POLITECNICO
MILANO 1863

Department of Civil and Environmental Engineering
Master of Science in Civil Engineering
Design of New Structures

Scan-to-BIM workflow:
an overview and case study

Supervisor: Professor Carlo De Gaetani
Thesis by: Letícia Brumatti Pinho

Academic Year 2020 – 2021

Abstract: Laser scanning and photogrammetry are remote sensing technologies that have significantly evolved in the scan-to-BIM workflow in the recent years, being indispensable tools for modeling as-built structures. They can be used to capture dense 3D measurements of a facility's condition and the resulting point cloud can be processed to create the as-built BIM, providing building information to document as-built conditions, and serving as a knowledge base for supporting decision-making and problem-solving issues in the field of civil engineering. Allied to a detailed and comprehensive quality information about the data and the elaborated as-built model, which can be provided by quality assessment verifications, the proactivity of the decision making is improved within the workflow.

This study addresses an overview of the scan-to-BIM workflow and discusses the application of the process in a case study, where an as-built BIM model of an existing bridge was developed based on a point cloud generated by the combination of two reality capture surveying techniques: laser scanning and photogrammetry. The aim of the work is then to analyze the effectiveness of the applied workflow in representing the real state of the construction by qualitatively comparing the deviations in the generated as-built model with the captured conditions of the existing structure.

Keywords: Scan, BIM, Laser Scanning, Photogrammetry, Deviation Analysis

Summary

1 Introduction....9
2 Scan-to-BIM Overview....11
2.1 Data Acquisition....12
2.2 Data Processing....21
2.3 BIM Modeling....25
3 Case Study....29
3.1 Data Acquisition....34
3.2 Data Processing....37
3.3 BIM Modeling....39
4 Deviation Analysis....50
5 Final Considerations....59
References....61
Annex....66
A.1) Piers....67
A.2) Abutments and Wing Wall....75
A.4) Decks....86
A.5) State of implementation of the public works of the Province of Piacenza....95

List of Figures

Figure 2.1: Standard san-to-BIM workflow. Font: (Yunos, 2020). 11

Figure 2.2: a) Terrestrial Laser Scanner. Font: (SpatialHumanities, n.d). b) LiDAR data acquisition. Font: (Tan et al., 2020). 12

Figure 2.3: ToF for range measurement. Adapted from (Groetelaars, 2015). 13

Figure 2.4: Phase-shift techniques for range measurement. Adapted from (Groetelaars, 2015). 14

Figure 2.5: (a) RIEGL VZ-6000. Font: www.riegl.com; (b) Leica ScanStation P40 / P30. Font: www.leica-geosystems.com; (c) FARO Focus3D X 330. Font: www.knowledge.faro.com; (d) Z+F IMAGER® 5010C. Font: www.zf-laser.com. 14

Figure 2.6: Principle of a laser triangulation sensor. Font: Adapted from (Groetelaars, 2015). 15

Figure 2.7: Romer Infinite 2.0. Font: www.tjaerostructures.com/metrology-equipment. 15

Figure 2.8: Photogrammetry. Font: (Mason, n.d.). 16

Figure 2.9: Variety of cameras and platforms used in close-range photogrammetry. Font: (Breithaupt et al., 2004) 17

Figure 2.10: Timeline for 3D imaging project. Font: Adapted from GSA BIM Guide for 3D Imaging. 18

Figure 2.11: Mapping of the spaces. Font: Scan to BIM 102: Project Planning Best Practices. 20

Figure 2.12: Typical processing procedures of point cloud data. Font: Autor. 21

Figure 2.13: Types of targets and control points. Font: Scan to BIM 104: Registration Methodologies and Pro Tips. 22

Figure 2.14: Parametric modelling of an object. Font: (Autodesk, 2018) 25

Figure 3.1: Lateral view of the bridge. 29

Figure 3.2: Top view of the bridge. 29

Figure 3.3: Signs of material degradation in the piers. 30

Figure 3.4: Water seepage and concrete spalling in the spandrel walls. 31

Figure 3.5: Invasion of soil and vegetation and signs of material deterioration of the abutment 32

Figure 3.6: Superficial cracks in the concrete decks. Font: Google Maps. 33

Figure 3.7: Point cloud by LiDAR data. Font: Autor. 34

Figure 3.8: Point cloud by Photogrammetry. Font: Autor. 35

Figure 3.9: Details of the point cloud provided by the laser scanner. Font: Autor. 36
Figure 3.10: Details of the point cloud provided by the drone. Font: Autor. 36
Figure 3.11: Aligned and merged point clouds. Font: Autor. 38
Figure 3.12: Post-processed point cloud. Font: Autor. 38
Figure 3.13: Principal elements of a masonry bridge. Font: (Pipinato, 2016) 39
Figure 3.14: Visualization of automatic wall fitting. Font: Autor. 40
Figure 3.15: Automatic wall extraction from the point cloud. Font: Autor. 40
Figure 3.16: Building tools. Font: ClearEdge3D Support. 40
Figure 3.17: 3D model output from Edgewise. Font: Autor. 41
Figure 3.18: Pre-modeling phase. Font: Autor. 42
Figure 3.19: Creation of new levels. Font: Autor. 43
Figure 3.20: Family of central piers and its parameters. Font: Autor. 44
Figure 3.21: Family of piers and its parameters. Font: Autor. 45
Figure 3.22: Family of abutments and its parameters. Font: Autor. 46
Figure 3.23: Family of arches and its parameters. Font: Autor. 47
Figure 3.24: Family of decks and its parameters. Font: Autor. 48
Figure 3.25: a) BIM model and point cloud data representation; b) only BIM model representation. Font: Autor. 49
Figure 3.26: Point cloud data, EdgeWise Model, and the parametrized family modelled in Revit. Font: Autor. 49
Figure 4.1:a) Inputs for the deviation analysis; b) APL Face deviation style. Font: Autor. ..51
Figure 4.2: Schematic representation of the bridge elements. 52
Figure 4.3: a) Right view of the Pier 5; b) deviation patterns; c) curvature of the pier cap. Font: Autor. 53
Figure 4.4: Pier 3 - Lateral view of the point cloud. Font: Autor. 54
Figure 4.5: Pier 3 - Lateral view of the deviation results. Font: Autor. 54
Figure 4.6: Pier 3 - Front and back view of the deviation results. Font: Autor. 54
Figure 4.7: Reduction in stiffness caused by scour. Font: (Prendergast et al., 2014). 55
Figure 4.8: Front view of the a) Abutment 1; b) Abutment 2. Font: Autor. 56
Figure 4.9: Top view of the Abutment 2. 56
Figure 4.10: a) Data quality issue; b) modeling quality issue. Font: Autor. 56

Figure 4.11: Arch 4. a) Back view; b) bottom view.....57
Figure 4.12: a) Back view of Arch 4; b) data quality issue. Font: Autor. 58
Figure 4.13: Deviation results of the decks. Font: Autor. 58

List of Tables

Table 3.1: List of software used in each phase of the proposed workflow. 33

1 Introduction

As-built capture and modelling is the process of deriving measurements and dimensions of a constructed entity and thereafter modeling the constructed entity based on the derived measurements to represent its completed state. In the past, this task has been purely manual, cumbersome, and inaccurate. Fortunately, with the progression in design tools and technology, this process has been made easier with the combination of reality capture technologies and BIM (Building Information Modeling), commonly known as scan-to-BIM workflow. The workflow consists of three major phases, including data collection, data processing and BIM modeling. Commonly, the data (in form of point clouds) are obtained through photogrammetry and LiDAR techniques, proving to be extremely accurate at registering complex geometries of buildings and infrastructures while saving time in the field. After a series of processing steps of the data obtained on site, such as data cleaning and data registration, a final point cloud that describes the scanned environment is obtained so that the post-processed data can be used in future BIM modeling.

With the ability of capturing complex geometries in reasonable time along with high quality, laser scanning and photogrammetry have attracted the interests of researchers in the domain of documentation and maintenance of historic buildings in the last decade. Usually, these constructions present complex architectural and structural elements, having walls with non-homogeneous thicknesses, deviations, and the lack of perpendicularity. Additionally, the possible variation in their constituent materials, the traditional design criteria and methods used for their construction, their deterioration over time caused by weathering processes and the development of other defects, significantly influence the capacity of stakeholders to correctly document these historic structures. Constructions like these typically require more measurements and detailed surveys to monitor and record the physical conditions of the building at a level that allows them to be correctly interpreted and represented as 3D models, which makes the combination of reality capture surveying and BIM modeling the ideal approach for this type of work. As BIM can incorporate both qualitative and quantitative information about a facility to represent its physical and functional characteristics, by incorporating high-quality digital survey datasets provided by laser scanning and photogrammetry these characteristics can be integrated into the as-built model in a structured and consistent way, recording in detail the state of the building, which can be useful for heritage representation and interpretation, allowing an easier information extraction of the heritage building. Although scan-to-BIM processes applied for historic buildings is a relatively new field of academic research (Baik, 2017), it has already proven to be very effective in providing new tools for the sector to support activities such as building retrofitting (Wang et al., 2015 and Oreni et al., 2014), historic asset management (Brumana et al., 2013), preventive maintenance (Angulo-Fornos et al., 2020), and documentation (Murphy et al., 2009 and Martins, 2019). And, in cases where the integration between terrestrial laser scanning and photogrammetry were applied for surveying and as-built modeling techniques, achieved results have shown that the hybrid methodology can successfully supplement each other in creating high-quality 3D recordings and as-built models of the physical scanned space (Guarnieri et al., 2006, Rocha et al., 2020 and Böhm et al., 2007).

A major problem with the creation of as-built BIM projects is that it has been largely a manual process, and, depending on the complexity of the facility and modeling requirements, the project may require several months to be completed. The manual process is time-consuming, and even though modeling of individual geometric primitives can be quick, modeling an entire facility may require thousands of primitives. Nowadays, with the incorporation of point cloud extraction technologies, semi-automated and automated techniques have been used to streamline the as-built BIM modelling and make the process more efficient. These technologies allow the geometry reconstruction of scanned environment from the point clouds to be semi or fully automated by reducing the human intervention in the process of model generation. Nevertheless, depending on the scope of the project, the problem of as-built BIM reconstruction can be very complex in terms of available inputs and expected outputs. (Tang et al., 2010) identified and discussed in their studies a number of technology gaps in automated as-built BIM creation capabilities, revealing areas where research on this problem should be concentrated, for instance, modeling of complex structures and representing non-ideal geometries that occur in real facilities, handling realistic environments with clutter and occlusion, representing models using volumetric primitives rather than surface representations, and developing quantitative performance measures for tracking the progress of the field.

This study addresses an overview of the scan-to-BIM workflow, covering the main issues of the process and discussing the application of the workflow in a case study, where an as-built BIM model of an historical bridge was developed based on a point cloud generated by the combination of two reality capture surveying techniques: laser scanning and photogrammetry. The aim of the work is then to analyze the consistency of the applied workflow in representing the actual conditions of the existing structure by means of a qualitative comparison between the generated as-built model and the point cloud data. The case study begins with a brief characterization of the real state of the structure, an existing masonry bridge placed at Ciriano, Italy, followed by the presentation of the two point clouds obtained by a terrestrial laser scanner and a drone, which were processed (merged and registered in a unique point cloud) in such a way that the final data could be used for the creation of the 3D BIM model. To further automate the modeling process, the proposed workflow accounted with an object recognition tool, acting as a pre-modeling phase which resulted in time saving and increased efficiency of design intent. Once the 3D parametric model was concluded, a deviation analysis between the point cloud data and the surfaces of BIM model was carried out. Then, the results of the deviation analysis were analyzed and the effectiveness of the applied scan-to-BIM workflow was tested by comparing the deviations in the generated as-built model with the real conditions of the existing structure.

The paper is organized as follows. In Section 2 is given an overview of the scan-to-BIM workflow, where the process of data acquisition, the main steps performed during the processing of 3D imaging projects, and the basic concepts related to the BIM modeling methodology are explained. In Section 3 the case study is addressed along with the steps followed during the proposed scan-to-BIM workflow. The application of a deviation analysis in the case study and its relevance in the scope of civil engineering is discussed In Section 4. The article concludes in sequence, in Section 5, where a resume of the main consideratons about the scan-to-BIM worflow is made, providing the main findings and perspectives of the research.

2 Scan-to-BIM Overview

The traditional scan-to-BIM workflow can be divided into three main steps, as illustrated in Figure 2.1: data collection, in which dense point measurements of the facility are collected using reality capture technologies (laser scans, photogrammetry, etc.); data processing, in which the data acquired is processed producing as output a point cloud as discrete representation of the reality; BIM modeling, in which the point cloud is used for the creation of a BIM model virtualizing the surveyed object.

Figure 2.1: Standard san-to-BIM workflow. Font: (Yunos, 2020).

The major benefit of 3D imaging systems is the ability to capture existing conditions more completely with a higher level of detail than most manual methods, especially in the cases of complex geometries and inaccessible areas, reducing in this way errors and reworks on site. Along with BIM modeling, all relevant information related to the captured and modeled building and its components, including geometric, topological, and semantic attributes, can be used to analyze, document, and monitor buildings and infrastructure more efficiently. Moreover, the scan-to-BIM workflow could benefit significantly from automation with the incorporation of point cloud extraction technologies. Although automatic segmentation of point cloud is one of the most challenging issues in the image-based 3D reconstruction panorama, properly applied it significantly reduces the modeling time by further automating the process, with the so called “Refined Scan-to-BIM Workflow”. The main idea of the refined workflow is that, from a point cloud describing an environment, it is possible to recognize and extract 3D models of each object instance and combine them to generate a 3D representation of the scanned scenario.

2.1 Data Acquisition

First step of the scan-to-BIM workflow is the data acquisition aiming at obtaining a point cloud of the surveyed object and/or scenario. Point clouds are large collections of 3D points, that store their cartesian coordinates (x, y, z) along with additional attributes such as intensity values or color measurements (RGB values). They are commonly obtained through laser scanning and photogrammetry, proving to be extremely accurate at surveying non-regular geometries and saving time in as-built modeling of complex building and infrastructures. This section focuses on terrestrial laser scanning and close-range photogrammetry, which are the two surveying techniques that have been progressed significantly and implemented for 3D digital documentation of buildings in recent years (El-Din Fawzy, 2019).

Laser scanning, also known as LiDAR (Light Detection and Ranging), is an optical remote-sensing technique that uses laser light to densely sample the surface of the scanned environment, producing highly accurate measurements, with accuracies from millimeters to centimeters, in short periods of time (ArcMap, 2019). Basically, a laser scanner measures the distance from the instrument to a target by means a laser beam that travels towards the object being scanned which is detected by receivers in the LiDAR sensor when back scattered or reflected. As shown in Figure 2.2, at each scanning location the distance "D" from the LiDAR to the target and its incident angle "α" is recorded. By combining these two measurements, the relative position of the target with respect to the equipment can be recovered. Then, through a series of processing steps, a point cloud is produced that aims to preserve the original complexity of elevations of the ground, buildings, and anything else that the laser beam encounters during the survey.

a) b)

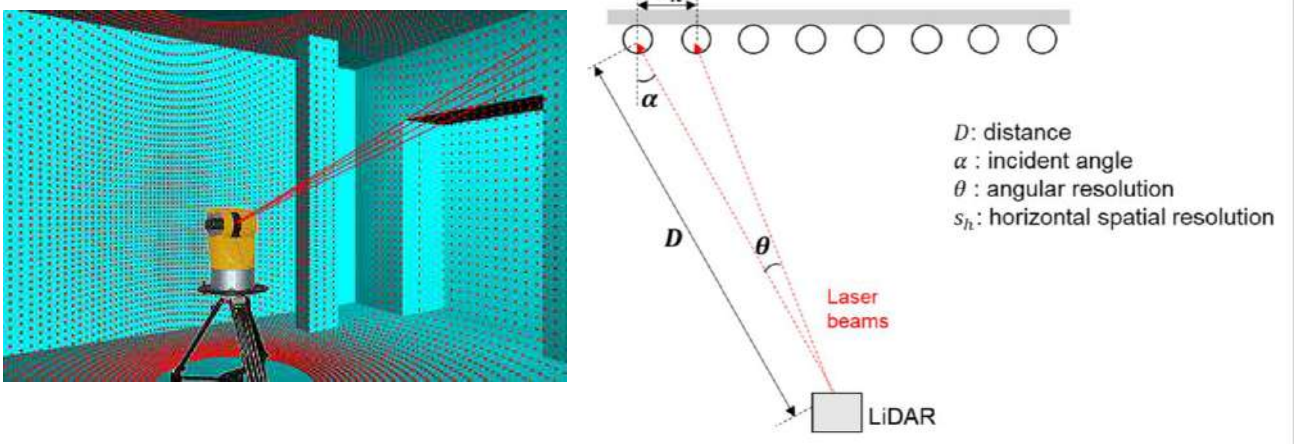

Figure 2.2: a) Terrestrial Laser Scanner. Font: (SpatialHumanities, n.d). b) LiDAR data acquisition. Font: (Tan et al., 2020).

A measure of point cloud resolution is the spatial resolution between points. It governs the level of recognizable detail within the scanned point cloud. The horizontal resolution "sh" of the acquired data (see Figure 2.2b) is determined by the scanning angular resolution "θ"

(angle increment) and scanning location, including distance “D” and incident angle “α”, and can be estimated as:

$$sh = \frac{\theta D}{\cos\alpha}$$

Accordingly, the vertical resolution is calculated with the corresponding vertical incident angle. The range distances “D” of commercial laser scanners may vary from 5 m to values above 3500 m, thereby, a classification between scanning systems is provided strictly based on the range of the equipment, as follows:

- Ultra-long range: for distances more than 3500 m;
- Long-range: for distances up to 3500 m;
- Medium-range: for distances up to 500 m;
- Short-range: for distances up to 120 m;
- Very short-range: for distances up to 25 m.

There is a wide variety of laser scanners on the market, which vary depending on the technology used for range measurement and their working platforms. Each type comes with its own range and accuracy that is suitable for the use to which it will be destined. According to the range measurement methodologies, they are commonly differentiated into three main principles: time-of-flight, phase-shift and triangulation. In the Time of Flight (ToF) technique, the receivers of the LiDAR sensor record the traveling time “T” from its emission to the detection of the reflected laser from a target to calculate the range distance between the sensor and the scanned object. By taking into account the refraction index of the medium and the speed of light, it is then possible to deduce the laser’s travel distancing through basic principles of Optics. Figure 2.3 illustrates the mentioned working principle. Combined with the positional information of the equipment, these measured distances are lead to three-dimensional points of the scanned scenario. ToF technique is commonly used for long-range distance measurements, achieving measurement accuracies ranging from 3 mm to 20 mm (Groetelaars, 2015).

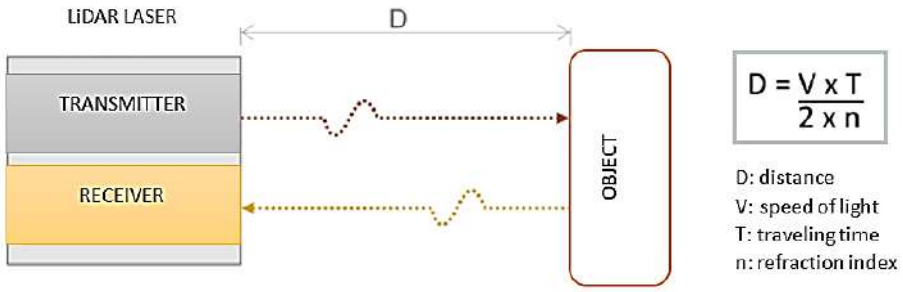

Figure 2.3: ToF for range measurement. Adapted from (Groetelaars, 2015).

In the phase-shift technique, scanners emit a continuous and modulated wave (in amplitude or frequency) and measure the phase shift between the emitted and reflected signals. The phase difference “Δφ” correlates to the distance measurement “D” from the LiDAR to the target as can be seen in Figure 2.4. These measuring systems generally have a higher data acquisition speed and higher accuracy than time-of-flight measuring systems (Wang et al., 2019), and are commonly used in medium-range systems, such as terrestrial and indoor LiDAR scanners (YellowScan, 2020), achieving measurement accuracies in the order of 5 mm (Groetelaars, 2015). Figure 2.5 shows some laser scanners that work according to the principles of the two range measurements mentioned: ToF (the first two images) and phase shift (the last two).

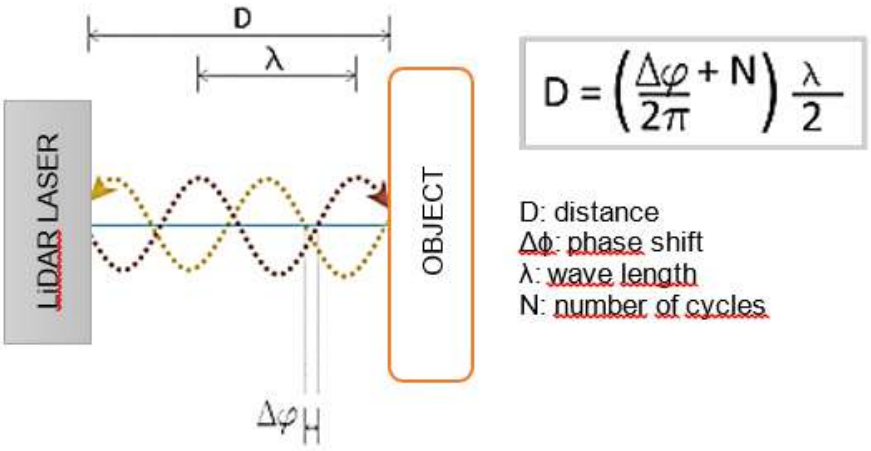

Figure 2.4: Phase-shift techniques for range measurement. Adapted from (Groetelaars, 2015).

Figure 2.5: (a) RIEGL VZ-6000. Font: www.riegl.com; (b) Leica ScanStation P40 / P30. Font: www.leica-geosystems.com; (c) FARO Focus3D X 330. Font: www.knowledge.faro.com; (d) Z+F IMAGER® 5010C. Font: www.zf-laser.com.

In triangulation measurement systems, the distance and orientation between the receiver and the laser transmitter are known (see Figure 2.6). At each pulse emission, the angles “α”

and “β” are registered in the system and, through knowledge of the distance “D” between the laser transmitter and the camera lens which are coupled in the laser receiver, the coordinates of the illuminated point on the surface of the target object are determined by the principle of triangulation. In this type of system, the measurement error is directly related to the distance to the measured object. This technique is mainly used to a limited range of applications that operate at short distances, often less than 5 m, achieving measurement accuracies ranging from 0.05 mm to 0.5 mm (Groetelaars, 2015). In Figure 2.7 is shown an example of laser scanner with an articulated arm system which uses active laser triangulation for 3D line imaging.

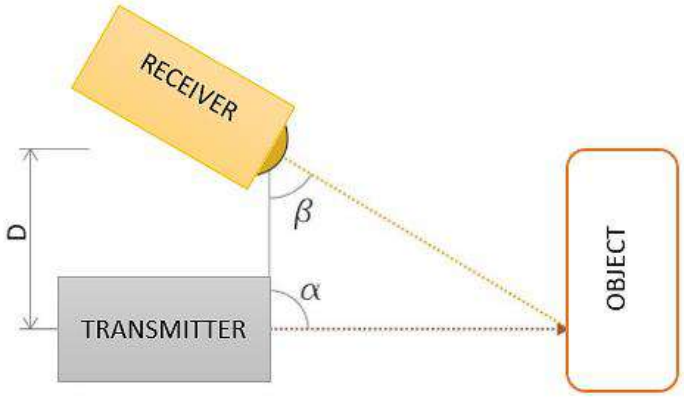

Figure 2.6: Principle of a laser triangulation sensor. Font: Adapted from (Groetelaars, 2015).

Figure 2.7: Romer Infinite 2.0. Font: www.tjaerostructures.com/metrology-equipment.

As previously discussed, another way to classify laser scanners is according to their working platform. In this way, laser scanners can be divided in two main groups: airbone and terrestrial (ArcMap, 2019). While in the Airbone Laser Scanners (ALS) the laser system is mounted on an aircraft during flight, Terrestrial Laser Scanners (TLS) are usually mounted

on a tripod positioned over the ground (see Figures 2.2a, and 2.5). TLS has been very utilized for applications that require high accuracy such as surveying, documentation and monitoring of buildings and civil infrastructures (Riveiro et al., 2016) that can be directly extrapolated to cultural heritage (Rocha et al., 2020), including defect detection (J. et al. 2010), and production of as-built models (Ahmad Fuad Bin Che Ku Abdullah et al., 2016). However, many professionals are resistant to this technology due to its high cost (it can cost hundreds of thousands of dollars) and the processing time involved to deal with the huge volume and complexity of these data. Also, LiDAR projects require an expert who understands the workflow and details of each subsystem and is able to recognize consistent and accurate data. Furthermore, the poor mobility in case of TLS is a limitation factor and, generally, it is not possible to capture all information required from a single scanning position, therefore it may be necessary to place the scanner in different positions with respect to the target object to make sure that the scanned environment is captured correctly without occlusions. These precautions are very important to be taken because they ensure that the software used to process the acquired data will be able to recognize corresponding points at different scans and align them. Yet, environmental factors like rain, snow, wind and moving cars or pedestrians will also result in spurious and unwanted data by causing vibration of the equipment or the structure on which the equipment is stationed.

Photogrammetry is a precise, non-contact 3D measurement technique which is based on the acquisition of several high-quality images that allow the collection of semantic and spatial data of a building or object to be accelerated thanks to its fundamental operating principle: the triangulation. By taking pictures of the object from different perspectives and under constant lighting, the specialized software can find representative or characteristic points of the model that are repeated in all the photos (target objects). The lines of vision of the cameras, also called as "lines of sight", by mathematically intersecting at a common point in the object, allow the production of the 3-dimensional coordinates of the points of interest, as schematically represented in Figure 2.8.

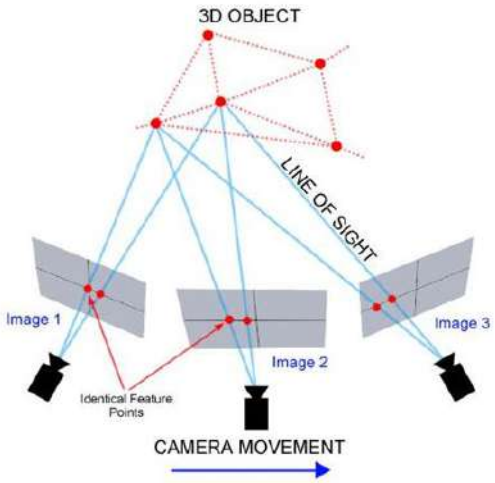

Figure 2.8: Photogrammetry. Font: (Mason, n.d.).

The two main types of photogrammetry that are used in geomatics are close-range and aerial photogrammetry, sharing the same basic principles of photogrammetry. The main difference between the two is that, in Close-Range Photogrammetry (CRP), the distance between camera and the objects is limited to 300 meter maximum (Doumit, 2019). Since the same basic principles apply to photographs taken from a camera mounted on a tripod (terrestrial) or suspended from a light sport aircraft, both survey techniques are commonly referred as close-range photogrammetry (Matthews, 2008). A variety of cameras and platforms may be used to obtain the photographic images, including cameras housed in unoccupied airborne vehicles, suspended below helium-filled blimps, and mounted on tripods (Figure 2.9).

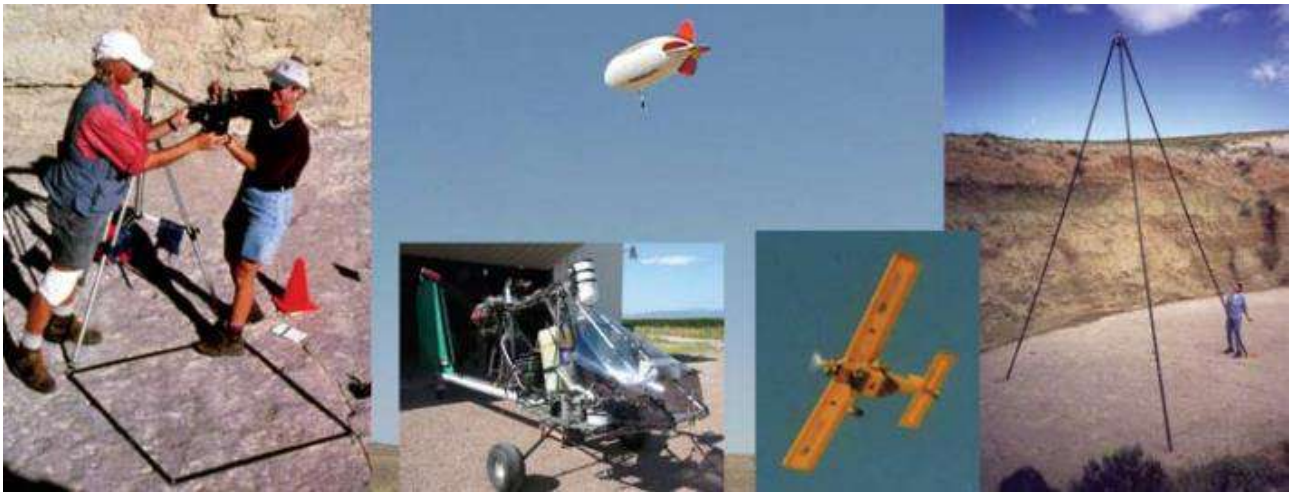

Figure 2.9: Variety of cameras and platforms used in close-range photogrammetry. Font: (Breithaupt et al., 2004)

The main advantage of CRP is the ability to use simple cameras, sometimes self-calibrated, due to the recent advancements in the mass market image acquisition technologies and modeling software, which translates into greater operational flexibility and overall reduced costs. With the self-calibration feature, internal parameters of the camera such as focal length, key point location, lens distortions, sensor size and image resolution, are resolved automatically, without the need to perform the interactive association of homologous points (Groetelaars, 2015). In the specific case of lens distortion phenomenon, this is one of the major factors that can affect the accuracy of the resulting model obtained through photogrammetry and it is present in all camera lens systems because of the curvature of the lens and their alignment with the sensor, which causes the point to shift from its true position to a skewed position (Dai et al., 2010). The main limitations of CRP systems, in turn, include the short flight distances, low battery life and the use of low weight navigation units, which implies less accurate results for the orientation of the sensors (Doumit, 2019). For this reason, proper planning is essential to obtain good quality data on site and ensure the desired point density and accuracy of the deliverable model.

Actually, when scanning complex environments, the ideal data acquisition approach is to make use of hybrid methodologies to supplement and compensate the limitations of each

technique. Alternatively, and especially for the complementation of TLS surveys, aerial surveys can be performed using Unmanned Aerial vehicles (UAVs), commonly known as Drones. Depending on the type of sensor installed in the vehicle, it can collect point clouds both from LiDAR as well as digital images (produced from photogrammetry). Achieved results have shown that these two technologies, 3D laser scanning and photogrammetry, can supplement each other in creating high-quality surface geometries for survey and documentation of as-built structures over the last decade (El-Din Fawzy, 2019). As explained by (Guarnieri et al., 2006), generally, laser scanning produces dense 3D point-cloud data that is required to create high-resolution geometric models, while digital photogrammetry is more suited to produce high resolution textured 3D models representing just the main object structure. In the context of historic monuments, (Rocha et al., 2020) combined these two survey techniques for the creation of an HBIM model. In his study, drone was used to access and capture the roof of an historic engine house, which was not possible with the 3D laser scanner. (Mateus et al., 2019) discussed in his studies the graphical data flow based on the hybrid methodology for the conservation and rehabilitation of a medieval fortress, where a photogrammetric model was used to identify all the problems with materiality and discover old constructions techniques and the TLS model was used to give the precise information about measurements needed to develop the design project. In the context of structural health monitoring, (Riveiro et al., 2013) proposed a novel methodology based on the application of the hybrid techniques as auxiliary metric tools for bridge inspections procedures.

According to the GSA BIM Guide for 3D Imaging, a North American guide prepared to assist project teams in contracting for and ensuring quality in 3D imaging contracts, the scanning projects consists of three major phases: procurement (solicitation), planning, and execution. A possible timeline for 3D imaging project is shown in Figure 2.10.

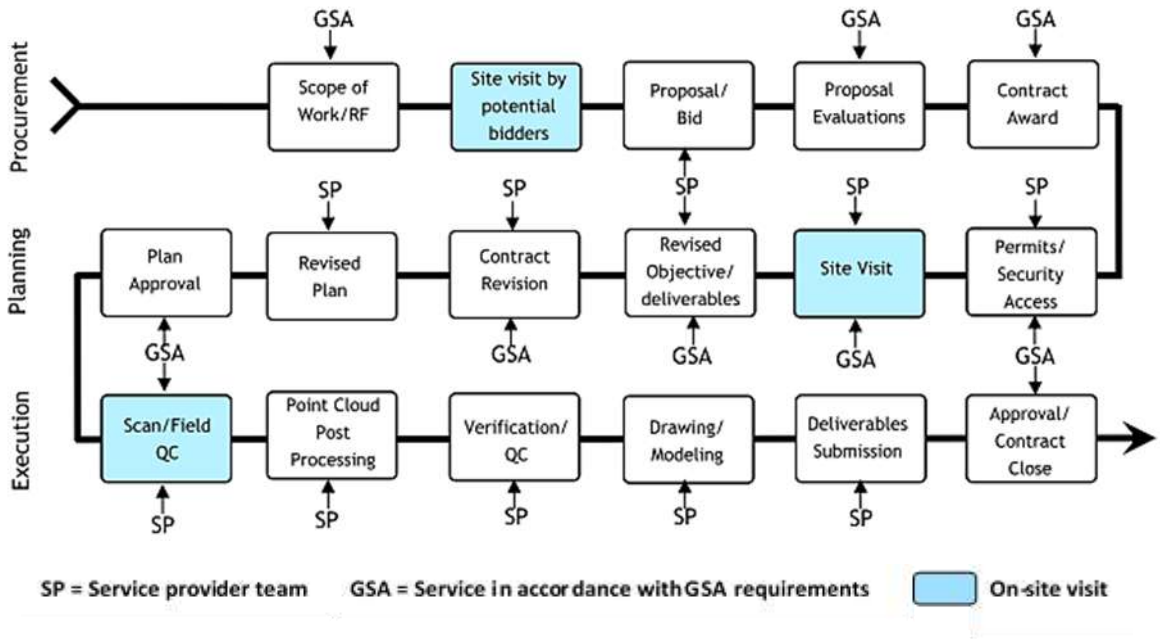

Figure 2.10: Timeline for 3D imaging project. Font: Adapted from GSA BIM Guide for 3D Imaging.

The procurement phase begins with the creation of a Request for Proposal (RFP) that includes a Statement of Work (SOW). A very critical part of the development of the SOW is defining the objectives and the deliverables of the project, which should include the deliverable document type (e.g., point cloud, 2D drawings, 3D models) and desired point density and accuracy that the client is looking for. Within this phase, the potential challenges faced when scanning should also be clarified, which may be suggested by the type of the environment to be scanned (office indoor, open space, school, industrial, residential, or commercial spaces), the access restriction to certain areas and limited periods of time that the scan team can work, obstructions caused by heavy vegetation or overcrowded workspaces, and environmental conditions. The choice of the best surveying techniques and equipment will be based on the solution that offers the desired deliverable even with the restrictions and challenges imposed during the project. However, understanding the customers' goal is a great start, but this is meaningless if the data acquisition approach is not planned and executed properly.

The planning phase generally initiates with an on-site meeting. Site reconnaissance not only aids in identifying strategies for capturing complete environment but can also be used to identify obstacles to imagery acquisition (e.g., vegetation, structures, traffic, surface finish), which can obscure points of view. Objectives must be defined clearly and be vetted by all parties so that the service provider can revise the plan if needed, in order to furnish the deliverables in the most efficient manner. Permissions and site access should also be discussed at this time. At this stage, logistics is very important to optimize the overall work. Mapping the spaces (see Figure 2.11), determining the type of instrument to be used in each of them, as well as the periods of the day when the scan can be performed and those when it cannot, defining a scan walkthrough, scheduling the scan team according to their expertise and availability, all they are crucial decisions to optimize time, effort, avoid redoing work and so reduce costs. The scan plan should describe the general procedures used to obtain the spatial data and to achieve the specified tolerance of the deliverables and estimate the work in terms cost and time length.

Finally, the execution phase involves acquisition of the data itself and data post-processing to obtain the required deliverables (e.g., registration, cleaning, exporting data into required formats). In most cases, the post-processing of the scans is more time consuming than obtaining the scans, and underestimations of the time required for post-processing results in project delays. There are many other factors which may affect the project schedule: the size of the project (e.g., single building versus a composition of buildings), specified tolerances and resolutions (tighter tolerances and higher resolutions increase time and cost, affecting mainly the scanning and post-processing phases), the complexity of the region scanned (scanning in low light or highly reflective surfaces like glass or mirrors), the security/site access (limited access, restricted work times), required deliverables (any modeling will increase the time and cost), skill of the service provider (mainly affects scanning and post-processing phases), and change in scope of work.

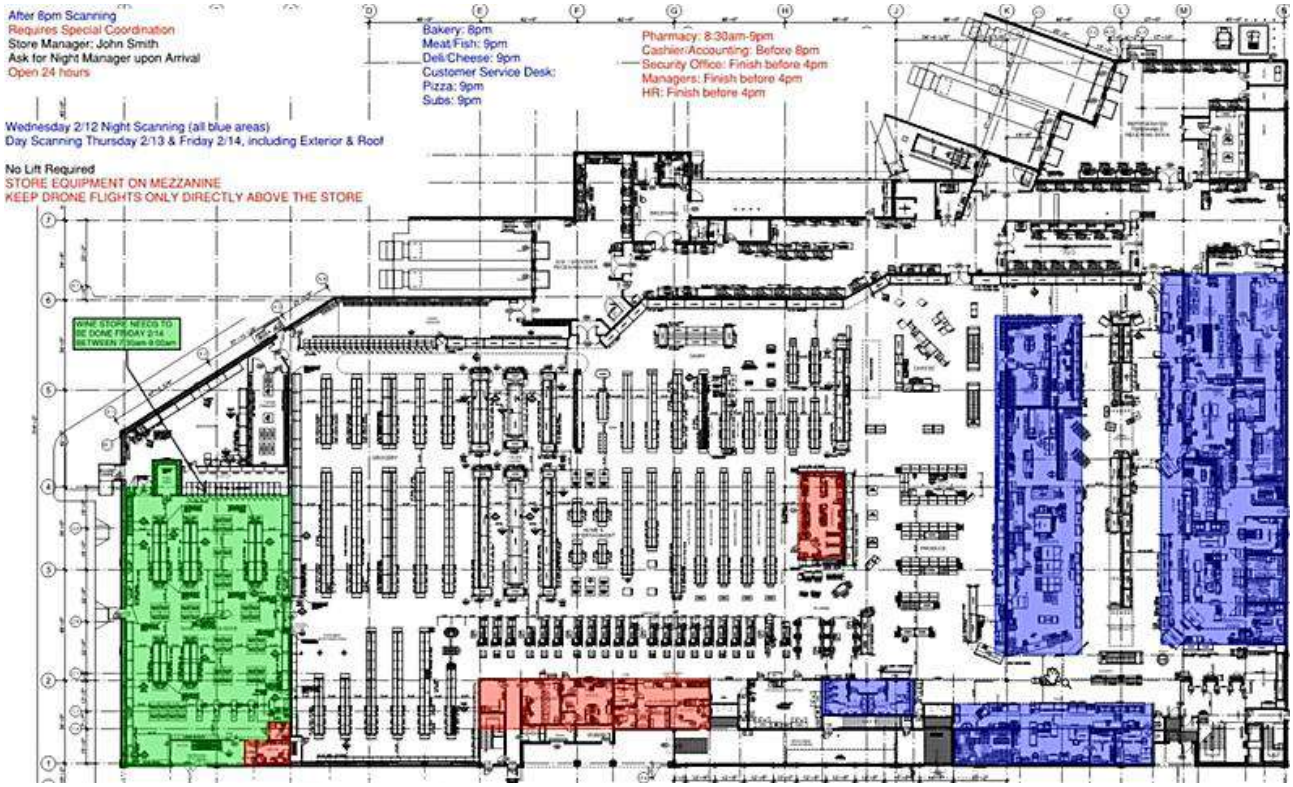

Figure 2.11: Mapping of the spaces. Font: Scan to BIM 102: Project Planning Best Practices.

2.2 Data Processing

The acquired raw point cloud needs to pass through a series of processing steps so that the post-processed data can be used for further 3D modeling. Commonly, in scan-to-BIM workflow, the processing procedures consist of three main phases: (1) data registration, (2) data cleaning, (3) data segmentation, as schematically shown in Figure 2.12 below.

Figure 2.12: Typical processing procedures of point cloud data. Font: Autor.

Data registration aims to align multiple point clouds collected from different locations in a common reference coordinate system. The point clouds from each scan are initially represented in the scanner's local coordinate frame, then these point clouds are aligned through a certain spatial transformation (e.g., scaling, rotation, and translation) and merged to give rise to a global cloud that will describe the scanned area.

The traditional approach to register datasets is the so-called target-based method. It involves the use of artificial targets that are placed along the environment being scanned, or natural targets like corners, signs, and salient characteristics, so that the processing software could align and match the individual scans into one common point cloud. Since artificial targets are coded, they are easily identifiable inside the scanned data, allowing specific software to be able to perform the registration of the point clouds more easily. It is important to emphasize that in order to register scans together, the algorithms must first have at least three reference points that correlate between scans, that means, if we have two scans that we are going to register together, the first scan must include three geometric references that the second scan can also see. The minimum and essential amount of three corresponding points in each scan is foreseen to interlock the six degrees of freedom and the scale factor between the two point clouds to be aligned, but obviously, the greater amount of matching points in different scans, the greater the overlap between point clouds and a stronger link between them is established.

There are many different types of targets available in the market: they can be patterned, such as a black and white checkerboard, or a retro-reflective dot, or they can be geometric objects, like spheres of known dimensions, as can be seen in Figure 2.13. Their applicability will fundamentally depend on the objectives of the measurement. The appropriate target size for a measurement, for example, depends on several factors which include the distance from the instrument to the object, the resolution of the instrument, and the target exposure (Tian, 2011). Regarding the distance from the instrument to the object and the instrument's

resolution, plane-based checkerboard targets have an effective range of approximately 15 meters, while smaller reflective spheres have a range usually no greater than 18 meters and larger reflective spheres greater than 45 meters in optimal conditions (Cox, 2015).

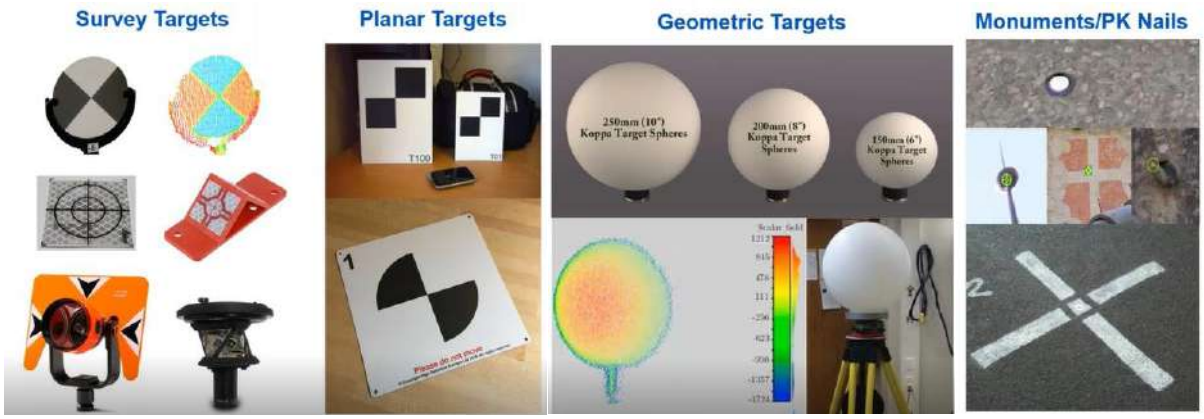

Figure 2.13: Types of targets and control points. Font: Scan to BIM 104: Registration Methodologies and Pro Tips.

The registration error using target-based methodology is dependent on how well the targets can be measured, which requires that the operator possesses some expertise to be able to place the targets efficiently. Basically, good geometry implies that targets should be placed at differing distances and elevations from the scanner and far apart from each other in all three dimensions, so that they are visible from several different scan locations. Other aspect to be discussed in the target-based technique is that some final deliverables may require that the final registered point cloud representing the as-built environment is free from artificial targets, and the task of removing them from the point cloud can become quite time-consuming (Cox, 2015).

Recently, with improvements to point cloud processing software, the registration of point clouds can be performed without the use of targets. This method of point cloud registration, referred as targetless registration, seeks to solely use the overlapping scan data to align separate local point clouds into a common global point cloud. Although automated registration methods have been developed, targetless registration is still a semi-automated process, which can be divided into two categories: coarse registration and fine registration (Wang et al., 2019). A commonly used solution for fine registration is the Iterative Closest Point (ICP) algorithm due to its simplicity. The algorithm is an iterative process employed to identify corresponding points between the data sets and find a transformation that minimizes the difference between two point clouds. More formally, the aim of the geometric registration is to be able to represent a shape, called reading, in the same coordinate frame as another, called reference (Pomerleau et al., 2015). A shape "S" is a set of points including both geometric (e.g., coordinates of points, surface normals or tangent vectors) and non-geometric information (e.g., color, temperature and identifier, also called as descriptors). Letting ${}^{A}P$ be the shape representing reading in a coordinate frame A and ${}^{B}Q$ the shape

representing the reference in its coordinate frame B, the aim of registration is to estimate the transformation ${}^{B}_{A}T$ by minimizing an error function:

$$ {}^{B}_{A}T = \arg\min(error\ (T\ ({}^{A}P,\ {}^{B}Q\ ))) $$

where $T\ (S)$ is the application of the geometric transformation T to the shape S.

Actually, the idea of the algorithm is to build a sequence of transformations ${}^{i+1}_{i}T$ that are successively applied to P so that the registration error slowly decreases. In the case of the open source software CloudCompare, a 3D point cloud editing and processing software, it is possible tell the software to stop this process either after a maximum number of iterations, or as soon as the error difference between two iterations becomes lower than a given threshold. The smaller this threshold is, the longer it will take to converge, but the finer the result should be (Girardeau-Montaut, 2015). Unfortunately, the popular ICP algorithm only works well in ideal scenarios (Pomerleau et al., 2015). In practice, two point clouds are usually first roughly registered with a robust but less accurate methodology, named as coarse registration. With the coarse registration, an initial solution can be obtained to align these point clouds, afterwards, the ICP-based algorithm is adopted for fine registration to further improve the initial solution (Wang et al., 2019).

One of the coarse registration techniques relies on the use of local descriptors and keypoints to align two point clouds. Keypoints (also known as interest points) are points in point clouds that are stable, distinctive, and can be identified using a well-defined detection criterion (PCL, 2021). Descriptors, in turn, analyze the local neighborhood of a keypoint to form a compact and descriptive representation of the original data. During the coarse registration, point descriptors are first predefined to describe each point, highlighting the salient features. This information can then be used to classify the extracted keypoints among specific categories or for determining point-to-point correspondences between two point clouds (Tombari et al., 2013). Then, based on the descriptors, the original point cloud is reduced to a sparse set of keypoints and finally, the alignment between two point clouds is calculated based on these sets of keypoints. (Wang et al., 2019) review in their studies relevant literatures for coarse registration.

Following with the point cloud data processing, data cleaning aims to remove noise, outliers, and gaps, from the point cloud which are generated by environmental or technical limitations of sensors. Since the presence of noises inside the point clouds difficult latter registration, visualization, and 3D modeling of the scanned scenario, some algorithms are used to filter out useless and dirty data and retain the data of interest only (e.g., clean points from trees, people, moving objects, mixed pixel noise, reflected and refracted data). Basically, there are two types of cleaning processes: pre-processing and post-processing. The pre-processing cleaning is performed when the dirty data could cause registration errors. It speeds up the registration process and optimizes the alignment between scans. This is the case of reflection, refraction, and mixed-pixels noise, which are data points at spatial discontinuities. As explained by (Wang et al., 2014), reflective surfaces with general smooth geometry usually do not produce outliers as long as the sensor image is exposed properly, however,

extensive outliers will occur when scanning surfaces with edge features and small concave geometry. Two models, mixed reflections and multi-path reflections, are derived based on the principle of light reflection to characterize outlier formations when scanning such geometric features. The post-processing cleaning is performed to deliver a clean data for the client, so it is related with deliverable issues (removing trees, cars moving, etc.) The main points to be discussed are when to do Pre or Post registration clean up, and when we should not clean the data. The answer to the last point is based on the time-saving criterion: we should avoid clean data unnecessary, e.g., when the presence of noise will not affect the registration and the modelling team to extract the desired geometry form the point cloud.

Lastly, in data segmentation, points that share similar features in a continuous region are grouped to generate a segmented, spatially related, and organized point cloud. It can be carried out semi-automatically or fully automatically. The segmentation and recognition of point clouds currently represent the fundamental steps for identifying the correct surfaces and facilitating the tracing or the modeling of parametric objects. Ideally, from a point cloud of a given structure as an input, a system could produce an as-built BIM model as an output but, depending on the typology of the building and the level of complexity of the work, this task can be very challenging. (Yunos, 2020) highlights that the automatic point cloud geometry extraction reduces the modelling time by 50-70%, but do not automate the entire scan-to-BIM workflow in cases where the obtained results will be 2D and 3D CAD surface models, which must still be manually converted into parametric BIM models.

2.3 BIM Modeling

The acquired point clouds from laser scanners and photogrammetry describe, in detail, the surface geometry of the scanned environment but do not contain additional information about the objects whose geometry they represent. Geometrical, topological, and semantic attributes can be jointly managed through 3D parametric objects, and this is at the heart of BIM is. BIM (Building Information Modeling) is an intelligent 3D model process that, with the information and relationships established during the modeling process, promotes insights and tools to design, construct and manage buildings and infrastructures more efficiently, providing in this way building information to document as-built conditions and assist in developing architectural and engineering restoration and renovation designs.

The BIM methodology is based on the definition of objects: the components of the building are represented as digital parametric objects whose content is data (graphical and non-graphical data) and methods (codes). The graphical data is the 3D spatial data describing the geometry of the objects, while the non-graphical data describe its properties. The methods, in turn, describe the behavior of the single objects constituting the building. In other words, parametric modeling of an object is the art of defining not only the shape of the real object but also determining its properties and how it is connected to other objects (see Figure 2.14).

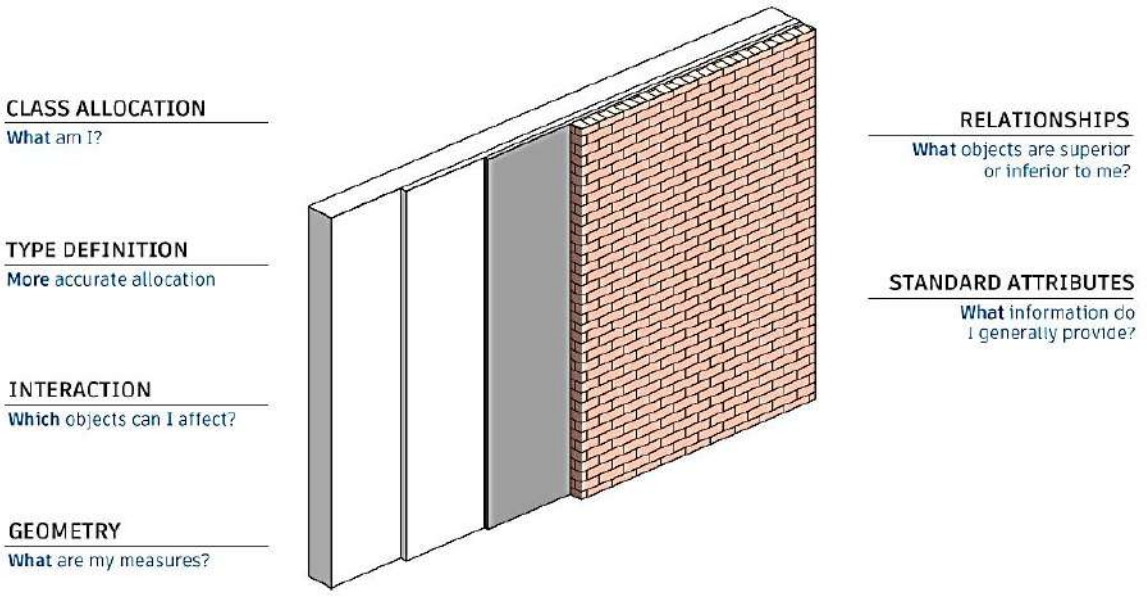

Figure 2.14: Parametric modelling of an object. Font: (Autodesk, 2018).

As explained by (Tang et al., 2010), from a given point cloud of a facility, the as-built BIM creation process involves three tasks: modeling the geometry of the components, assigning an object category and material properties to a component, and establishing relationships between components. Additionally, it is fundamental to ensure the interoperability of BIM content, which is one of the most challenging issues related to the work. In fact, the lack of

interoperability between software tools has been proven to be an obstacle to collaboration for the construction industry (Sattler et al., 2019).

Historically, the two forms to represent geometric shapes of the building elements are the boundary representation approach (B-rep), where shapes are represented as a closed, oriented set of boundary surfaces, along with connectivity information to describe the topological relationships between the elements, and the Constructive Solid Geometry approach (CSG), where shapes are represented by a set of functions that define primitives. A “primitive” can be described by a procedure which accepts some number of parameters; for instance, a sphere may be described by the coordinates of its center point, along with a radius value. The main advantage of CSG over B-Rep is that in CSG models use only primitive objects and Boolean operations (like spatial union, intersection, difference) to combine them, while in B-rep additional topological data is required, or consistency checks must be performed to assure that the given boundary description specifies a valid solid object. However, B-rep is more flexible and has a much richer operation set: Boolean operations; operations like extrusion (or sweeping), chamfer, blending, drafting, shelling, tweaking, etc. Recently, BIM software incorporates the “merged approach” to 3D object modeling: a CSG-like representation for editing purposes, and a B-rep representation for visualization and interaction (Migliaccio, 2019).

According to Autodesk specifications, object categories are subdivided into Model Categories, including beams, columns, doors, windows, and walls, and Annotation Categories, including dimensions, grids, levels, and textnotes. The importance of assigning to an object a category is that it can be used to classify elements, since the element category determines certain behaviors. For example, all elements in the same category can be included in the same schedule, being very useful for controlling visibility and graphical appearance in the software. Elements are also classified as family, type and instance, following a hierarchy among them. Each family object belongs to a category. The family object, in turn, contains a number of family types, defined by distinct parametric, graphical and documentation characteristics. Lastly, an element created using a specific family type is known as an instance. Instances represent transformed identical copies of an element type. Establishing relationships between elements and between elements and spaces is very important when working with digital objects. This is due to the fact that some properties of geometric objects do not depend on their shape and, as a consequence, the solution of some geometric problems does not depend on the shape of the objects involved but on how they are connected (Migliaccio, 2019). As outlined by (Tang et al., 2010), the common connective relationships modeled in the BIM model include aggregation relationships (e.g., a window is contained in a wall), topological relationships (e.g., wall 1 is connected to wall 2), and directional relationships (e.g., the second floor is above the first floor). These relationships can be established either manually or in a semi-automated manner. For example, if an object is modified, an adjacent element is automatically adjusted according to the predetermined relationship between them (rules such as “distance from”, “attached to”, “if-then”).

The interoperability issue is present throughout the entire scan-to-BIM workflow, starting from the point cloud data acquisition to the ability of BIM software to import point cloud datasets and export the 3D model into different BIM platforms. Different reality capture instruments produce raw data in multiple formats, but only certain processing software can accept some of these file types, and each software has different exporting capabilities.

Moreover, it can happen that Architecture, Engineering, and Construction (AEC) professionals involved in the modeling process are using different BIM software and, depending on the choice of the software, supported formats for point cloud data can vary. For these reasons, ensuring the interoperability of the scans and the BIM content is one of the most important and challenging issues in the AEC community. To overcome possible interoperability problems, numerous file formats were developed to facilitate the data exchange among programs that use point cloud data for processing and modeling purposes. As explained by (Thomson, 2018), the main difference between point cloud file types is the use of ASCII and binary codes. ASCII (American Standard Code for Information Interchange) is rooted in binary but conveys information using text, representing each character as a 7-bit binary number. Binary systems, in turn, store data directly in binary code. The common point cloud ASCII file types are XYZ, OBJ, PTX and ASC, while the point cloud binary formats include FLS, PCD, and LAS. In addition, several other regularly used file types are capable of both ASCII and binary formats, these include PLY, FBX, and E57. Once expressed data formats for point cloud data, also BIM content suffers for interoperability problems. In this context, the development of an open platform-neutral format is required. The OpenBIM approach, developed by buildingSmart (buildingSMART, n.d.) with its proposed IFC format (Industry Foundation Class), aims at managing and overcoming all possible problems related to the use of proprietary formats, for complete and consistent data exchange among all the involved stakeholders and a full exploitation of BIM capabilities.

In conclusion, it is important to emphasize that, despite advancements in scan-to-BIM tools, BIM modeling is still an arduous and time-consuming process. Consequently, the time and effort applied for the geometric parametric representation of a building is dependent on the complexity of the scanned environment, the Level Of Detail (LOD) and modeling tolerances required for the work. The commonly recognized reference document by practitioners for LOD Specifications is the (BIMForum, 2019). According to this reference, the various LODs from 100 to 500 specify how much information is known about a building element at a particular stage of the project and the expected geometric representations. In LOD 100 it is indicated the existence of a component, but not its shape or precise location. In LOD 200 the model elements are represented graphically but in a generic way just to recognize the element. In LOD 300 a detailed design of the element is provided, where non-graphic information may also be attached. In LOD 350, in addition to the detailed design and the non-graphic information, interfaces with other building systems are added to the model element. In LOD 400 the elements are graphically represented in an accurate geometry, with detailing, fabrication, assembly, and installation information. Finally, in LOD 500, the model elements are as-built and field verified representations in terms of size, shape, location, quantity, and orientation (Migliaccio, 2019). The LOD classes, if correctly used, will help to understand the usability and limitations of the modelled elements. However, LOD concept is commonly dedicated to new buildings, being not totally appropriate for already existing buildings, maybe of historical importance. (Fai et al., 2014) explain that the LOD definition in the context of heritage buildings is complicated because it is necessary to reconcile the level of detail of the BIM model with that used during the documentation process. For example, point clouds with a poor resolution may not be sufficient enough to produce highly detailed models of architectural elements since the density of the points may not be high enough to interpret the form of the element. Moreover, buildings with historic architectural styles often consist of highly complex geometries (sometimes including undefined shapes

as a result of weathering or structural deformation) which can be very difficult to represent accurately using parametric BIM objects. Yet, there is still no uniform criterion about the LOD for historic BIM modeling. According to (Yang et al., 2016), the level of “detail” in historic as-built BIM models is how complex, accurate and modifiable, with respect to the materials, the model is by considering spatial and temporal scale characteristics about the existing heritage. For this reason, they proposed a new LOD definition for historic models by considering their characteristics, and making a parallel numbering as in the BIMForum LOD Specification, as follows:

- LOD 100: the 2D outlines of different historic building, which means that the building is considered as an historic building.
- LOD 200: the simple models (but not box models) with size and basic shape.
- LOD 300: the detailed model with sub-structures including openings and roof superstructures in 2D and 3D.
- LOD 400: the accurate model with detailed structures such as the sculptures in the surface and complex shape about the openings (3D).
- LOD 500: the temporal model indicating the changes of historic elements.

3 Case Study

The structure is a masonry bridge located in Ciriano, a small town in the Province of Piacenza, Italy. It originally consists of seven shallow arches spanning about thirteen meters each for a total length of 90 meters, with a granular mixture fill and segmental brick vaults. Figure 3.1 shows the lateral view of the bridge while Figure 3.2 shows its top view. Additionally, the bridge is placed at Provincial Road n.6 bis of Castell'Arquato and crosses the Chero stream, a long stream that flows completely in the province of Piacenza.

Figure 3.1: Lateral view of the bridge.

Figure 3.2: Top view of the bridge.

Based on visual inspection of photographic recordings of the bridge, it was tried to characterize the real (superficial) conditions of the bridge elements, including the piers, spandrel walls, abutments, wing walls and the decks. As no type of visual observation of the foundation elements was possible, it was tried to find information about them in public sources.

Starting with the pier analysis, they showed several signs of material deterioration caused by weathering processes over the time (Figure 3.3), mainly at the pier top and at pier bed. The latter, probably due to erosional process caused by the interaction between the pier and the river flow, which compromised the integrity of the element.

Figure 3.3: Signs of material degradation in the piers.

The spandrel walls, in turn, presented signs of water seepage, judging from the black marks on the surface, and usual signs of deterioration due to spalling of concrete (Figure 3.4), which happens because of two main mechanisms: thermal stress and pore pressure, forcing the surface to peel, pop out, or flake off.

Figure 3.4: Water seepage and concrete spalling in the spandrel walls.

The abutments also showed a certain level of material deterioration and, mainly, the invasion of soil and vegetation, in such a way that it was possible to identify the presence of only two wing walls, as can be seen in Figure 3.5.

Figure 3.5: Invasion of soil and vegetation and signs of material deterioration of the abutment.

The bridge decks showed some signs of superficial cracks, which were better visualized through Google Maps (Figure 3.6). Lastly, with respect to the foundation elements, it was founded in public sources that the Province of Piacenza awarded an executive project of foundation consolidation of the studied bridge in December 2020 (Annex A.5), which can be found in “Cantieri aperti e trasparenti”, an open and transparent construction site to allow citizens to be informed about the progress of the works. The Viability Service foresaw the completion of works In July 2021 and the estimated amount was € 450,000.00.

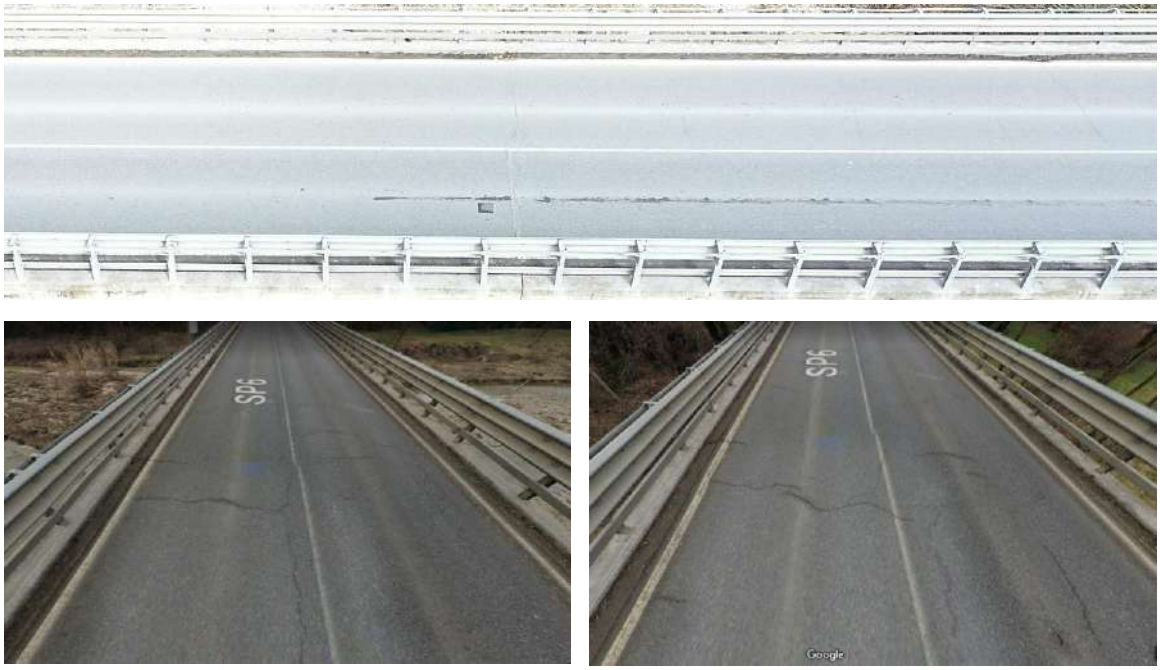

Figure 3.6: Superficial cracks in the concrete decks. Font: Google Maps.

Once the description of the site and the analysis of the physical conditions of the structure were made, the scan-to-BIM workflow was applied to the case study. For that, different software were used throughout this process, which are listed in the Table 3.1 bellow. The table lists the software used in each phase of the case study and their functionalities as engineering programs, which will be explained in more detail in the next subsections.

Table 3.1: List of software used in each phase of the proposed workflow.

Application phase	**Software**	**Software description**
Data processing		
Visualizationa interoperability	Autodesk ReCap Pro version 7.0.0.183	Reality capture and 3D scanning software and services
Meshing, cleansing, sub-sampling	CloudCompare (version 2.12.alpha)	3D point cloud editing and processing software
Object recognition	ClearEdge3D EdgeWise (version v5.5.0)	Automatic point cloud geometry extraction
BIM modeling	Autodesk Revit (version 2021)	Plan, design, construct, and manage buildings
Deviation analysis	Autodesk Point Layout (version 2021)	Construction layout software. Requires AutoCAD, Revit, or Navisworks

3.1 Data Acquisition

The survey of the exterior of the bridge was performed using the combination of a terrestrial laser scanner and an Unmanned Aerial vehicle. The registered and georeferenced point clouds were given as input for this study.

The laser scanner used was the Leica Nova MS60, a MultiStation combining total station functionality with 3D laser scanning, GNSS connectivity and digital imaging. The Nova MS60 is a time-of-flight range scanner and features an electro-optical distance measurement system based on the wave form digitizer technology (WFD). In this technique, as explained by (Maar et al., 2017), the instrument sends out short pulses where a small part of each pulse gets directly guided onto a photo detector inside the telescope and serves as internal calibration measurement, called start pulse. The rest of the pulse is emitted out of the telescope and reflected by the object, therefore called stop pulse. Both pulses are digitized as full waveform and accumulated from multiple signals. The time difference between accumulated start and stop pulse is used to calculate the distance as it is done in a standard time-of-flight method. The main advantages of the WFD technology are the fast distance measurements, high measurement accuracy and long ranges that are available at the same time. The post-processed point cloud obtained with the laser scanner accounts to 1995288 points, approximately, and is presented in Figure 3.7. In the case of the photogrammetry by the unmanned aerial vehicle, algorithms were used to transform the digital images taken on site into a 3D point cloud, obtaining the point cloud illustrated in Figure 3.8, with a total of 20214429 number of points.

Figure 3.7: Point cloud by LiDAR data. Font: Autor.

Figure 3.8: Point cloud by Photogrammetry. Font: Autor.

As expected, the two registered point clouds presented a high level of detail, however, it is possible to notice the occurrence of some occlusions in both of them. In the case of data associated to the laser scanner, for example, the concrete deck was completely occluded. The same happened for some regions in the bottom of the arches, some piers and an abutment (see Figure 3.9). The point clouds produced by photogrammetry, in turn, produced a higher resolution textured 3D representation which, fortunately, was capable to represent the absent data produced by laser scanning. And this is exactly the scope of the hybrid surveying methodology, e.g., when the instruments and techniques implemented can successfully supplement each other in creating high-quality 3D recordings of the scanned environment. However, it is important to highlight that all data collection techniques have their limitations, and therefore, the point cloud generated by photogrammetry also presented some occlusions, such as some regions in the bottom of the arches and in the façade of the spandrel walls, as can be seen in Figure 3.10.

Figure 3.9: Details of the point cloud provided by the laser scanner. Font: Autor.

Figure 3.10: Details of the point cloud provided by the drone. Font: Autor.

3.2 Data Processing

The two software used in this phase of the scan-to-BIM were the Autodesk Recap and CloudCompare. The former is a reality capture and 3D scanning software, which was used to import and export the point cloud files with different formats. The latter is a point cloud editing and processing software, which was used to process the data with many different tools. Even though CloudCompare has a huge list of supported file formats for importing /exporting data, rcs format files (the ones used for the case study), are not included in it. For this reason, Autodesk Recap was only used to convert the rcs file format of the two registered point clouds into pts file format, which is supported by CloudCompare. Once the interoperability issue was solved, the point clouds were imported to CloudCompare to be properly processed.

In a first processing stage, the data collected from both surveying methods were merged to achieve a unique and richer virtual representation of the bridge (Figure 3.11). As the point clouds were already registered and georeferenced, it was not necessary to align them before merging them properly. Then a post-processing cleaning process was performed to deliver a clean data for the modeling phase. Initially, an automatic off-ground segmentation was performed by applying a Cloth Simulation Filter (CSF). This method is based on cloth simulation, where the original point cloud is firstly inverted, and then a rigid cloth is used to cover the inverted surface. By analyzing the interactions between the cloth nodes and the corresponding LiDAR points, the locations of the cloth nodes are determined to acquire an approximation of the ground surface. After that, by comparing the distance between original point cloud and the final shape of the simulated cloth, the point cloud can be classified to ground and non-ground points (Zhang et al., 2016). The parameters which need to be set by the user include the Scenes, Cloth resolution, Max iterations and Classification threshold. The first parameter helps users to set scenes type of the point cloud (e.g., steep slope, relief, or flat). The cloth resolution refers to the grid size of cloth which is used to cover the terrain. Max iterations refers to the maximum iteration times of terrain simulation (500 is enough for most of scenes). Lastly, classification threshold refers to a threshold to classify the point clouds into ground and non-ground parts based on the distances between points and the simulated terrain (0.5 is adapted to most of scenes). For the case study, this tool proved to be efficient because it was able to automatically reduce much of the vegetation present in the point cloud that was undesired for the BIM modeling. It was tried to respect the integrity of the structure in the data by choosing the parameters that lead to a removal of a certain layer of vegetation without reaching the level of the points belonging to the bridge. Therefore, it was settled: steep slope scene, cloth resolution 2.0, maximum iterations 500 and classification threshold 0.2. Finally, to remove the remaining ground vegetation, a manual segmentation of the ground was performed.

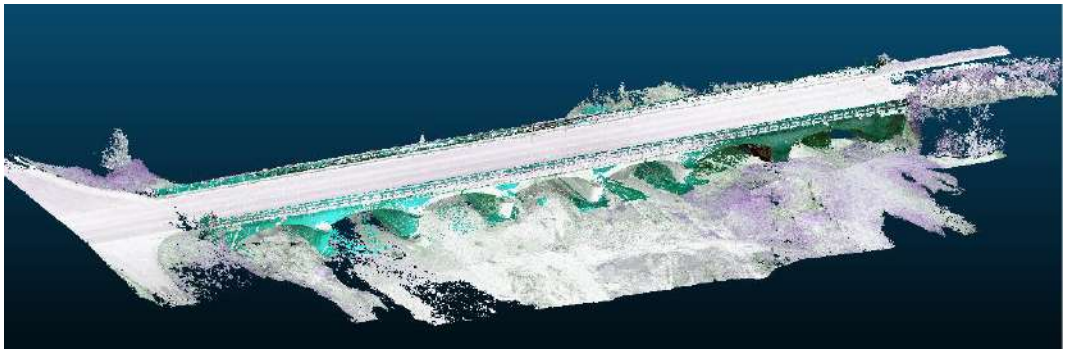

Figure 3.11: Aligned and merged point clouds. Font: Autor.

Often, it can happen that the data density may be more than necessary for a given application, which leads to higher computational cost in subsequent data processing or visualization (Poux, 2020). In this instance, it is useful to decimate (sub-sample) the data, without reducing its quality, to improve computing time. Sub-sampling the data density is basically to make dense point clouds become more manageable for further BIM modeling. The typical sub-sampling methods for point cloud data thinning are the random, the spatial and the octree. The random method is the simplest for reducing data density, in which a specified number of data points is selected randomly. In the spatial method, the data point selection is constrained by a minimum distance so that no data point in the selected subset is closer to another data point than the minimum distance specified. In the octree method, a grid structure is created with the definition of a certain subdivision level (the higher the level is, the smaller the cells are, so the more points will be kept), and a representative data point is selected. The latter two methods can achieve a more homogeneous spatial distribution of data points in the reduced point cloud. In such cases, the average data spacing is determined by the minimal distance or the voxel edge length specified. Taking it in mind, the point cloud was sub-sampled to facilitate the modeling process in Revit, since not doing this at first, the modeling process was very slow and crashed the computer sometimes. Thereby, different sub-sampled levels were tested, aiming to achieve the one that combined the best point cloud visualization quality with a reasonable computer performance. At the end, the data was subsampled using octree method with subdivision level 15, obtaining the post-processed point cloud with a total of 10627880 points, as illustrated in Figure 3.12.

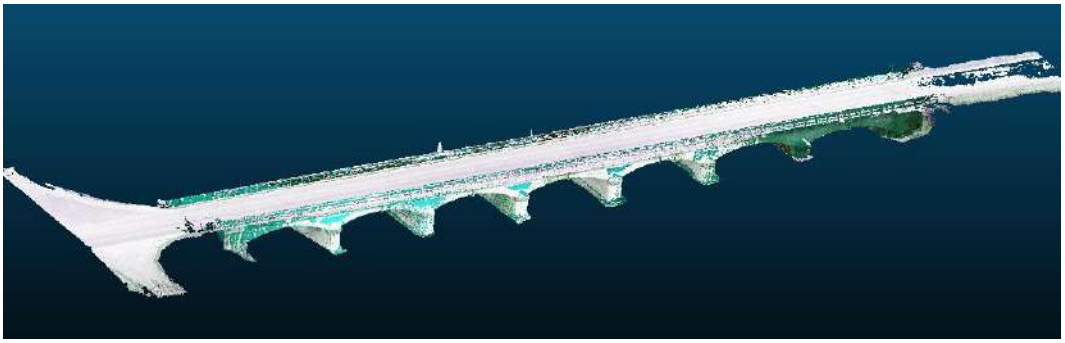

Figure 3.12: Post-processed point cloud. Font: Autor.

3.3 BIM Modeling

Being the case study an already existing construction, presenting architectural elements with lack of perpendicularity and signs of deterioration due to weathering or structural deformation, the BIM modeling process sought to stick to the creation of elements detailed enough to represent the as-built features of the bridge. For that, the acknowledgement of the aesthetics of this typology of bridge played a fundamental role for the modeling process. The masonry bridges have some common structural elements, varying in their constituent materials and executive details depending on the time of construction, the geographical area, and the designer. In this context, the shape of the arches may be semicircular, segmental, elliptical, or even pointed and might be of dressed stone voussoirs (wedge-shaped blocks), bricks or rough stone; the road may be level, sloping or humped; the spandrel walls may be filled with earth, stone, or concrete (or may also be hollow). Figure 3.13 illustrates the principal elements of masonry arch bridges.

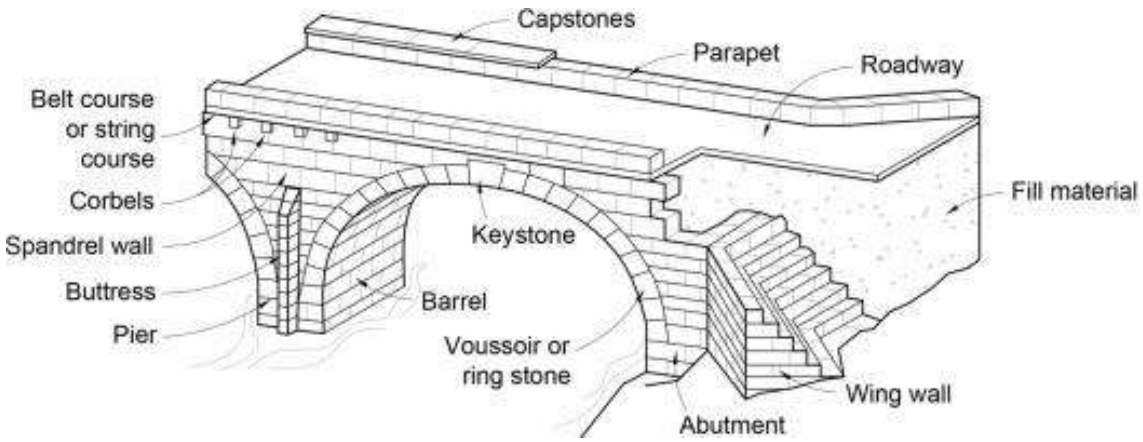

Figure 3.13: Principal elements of a masonry bridge. Font: (Pipinato, 2016)

Similar to the scanning and processing data phases, some steps need to be done before the modeling itself. In the present case study, the first one was to perform a pre-modeling phase, where the post-processed point cloud was used for automatic object recognition and extraction. By using ClearEdge3D, an as-built modeling platform offered by EdgeWise, walls were automatically extracted by advanced feature extraction algorithms and fitted to the point cloud precisely (see Figure 3.14). In Figure 3.15 it is possible to see the automatically extracted walls from the point cloud.

Figure 3.14: Visualization of automatic wall fitting. Font: Autor.

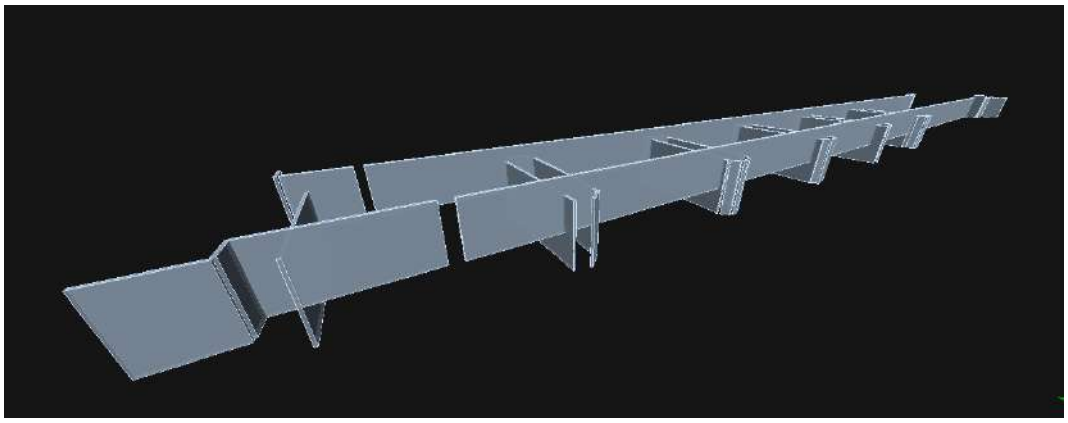

Figure 3.15: Automatic wall extraction from the point cloud. Font: Autor.

As the modeling platform was not able to extract all the existing walls of the real structure (evidenced by the presence of gaps in Figure 3.15) and the spandrel walls of the bridge are originally continuous along their depth, a manual improvement of the model was performed, which transformed the automatic extraction and modeling processes into semi-automatic ones. Semi-automated extraction tools (Figure 3.16) were applied to supplement the model generated from full automation by modifying previously extracted walls and levels and creating (extracting) new ones.

Figure 3.16: Building tools. Font: ClearEdge3D Support.

With Pick Level from Point tool, it is allowed to declare a new level at a point, while the Level Editor tool concedes to change the level names or “z” values by typing in new names or values, respectively. With Find Walls tool, EdgeWise reverts the walls to their original state. The Extract Wall tool is intended for semi-automated wall extraction and the Modify Wall to modify the walls length, or thickness. Said that, the walls were modified firstly in their thickness by extending them all over their depth, afterwards, new walls were extracted semi-automatically by selecting the region intended to recognize and extract the desired object. The same was done for the creation of new levels, e.g., by picking a point intended to declare a new a level. Finally, the walls were modified in their length, being limited accordingly to the predefined levels. The final 3D model, which is represented in Figure 3.17, was directed exported to Autodesk Revit for further BIM modeling as structural family objects, thanks to the Revit link provided by ClearEdge3D platform.

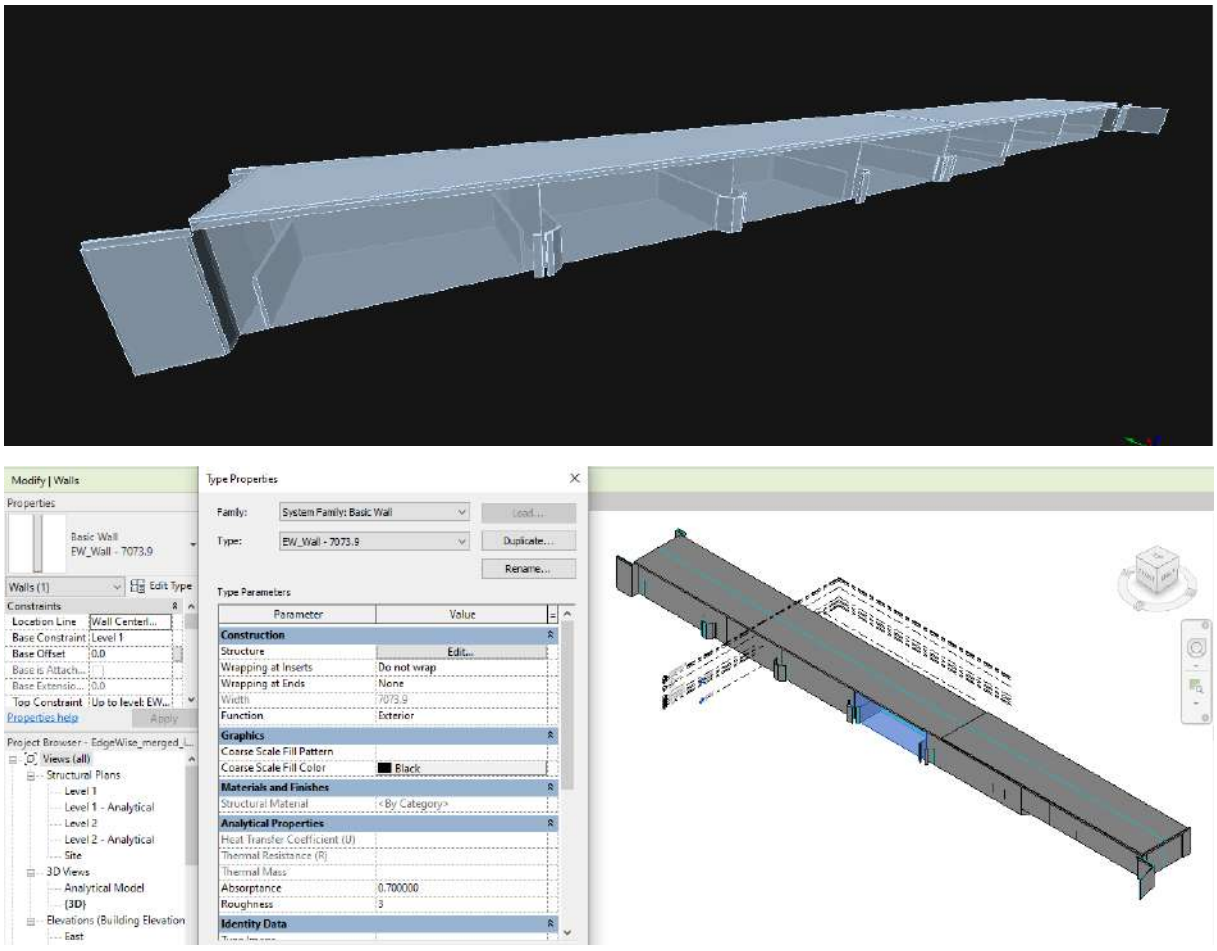

Figure 3.17: 3D model output from Edgewise. Font: Autor.

The second step was to link the 3D model output from EdgeWise and the point cloud to a new Revit project. Then, the point cloud was aligned to the model. After that, the profile of the walls belonging to the model were modified so that the model and the point cloud

matched geometrically and visually, obtaining the model illustrated in Figure 3.18, named in this paper as EdgeWise Model, just to facilitate the identification of the models by the lector during the reading.

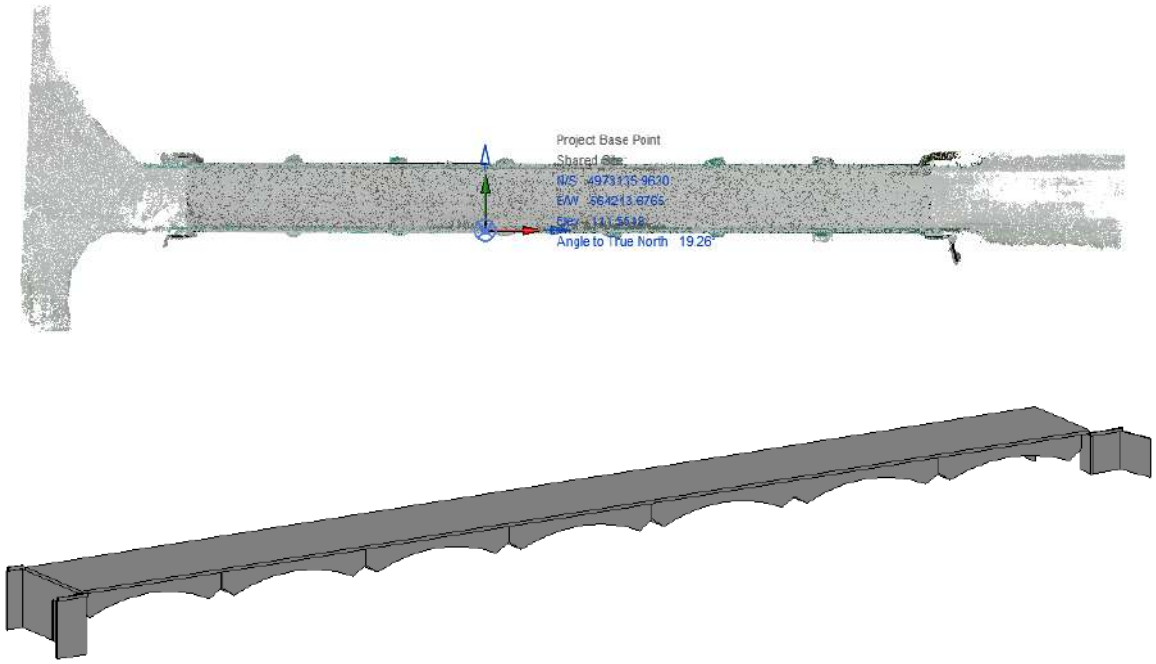

Figure 3.18: Pre-modeling phase. Font: Autor.

One time the pre-modelling step is concluded, the as-built modeling phase started. The point cloud and the EdgeWise Model remained linked to Revit throughout the overall modeling process, as guides for the BIM modeling. The reason why the EdgeWise Model was not directly used for the as-built modeling was because all elements semi-automatically extracted were defined by the Edgwise platform as structural walls, that is, all they belonged to the same object family. However, a real bridge has other types of structural elements, such as decks, abutments, piers, that is, elements from other object families, with different structural functionalities and geometries. Therefore, since the level of detail of the as-built BIM is associated with the attribution of geometric and non-geometric characteristics to the elements, it was sought to model different families for each type of structural element, assigning to each of them a family category and a structural classification. For example, piers and abutments were assigned as "Structural Columns", with the attribution of the "column slab frame" classification, spandrel walls were categorized as "Generic Models" along with "Masonry Structural walls" classification, concrete decks were also categorized as " Generic Models" but with the classification "Concrete Structural Floor Decks", and finally, the wing wall was kept with the structural wall properties of the EdgeWise Model.

Proceeding with the as-built modeling process, six new levels (dashed lines in Figure 3.19) of the building were created to help in the correct insertion of the building elements. In the same figure, the levels of the EdgeWise Model are represented by the continuous lines.

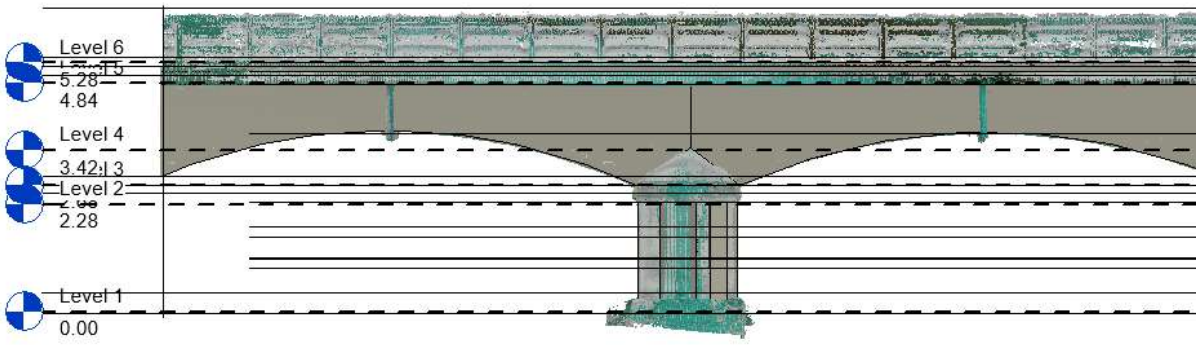

Figure 3.19: Creation of new levels. Font: Autor.

The approach adopted for modeling was to reconstruct the geometry of the building through the creation of parametrized families for the essential elements such as piers, spandrel walls, abutments, and decks, with the definition of which dimensions inside them would be necessary to be parameterized. The wing wall was automatically extracted by the EdgeWise and maintained as structural wall, while the foundations were not modelled since they are submerged, crossing the waterway, and are not visible in the point cloud data. The creation of parametric families is an integral part of working in Revit and the key to creating custom content and build with flexibility. Since, generally, these families are parametric elements, they can be adapted to different project needs, thus enhancing productivity of the BIM process (Baik, 2017). However, there is a deficiency of libraries that meet the requirements of HBIM projects, resulting in the need for the creation of new families by the combination of Boolean operations and operations like extrusion, blending, revolving, and sweeping. At the same time, creating custom families can be time-consuming, complex, and highly parameterized elements can often make the modeling as laborious as that of a complete building. Thereby it is necessary to understand the scope of the BIM modeling for developing an efficient and time-effective approach to achieve the desired project objective.

Having this in mind, for the creation of the object families, measurements of the geometry of the bridge were taken initially from the EdgeWise Model. Then, new measurements were taken from the point cloud since the bridge is also composed by curved shapes and EdgeWise platform is not able to extract curved walls. Finally, having defined the geometries of the bridge components, the families were customized with the definition of the parameters to be shared by each object family, as described in sequence. It is important to emphasize that the non-uniformity of geometry and imperfections of some bridge elements, which are present in the real structure, were not considered during the BIM modeling, since that the aim of this study was exactly to access the consistency of the applied workflow in representing the actual conditions of existing structure.

- **Piers**

In total, six types of piers were created, sharing the following parameters (see Figure 3.20):

— Material and finishes: masonry (brick, Norman) and concrete C50/60
— Dimensions:
  - Pier cap: Top height (h), Top radius (R),
  - Ring: height (H), radius (rr), height above (hsup) with and below (hinf) the half height of the ring (H).
  - Column: height (H), length (L), radius (R)

a)

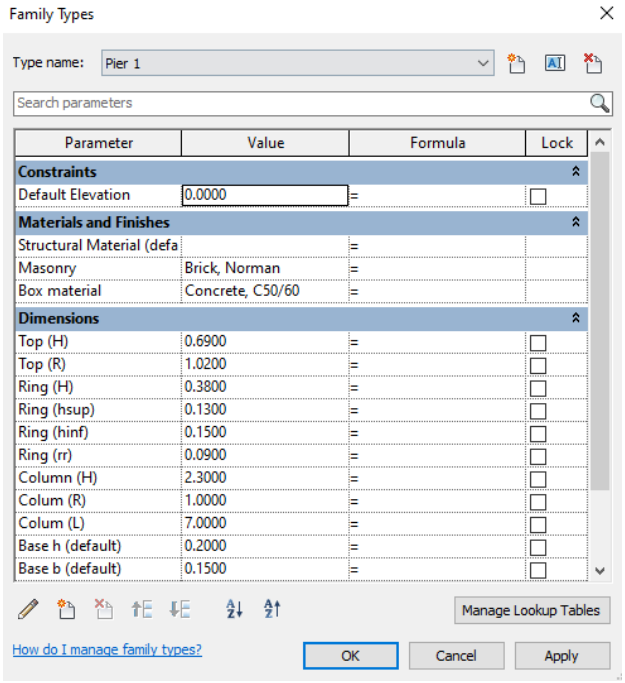

b)

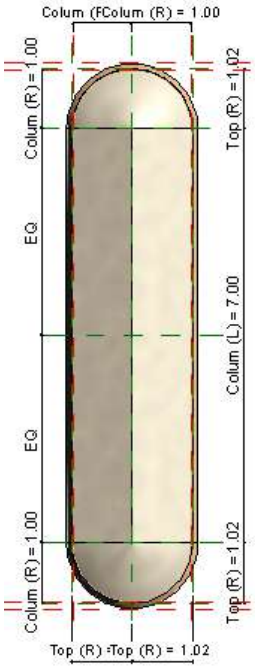

c)

d)

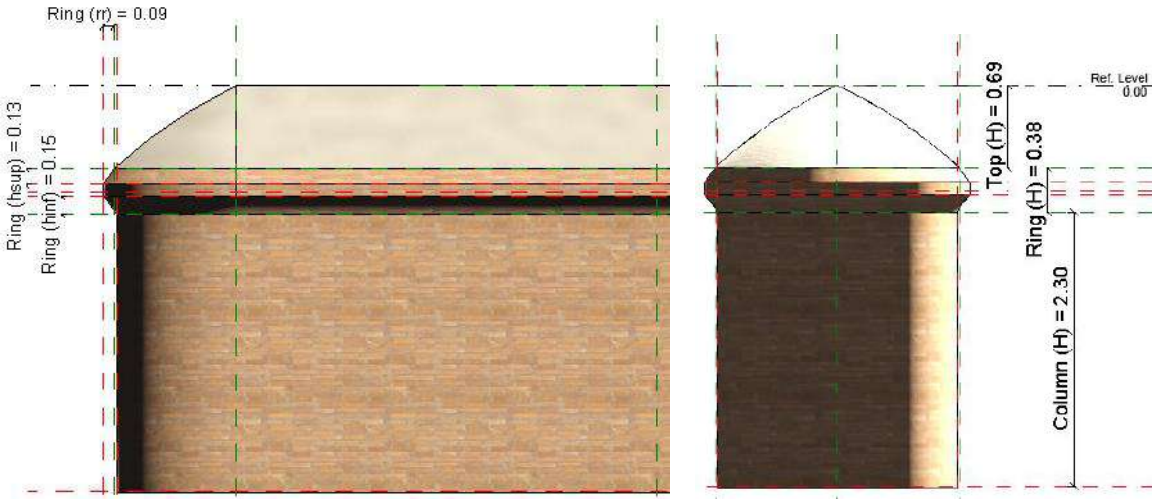

Figure 3.20: Family of central piers and its parameters. Font: Autor.

For the piers attached to the abutments, another family was created, having the same characteristics as for the central piers, but with only half of the column geometry, as can be seen in Figure 3.21 below.

a)

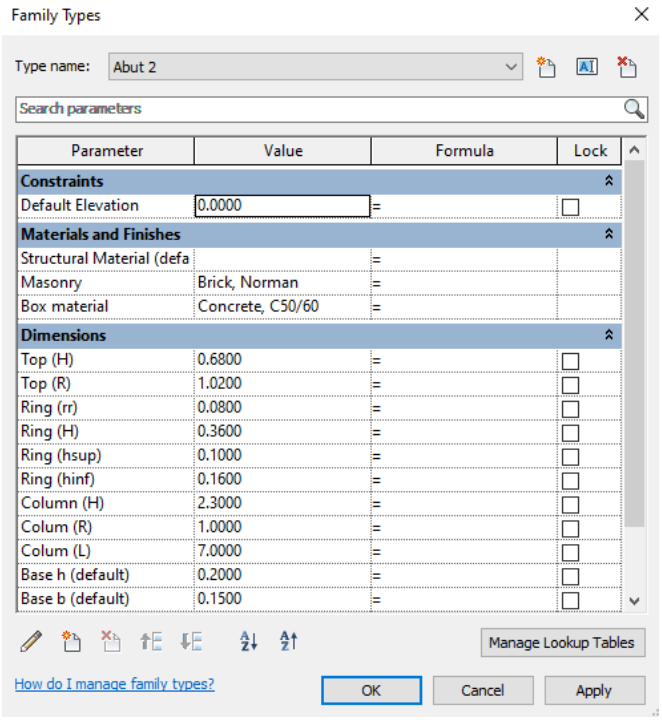

b)

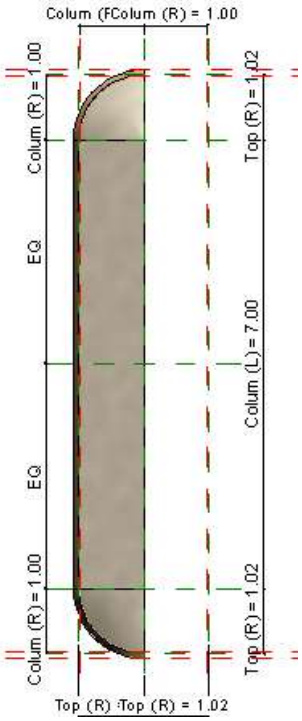

Figure 3.21: Family of piers and its parameters. Font: Autor.

- **Abutments**

For the abutments, only one family type was created, having the following parameters (see Figure 3.22):

— Material and finishes: masonry (brick, Norman) and concrete C50/60
— Dimensions:
  - Column height (H)
  - Abutment cap: top height (h), width (W), length (L), offset (b).

a)

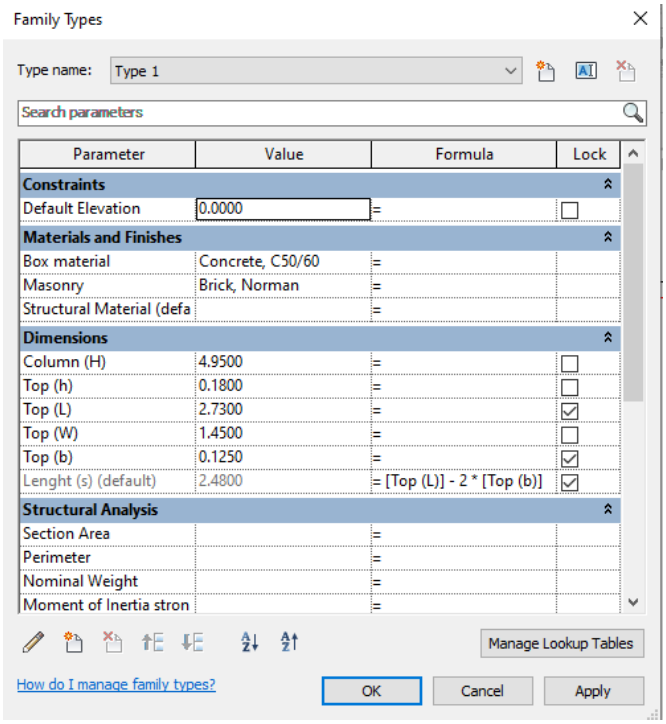

b)

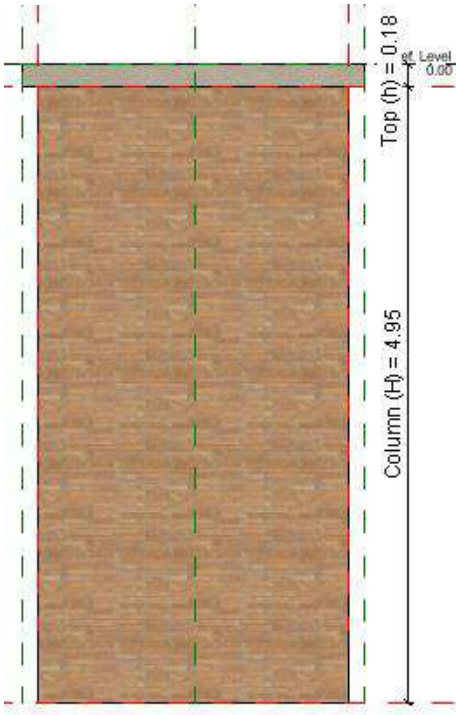

c)

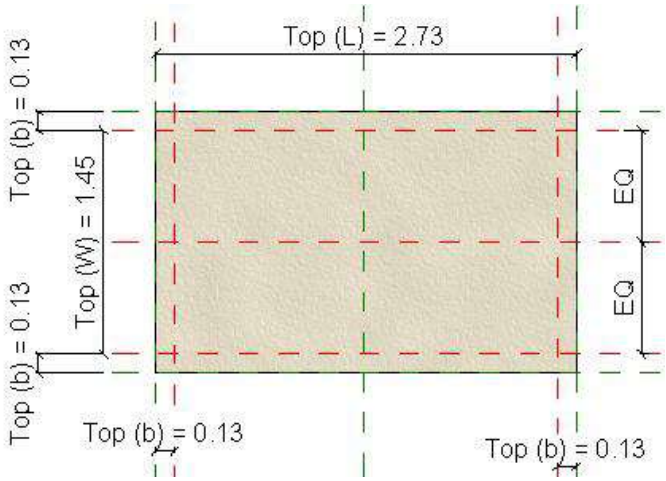

Figure 3.22: Family of abutments and its parameters. Font: Autor.

- **Spandrel walls**

In total, seven types of walls were created, and they group the following parameters (see Figure 3.23):

— Material and finishes: arches with voussoirs in mansory (brick, Norman) and filling material (Concrete, C50/60)
— Dimensions:
  - Deck span, deck width
  - Spandrel height (H)
  - Arch – span (S), rise (h), skewback (h), skewback angles (left and right)

a)

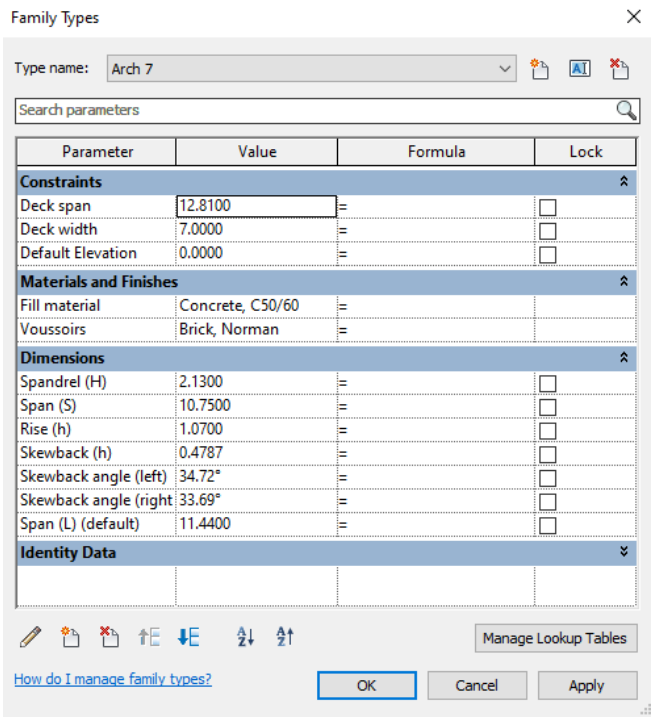

b)

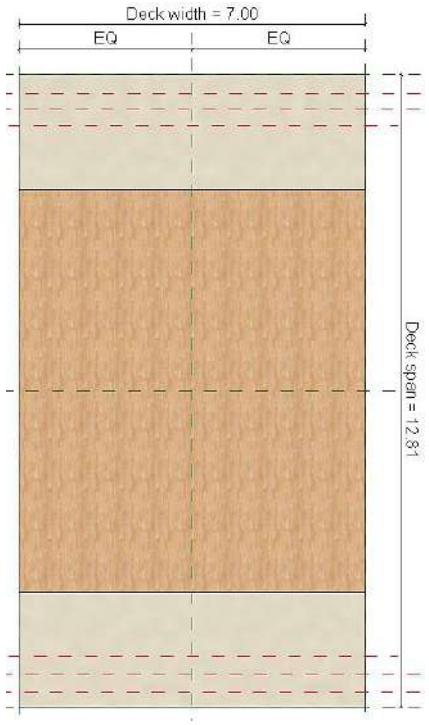

c)

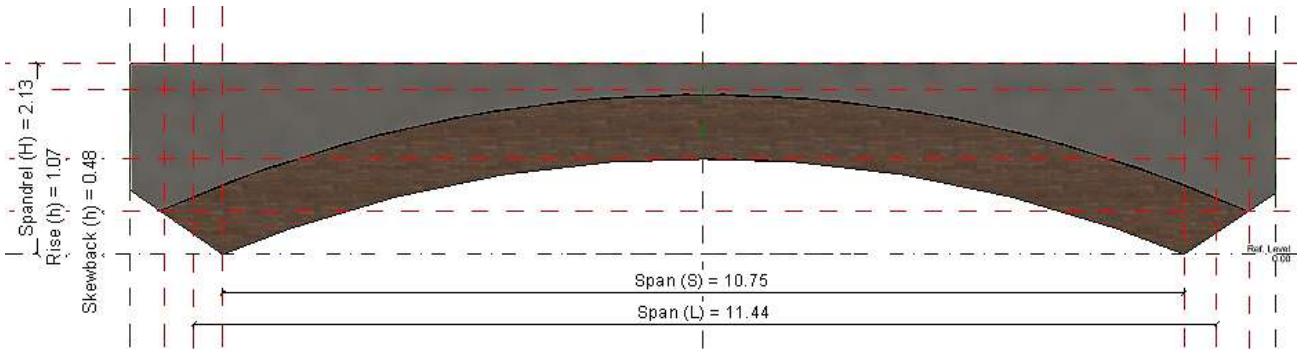

Figure 3.23: Family of arches and its parameters. Font: Autor.

- **Decks**

In total, nine types of decks were created, and they group the following parameters (see Figure 3.24):

— Material and finishes: concrete C50/60
— Dimensions:
  - Deck: span (S), width (W), thickness (t)
  - Guardrail: base “bottom” (bb), base “top” (bt), height (h)

a)

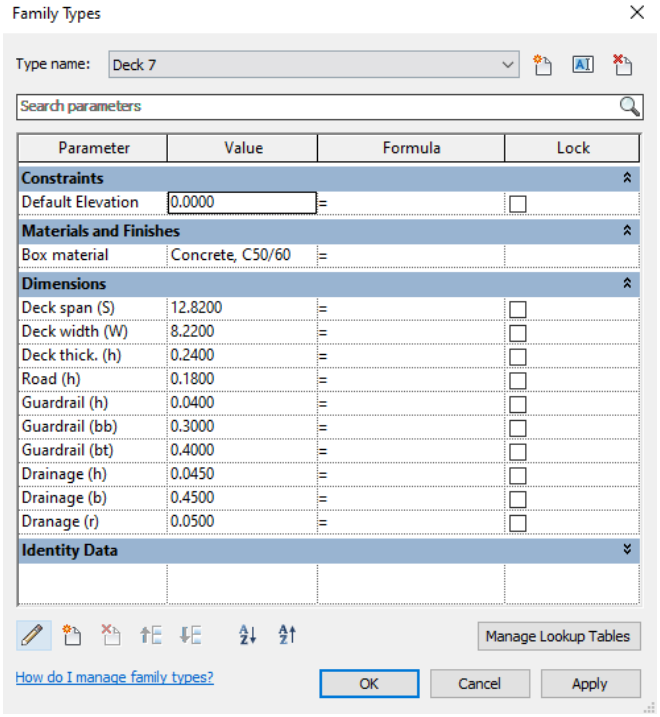

b)

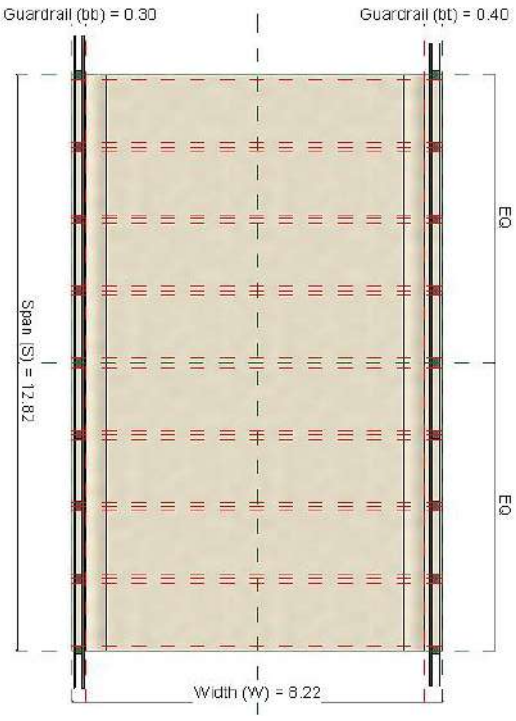

c)

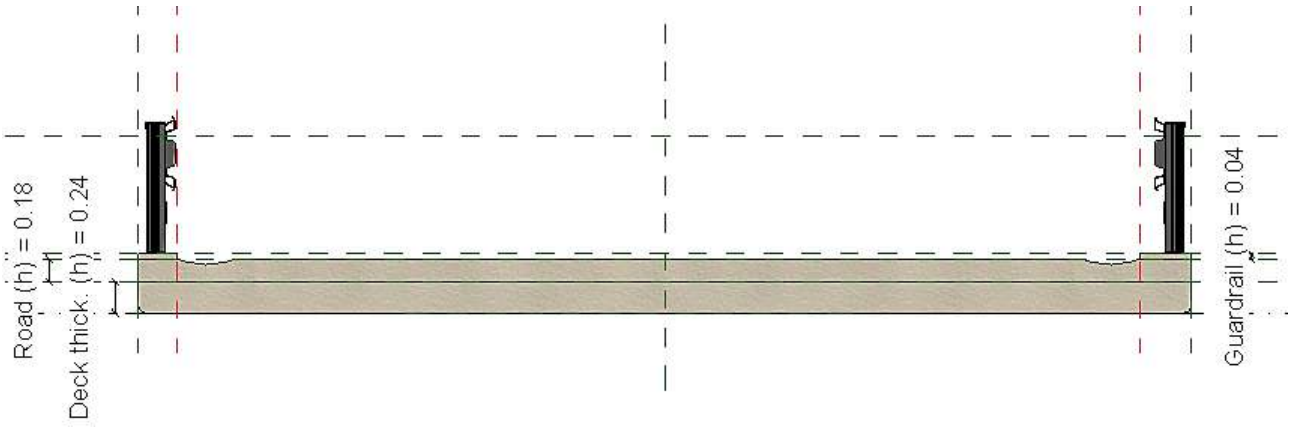

Figure 3.24: Family of decks and its parameters. Font: Autor.

The final model is illustrated in Figure 3.25. In Figure 3.26 is also possible to see the presence of the two links in Revit, the point cloud data and EdgeWise Model, and the modelled pier family.

a)

b)

Figure 3.25: a) BIM model and point cloud data representation; b) only BIM model representation. Font: Autor.

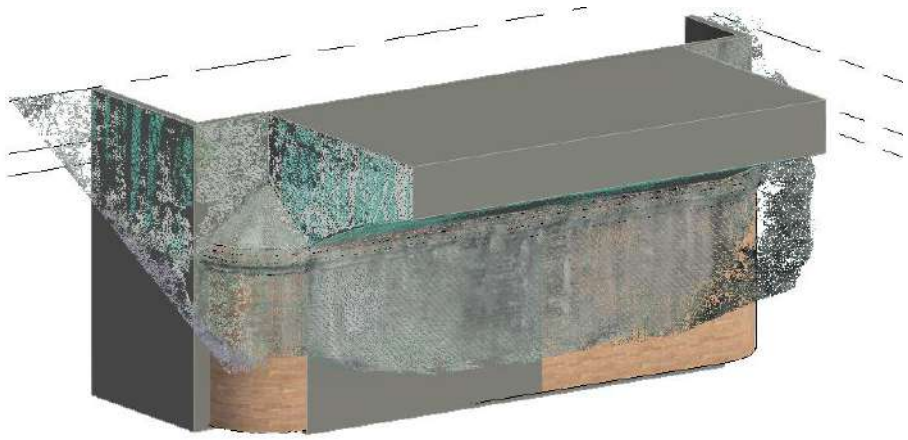

Figure 3.26: Point cloud data, EdgeWise Model, and the parametrized family modelled in Revit. Font: Autor.

4 Deviation Analysis

As discussed in previous sections, reality capture surveying techniques allied to the as-built BIM methodology have been proven to be a powerful combination in the scope of civil engineering, serving as a knowledge base for supporting decision-making and problem-solving issues in the field. In supporting such applications, thereby, it is essential to perform prompt, detailed, and comprehensive quality assessments of the scanned data and as-built BIM models before using them for making decisions about facilities. A detailed and comprehensive quality information about the data and the as-built models allows the better use of the data and models, reduces the project delays and improve the proactivity of the decision making, as pointed out by (Tang et al., 2011).

The Quality Assessment (QA) process in the scan-to-BIM workflow is based on two major requirements. First, engineers must be able to identify in the BIM model the different types of quality issues occurred during the workflow so that they can make conscious decisions to solve the existing errors. Then, engineers need to quantify the magnitudes of these deviations or errors and understand their implications to the domain applications. In the 3D imaging projects as the present study case, QA information can be derived by analyzing the patterns in the deviations between the point cloud data and the as-built model. Basically, the deviation analysis method consists in computing the deviations and then visualizing them. In a first step, the algorithm computes the deviations of data points from the surfaces of the model. This can be done through different ways, being the minimum Euclidian distance from each point to its nearest surface in the BIM the most commonly used (Tang et al., 2011). Other methods include the computation of point-surface distances along user-specified directions or the direction of the surface normal. The visualization of the deviation patterns can configure color maps, like continuous color map or binary color map. In the former, the user can configure it as unsigned (deviations of the same absolute values have the same color) or signed (positive and negative deviations with different colors). In addition, the user is able to define the scale of the color map by controlling the maximum and minimum deviation values visualized or by setting the threshold value for the binary color map to only distinguish deviations larger and smaller than that threshold. Other QA methods for as-built BIM project include simple visual inspection, clash detection, and the physical measurement method (Tang et al., 2013). With the physical measurement technique, virtual measurements are made on the BIM model and are compared with the corresponding physical measurements made on the real structure. The compared values can be then statistically analyzed to obtain a confidence value for achieving a given accuracy requirement.” (Anil et al., 2013). However, this quality assurance method goes totally against the scan-to-BIM philosophy, because it is a time-consuming process, requiring the acquisition of large number of physical measurements. Additionally, it is difficult to achieve highly accurate data with contact-based measuring methods, and sometimes some measurements cannot be taken due to accessibility limitations. Basically, scanning means that the working team should not go back to the site to redo the survey, so the scan plan should be strategically decided in order to guarantee the best data coverage and quality. With clash detection, spatial interferences between objects are detected by comparing the locations between components in the model and declaring a clash if they are closer than a given threshold or are occupying the same space. The application of this method is essential to recognize and report conflicts that occur in BIM, reducing in this way errors in the project, especially when

several models are integrated into one main BIM model. A negative point of using this method is that, in a QA procedure, we are more interested in determining amounts of deviations than defining the conflicting components.

For the case study, a face deviation analysis was performed using Autodesk Point Layout Add-in for Revit. The tool, in addition to support the interoperability of the workflow (as it is a tool of the BIM platform), provides ease of use and interpretation, through the visualization of heatmaps with signed colors that describes how much deviation the various faces of the BIM model have with respect to the point cloud data. The selection of the threshold depends on several factors, such as scene complexity, accuracy requirements of the project and the type of deviation pattern to be analyzed (e.g., data quality, registration error and modeling error). In this instance, (Anil et al., 2013) explain that smaller thresholds are more effective for visualizing detailed deviations, such as local geometrical errors. Even though the definition of the modeling accuracy and level of detail for as-built HBIM model is still an open question, the maximum point distance from face settled for the case study was 50 mm and the desired average distance between adjacent cloud point was 0.1 mm (see Figure 4.1). The deviation analysis was performed individually for each structural family.

This section focuses on the evaluation of the proposed deviation analysis method on satisfying QA requirements without detailing data processing steps and the definitions of all error types. To facilitate the discussion, a schematic representation of the modelled BIM components is provided in Figure 4.2. This section does not address deviation results for all bridge elements, presenting only the most evident deviation patterns of the case study. A more detailed presentation of the deviation results is provided in the Annex section.

a)

b)

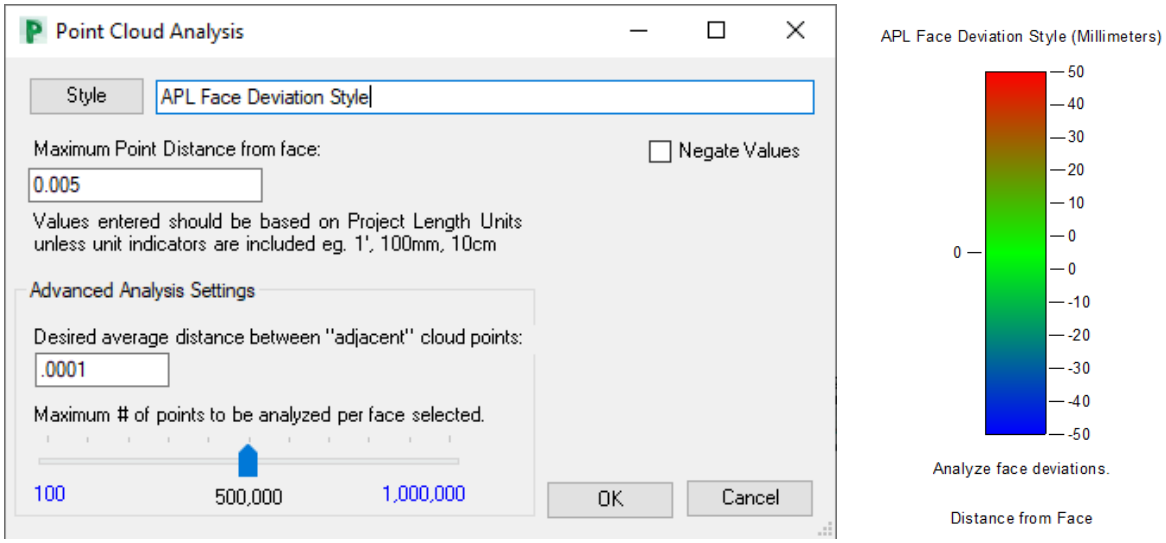

Figure 4.1:a) Inputs for the deviation analysis; b) APL Face deviation style. Font: Autor.

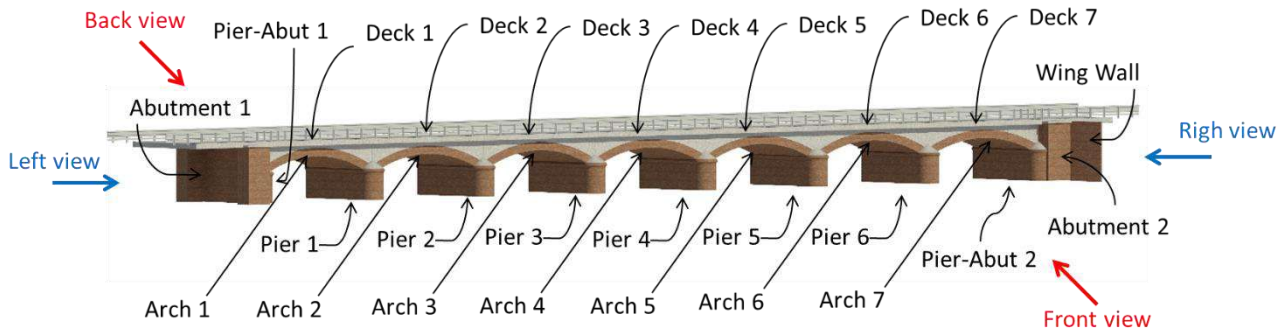

Figure 4.2: Schematic representation of the bridge elements.

Based on visual inspection of the results detailed in Annex A1, section dedicated to presentation of the deviation results of the piers, the deviation patterns observed indicated in great part the presence of vegetation and material degradation, as has already been seen through the photographic images. In Figure 4.3, for instance, it is possible to see some of these patterns, being evidenced by the dashed rectangle icons with different colors. The region limited by the white lines indicated a modeling error of the pier since a major part of the points belonging to this region are almost equally far from the model surface. This error occurred because the structural elements were analyzed individually, therefore, the region that was originally filled with the arch contact was identified as a "free" surface by the QA, that is, the pier and the arch were not in contact. Actually, they were. The region limited by the blue lines may indicated a modeling error, generated by a wrong definition of the curvature of the pier cap, or/and the deterioration of this element. The region limited by the yellow lines, in turn, clearly support the poor conditions of the material in that region since the surface of the model presented very concentrated deviations. Finally, the region limited by the red lines, clearly state the invasion of the soil and vegetation in that region.

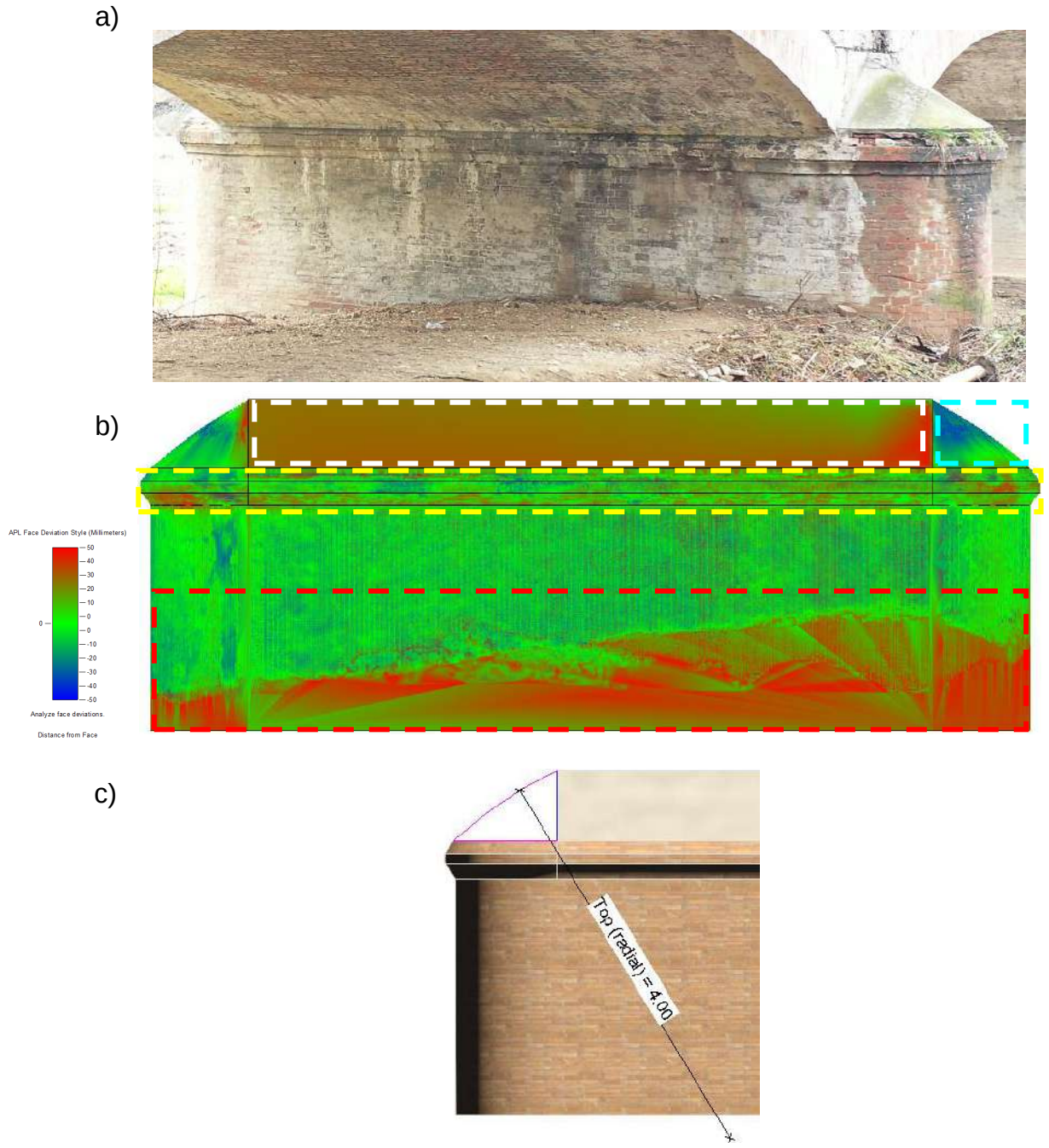

Figure 4.3: a) Right view of the Pier 5; b) deviation patterns; c) curvature of the pier cap. Font: Autor.

For Piers 3 and 4, instead, a different deviation pattern was observed, which indicates that the source of error for these components was different from those mentioned above. As can be seen in Figure 4.4, the red line indicates a certain structural unevenness, which was captured by the QA method (Figures 4.5 and 4.6). The unevenness, which was captured by the scans and successfully pointed out by the deviation analysis support the potential of the scan-to-BIM workflow for achieving detailed, qualitative, and quantitative assessment of the investigated construction. Once this paper is focused only on the qualitative assessment of the information about the data and the as-built model, it is necessary to carry out further

studies to quantify the magnitudes of these deviations and understand their implications in the domain of structural monitoring and documentation.

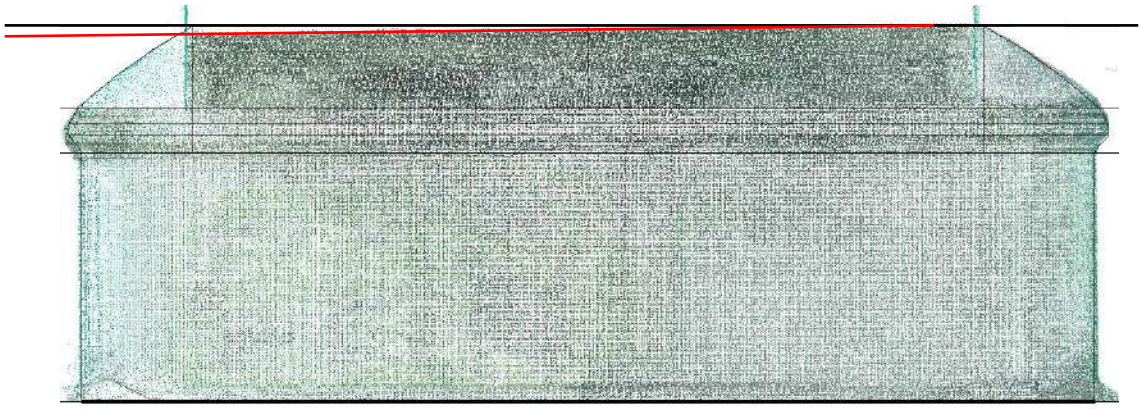

Figure 4.4: Pier 3 - Lateral view of the point cloud. Font: Autor.

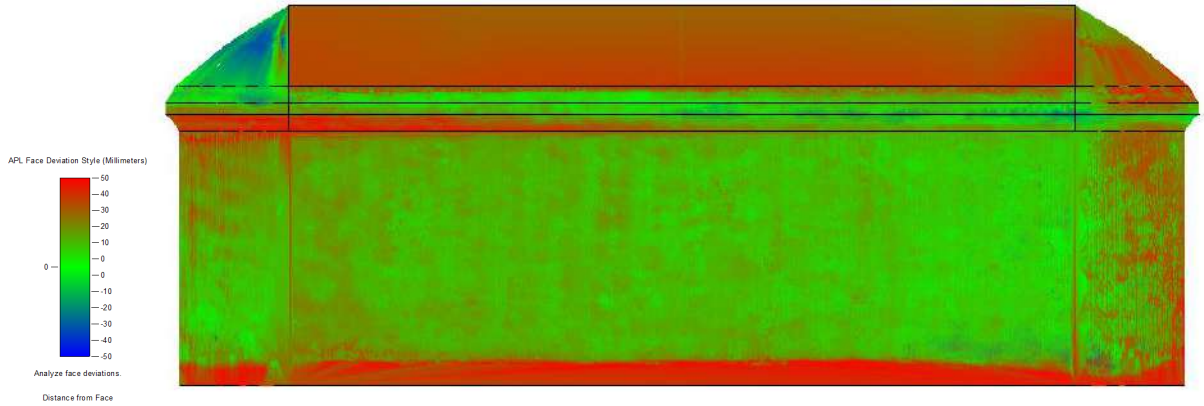

Figure 4.5: Pier 3 - Lateral view of the deviation results. Font: Autor.

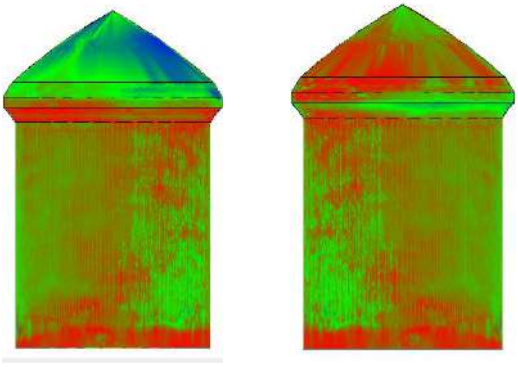

Figure 4.6: Pier 3 - Front and back view of the deviation results. Font: Autor.

In terms of curiosity, among the different types of bridges, masonry arch bridges are particularly vulnerable to the problem of scour and scour-induced settlements, due to their high stiffness and the fact that they are often built on shallow footings resting on the riverbed (Scozzese et al., 2019), as in the present case of study. Scour is an erosional process due to the interaction between any type of structure located underwater and the river flow, compromising the integrity of the structure (Pizarro et al., 2020). As explained by (Prendergast et al., 2014) and illustrated in Figure 4.7, the removal of material under (or around) the foundation during scour causes increased stress and consequently reduced stiffness in the remaining soil. Scour is by far the leading cause of bridge failure worldwide, resulting in significant direct and indirect losses (disruption to road networks in terms of transportation operation, losses of cultural heritage.

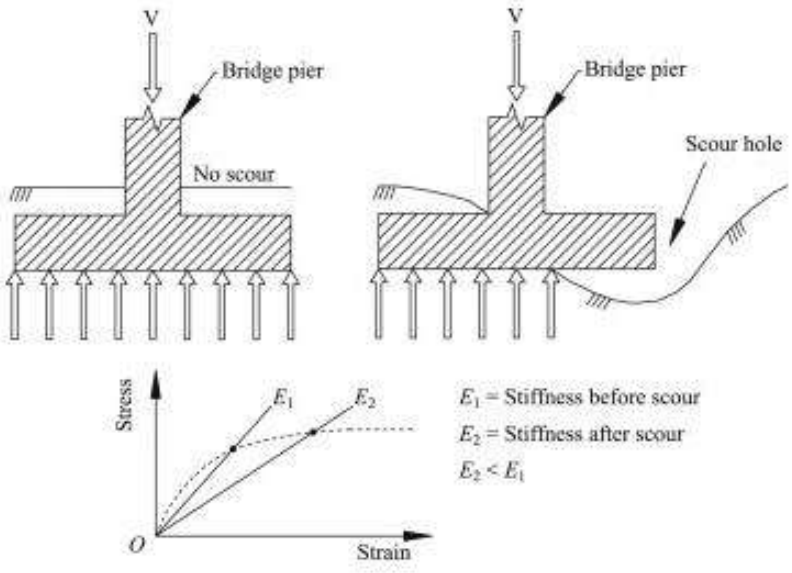

Figure 4.7: Reduction in stiffness caused by scour. Font: (Prendergast et al., 2014).

In the case of the abutments, the deviation patterns presented in the QA are various, including the invasion of vegetation in the structure (red dashed rectangles in Figure 4.8), the deterioration of the masonry (yellow dashed rectangles in Figure 4.8), regions with the superposition of objects (white dashed rectangles in Figure 4.9, where the bridge deck is supported by the abutment), and quality issues related to the data (pink dashed rectangle in Figure 4.8). The latter is better visualized in Figure 4.10 a), where is possible to see some irregularities in the region corresponding to the pink dashed line. In the specific case of the wing wall, the deviation pattern indicated by the blue dashed rectangle in Figure 4.8 addresses the incorrect modeling of the shape of the wall, being the correct geometric representation visible in the data (Figure 4.10 b). Deviation results for all abutments are detailed in Annex A2.

a) b)

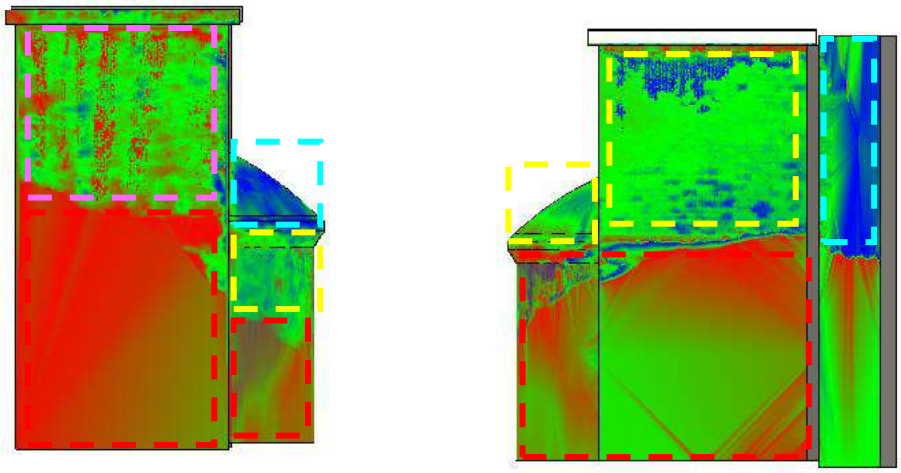

Figure 4.8: Front view of the a) Abutment 1; b) Abutment 2. Font: Autor.

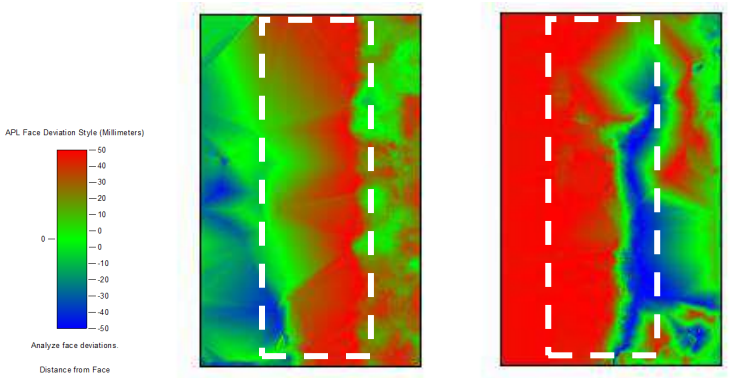

Figure 4.9: Top view of the Abutment 2.

a) b)

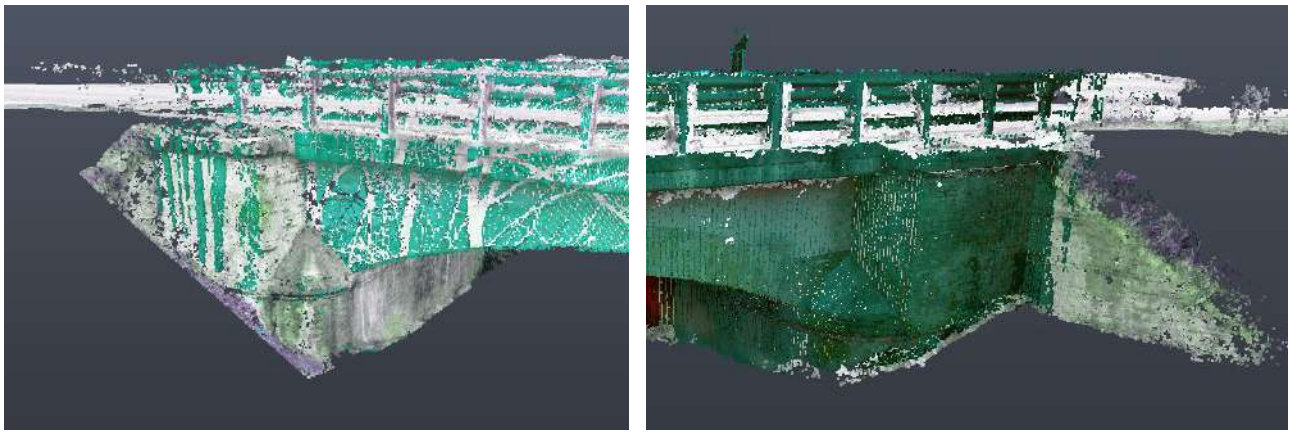

Figure 4.10: a) Data quality issue; b) modeling quality issue. Font: Autor.

The spandrel walls did not present very high deviations values, in general, presenting only concentrated deviations in their façade due to the deterioration of the structure (Figure 4.11a, and deviations distributed over larger regions at its base (Figure 4.11b) which would indicate a possible error committed during the modelling of the arches. Also, in the case of the object Arch 4, data quality issues were identified and outlined by the pink dashed rectangle in Figure 4.11b. As explained earlier, the data presented some occlusions in the bottom of the arches (see Figure 4.12 b), which were successfully captured by the QA method. Deviation results for all spandrel walls are detailed in Annex A3.

a)

b)

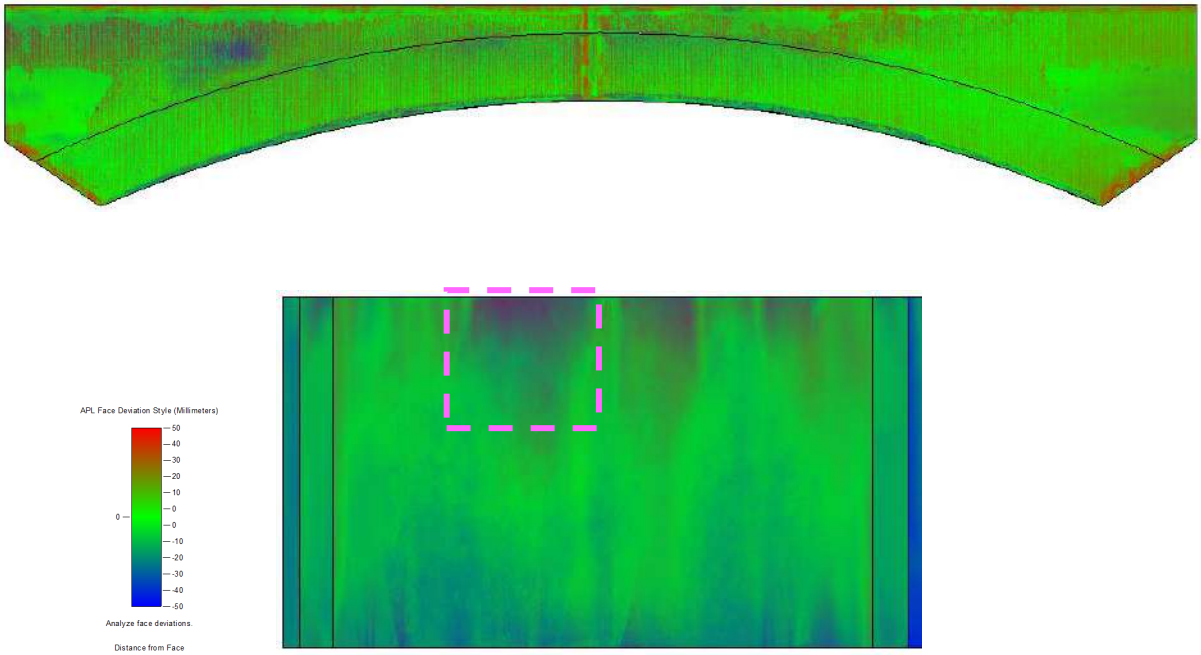

Figure 4.11: Arch 4. a) Back view; b) bottom view.

To finish the analysis, Figure 4.13 presents the poor conditions of the widening decks. The negative deviation patterns (in blue color) in the third, fourth and fifth decks could be generated by the structural unevenness of the 3rd and 4th central piers. The red points, associated to the positive deviation pattern, could be explained by the wear of the asphalt layer of the road deck. Deviation results for all concrete decks are detailed in Annex A4.

a)

b)

Figure 4.12: a) Back view of Arch 4; b) data quality issue. Font: Autor.

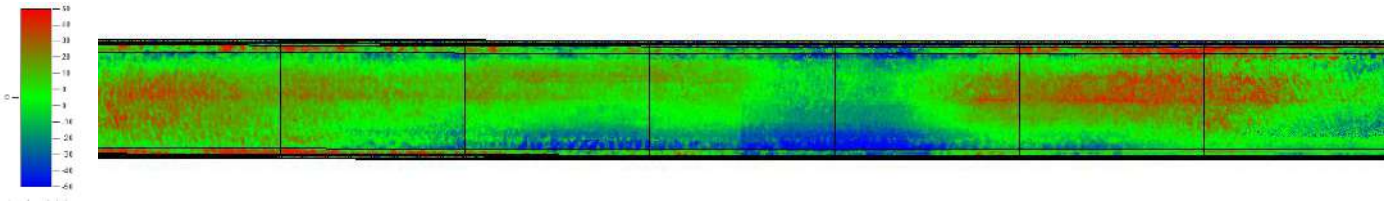

Figure 4.13: Deviation results of the decks. Font: Autor.

5 Final Considerations

Scan-to-BIM workflow has been proven to be an indispensable tool for the creation of as-built models of buildings and infrastructures. By incorporating high-quality digital survey datasets provided by laser scanning and photogrammetry, qualitative and quantitative information about the facility can be integrated into the as-built model in a structured and consistent way, recording in detail the state of the building. The major benefit of 3D imaging systems is the ability to capture existing conditions more completely with a higher level of detail than most manual methods, especially in the cases of complex geometries and inaccessible areas, reducing in this way errors and reworks on site. Additionally, the scan-to-BIM workflow could benefit significantly from automation with the incorporation of point cloud extraction technologies. The segmentation and recognition of point clouds currently represent the fundamental steps for identifying the correct surfaces and facilitating the tracing or the modeling of parametric objects but depending on the typology of the building and the level of complexity of the work, this task can be very challenging, as in the case of heritage buildings.

Although scan-to-BIM processes applied for historic buildings is a relatively new field of academic research, it has already proven to be very effective in providing new tools for the sector to support activities such as building retrofitting, historic asset management, preventive maintenance, and documentation. However, to support this domain of applications, it is essential to perform a prompt, detailed, and comprehensive quality assessments of the scanned data and as-built BIM models before using them for making decisions about facilities. The quality assurance approach plays a fundamental role in the quality assessment process of HBIMs, once that the LOD definition in the context of heritage buildings is complicated, being commonly dedicated to new buildings. Theoretically, the quality assessment approach should allow engineers to identify, classify and quantify different types of quality issues committed during the workflow, understanding their implications in the domain of its applications.

For this study, an as-built BIM model was developed based on a point cloud generated by the combination of laser scanning and photogrammetry survey techniques. The aim of the work was to analyze the consistency of the applied workflow in representing the real conditions of the scanned structure by means of a qualitative comparison between the generated as-built model and the point cloud data. The case study began with a brief characterization of the real state of the structure, followed by the presentation of the point clouds obtained by a terrestrial laser scanner and a drone, which were processed (merged and registered in a unique point cloud) in such a way that the final data could be used for the creation of the 3D BIM model. To further automate the modeling process, the proposed workflow accounted with an object recognition tool, acting as a pre-modeling phase which resulted in time saving and increased efficiency of design intent. Once the 3D parametric model was concluded, a deviation analysis between the point cloud data and the surfaces of BIM model was carried out. Then, the results of the deviation analysis were visualized and analyzed, and the consistency of the applied scan-to-BIM workflow was tested by comparing the deviations patterns in the generated as-built model with the real conditions of existing structure. They included the deterioration of the materials belonging to all elements analyzed, some quality data issues present in the spandrel walls and abutments, modeling issues

related to the creation of the piers, abutments, and wing wall, the invasion of soil and vegetation in elements such as piers and abutments, and, lastly, the wear of the asphalt layer of the road deck. However, other usual sources of errors involved in scan-to-BIM workflow include the incorrect calibration of the scanner, incorrect noise removals and data registration errors (Anil et al., 2013). Once this paper focused only on the qualitative assessment of the quality issues related to the data and the as-built model, it is necessary to carry out further studies to quantify the magnitudes of the deviations observed. By quantifying these magnitudes, engineers will be able to better understand the impacts of these deviations and precisely access the preservation conditions of the as-built structure analyzed.

Finally, it is important to emphasize that the scan-to-BIM workflows offer a considerable list of challenges to be faced for its properly application. Issues like operator expertise in all stages of the process, environmental conditions for scanning, high costs associated to the instruments and software for processing and modeling data (it will depend on the application and level of accuracy required for the project), and the interoperability between different platforms and file formats make the accessibility to this methodology more difficult. However, thanks to the correct choice of the tools that use point cloud data and BIM technology, the proposed scan-to-BIM workflow was successfully applied to the case study, being able to represent the real conditions of the existing structure, in its totally, and identify different quality issues committed during the process.

References

Ahmad Fuad Bin Che Ku Abdullah, C. K., & Ku Muhammad Umar, C. (2016). Application of Terrestrial Laser Scanner for Three Dimensional As-Built Building Model. 3. Available online: http://eprints.utm.my/id/eprint/78541/1/CheKuAhmadFuadMFGHT2017.pdf (accessed on 02 July 2021).

Angulo-Fornos, R., & Castellano-Román, M. (2020). HBIM as Support of Preventive Conservation Actions in Heritage Architecture. Experience of the Renaissance Quadrant Façade of the Cathedral of Seville. Applied Sciences (Switzerland), 10(7). Available online: https://doi.org/10.3390/app10072428 (accessed on 01 July 2021).

Anil, E. B., Tang, P., Akinci, B., & Huber, D. (2013). Deviation analysis method for the assessment of the quality of the as-is Building Information Models generated from point cloud data. Automation in Construction, 35, 507–516. Available online: https://doi.org/10.1016/j.autcon.2013.06.003 (accessed on 04 July 2021).

ArcMap. (2019). Fundamentals about lidar. What is lidar data?. Available online: https://desktop.arcgis.com/en/arcmap/10.3/manage-data/las-dataset/what-is-lidar-data-.htm (accessed on 15 October 2020)

Autodesk. (2018). Revit IFC manual. 1–52. Available online: https://damassets.autodesk.net/content/dam/autodesk/draftr/2528/180213_IFC_Handbuch.pdf (accessed on 01 July 2021)

Baik, A. (2017). From point cloud to Jeddah Heritage BIM Nasif Historical House – case study. Digital Applications in Archaeology and Cultural Heritage, 4(January 2016), 1–18. Available online: https://doi.org/10.1016/j.daach.2017.02.001 (accessed on 04 July 2021)

BIMForum. (2019). Level of Development (LOD) Specification Part I & Commentary. Bim-Bep, April, 254. Available online: https://bimforum.org/lod/ (accessed on 02 July 2021).

buildingSMART. (n.d). openBIM. Available online: https://www.buildingsmart.org/about/openbim/ (accessed on 06 July 2021).

Böhm, J., S. Becker, & N. Haala. 2007. “Model Refinement by Integrated Processing of Laser Scanning and Photogrammetry.” International Archives of the Photogrammetry, Remote Sensing and Spatial Information Sciences - ISPRS Archives 36(5W47). Available online: https://www.researchgate.net/publication/37685996_Model_Refinement_by_Integrated_Processing_of_Laser_Scanning_and_Photogrammetry (accessed on 02 July 2021).

Breithaupt, B. H., Matthews, N. A., & Noble, T. A. (2004). An Integrated Approach to Three-Dimensional Data Collection at Dinosaur Tracksites in the Rocky Mountain West. Ichnos, 11(1–2), 11–26. Available online: https://doi.org/10.1080/10420940490442296 (accessed on 02 July 2021).

Brumana, R., Georgopoulos, A., Oreni, D., Raimondi, A., & Bregianni, A. (2013). HBIM for Documentation, Dissemination and Management of Built Heritage. The Case Study of St. Maria in Scaria d’Intelvi. International Journal of Heritage in the Digital Era, 2(3), 433–451. Available online: https://doi.org/10.1260/2047-4970.2.3.433 (accessed on 02

July 2021).

Cox, R. A. K. (2015). Real-world comparisons between target-based and targetless point-cloud registration in FARO Scene , Trimble RealWorks and Autodesk Recap (Issue October). Available online: https://eprints.usq.edu.au/29195/1/Cox_R_Zhang.pdf (accessed on 02 July 2021).

Dai, F., & Lu, M. (2010). Assessing the accuracy of applying photogrammetry to take geometric measurements on building products. Journal of Construction Engineering and Management, 136(2), 242–250. Reston, VA: ASCE. Available online: https://ascelibrary.org/doi/10.1061/%28ASCE%29CO.1943-7862.0000114 (accessed on 25 November 2020)

Doumit, J. A. (2019). From Drones to Geospatial Data (pp. 1–109). Kuban State University. Available online: https://www.researchgate.net/publication/330555127 (accessed on 15 June 2021).

El-Din Fawzy, H. (2019). 3D laser scanning and close-range photogrammetry for buildings documentation: A hybrid technique towards a better accuracy. Alexandria Engineering Journal, 58(4), 1191–1204. Available online: https://doi.org/10.1016/j.aej.2019.10.003 (accessed on 30 June 2021).

Fai, S., & Rafeiro, J. (2014). Establishing an appropriate level of detail (LOD) for a building information model (BIM) - West Block, Parliament Hill, Ottawa, Canada. ISPRS Annals of the Photogrammetry, Remote Sensing and Spatial Information Sciences, 2(5), 123–130. Available online: https://doi.org/10.5194/isprsannals-II-5-123-2014 (accessed on 02 July 2021).

Girardeau-Montaut, D. (2015). CloudCompare Version 2.6.1 – User manual (p. 181). Available online: http://www.cloudcompare.org/doc/qCC/CloudCompare v2.6.1 - User manual.pdf (accessed on 01 July 2021).

Groetelaars, N. J. (2015). Criação de modelos BIM a partir de “Nuvens de Pontos”: estudo de Métodos e Técnicas para documentação arquitetônica. 372. Available online: https://repositorio.ufba.br/ri/handle/ri/20220 (accessed on 02 July 2021).

Guarnieri, A., Remondino, F., & Vettore, A. (2006). Digital photogrammetry and TLS data fusion applied to Cultural Heritage 3D modeling. The International Archives of the Photogrammetry, Remote Sensing and Spatial Information Sciences, 36(part 5). Available online: https://www.researchgate.net/publication/250198668_DIGITAL_PHOTOGRAMMETRY_AND_TLS_DATA_FUSION_APPLIED_TO_CULTURAL_HERITAGE_3D_MODELING/citations (accessed on 02 July 2021).

Martins, G. (2019). Desenvolvimento de as-built de patrimônios históricos com base em Heritage Building Information Modeling – Caso de Estudo: Solar Grandjean de Montigny.

Mason, A. (n.d.). Making 3D Models with Photogrammetry Getting Started with Agisoft PhotoScan. In The Haskins Society. Available online: https://thehaskinssociety.wildapricot.org/resources/documents/tutorials/photogrammetr

ywithphotoscantutorial.pdf (accessed on 02 July 2021).

Mateus, L., Fernández, J., Ferreira, V., Oliveira, C., Aguiar, J., Gago, A. S., Pacheco, P., & Pernão, J. (2019). Graphical data flow based in TLS and photogrammetry for consolidation studies of historical sites. The case study of Juromenha Fortress in Portugal. International Archives of the Photogrammetry, Remote Sensing and Spatial Information Sciences - ISPRS Archives, 42(2/W15), 767–773. Available online: https://doi.org/10.5194/isprs-archives-XLII-2-W15-767-2019 (accessed on 02 July 2021).

Matthews, N. A. (2008). Aerial and Close-Range Photogrammetric Technology: Providing Resource Documentation, Interpretation, and Preservation. (p. 42). Available online: https://www.blm.gov/sites/blm.gov/files/documents/files/Library_BLMTechnicalNote428_0.pdf (accessed on 02 July 2021).

Maar, H., & Zogg, H.-M. (2017). Leica Nova MS60. Leica Geosystems AG, 12. Available online: http://leica-geosystems.com/products/total-stations/multistation/leica-nova-ms60 (accessed on 03 July 2021).

Migliaccio, F. (2019). BIM: parametric object modelling. DICA – Sezione Geodesia e Geomatica.

Murphy, M., Mcgovern, E., & Pavia, S. (2009). Historic building information modelling (HBIM). Structural Survey, 27(4), 311–327. Available online: https://doi.org/10.1108/02630800910985108 (accessed on 02 July 2021).

Oreni, D., Brumana, R., Della Torre, S., Banfi, F., Barazzetti, L., & Previtali, M. (2014). Survey turned into HBIM: The restoration and the work involved concerning the Basilica di Collemaggio after the earthquake (L'Aquila). ISPRS Annals of the Photogrammetry, Remote Sensing and Spatial Information Sciences, 2(5), 267–273. Available online: https://doi.org/10.5194/isprsannals-II-5-267-2014 (accessed on 02 July 2021).

PCL (2021). Point Cloud Library 1.11.1-dev. Module keypoints. Available online: https://pointclouds.org/documentation/group__keypoints.html (accessed on: 20 June 2021).

Pizarro, A., Manfreda, S., & Tubaldi, E. (2020). The science behind scour at bridge foundations: A review. Water (Switzerland), 12(2). Available online: https://doi.org/10.3390/w12020374 (accessed on 02 July 2021).

Pomerleau, F., Colas, F., & Siegwart, R. (2015). A Review of Point Cloud Registration Algorithms for Mobile Robotics. Foundations and Trends in Robotics, 4(1), 1–104. Available online: https://doi.org/10.1561/2300000035 (accessed on 02 July 2021).

Poux, F.(2020). How to automate LiDAR point cloud sub-sampling with Python. Available online: https://towardsdatascience.com/how-to-automate-lidar-point-cloud-processing-with-python-a027454a536c (accessed on 06 July 2021).

Prendergast, L. J., & Gavin, K. (2014). A review of bridge scour monitoring techniques. Journal of Rock Mechanics and Geotechnical Engineering, 6(2), 138–149. Available online: https://doi.org/10.1016/j.jrmge.2014.01.007 (accessed on 02 July 2021).

Riveiro, B., DeJong, M. J., & Conde, B. (2016). Automated processing of large point clouds for structural health monitoring of masonry arch bridges. Automation in Construction, 72, 258–268. Available online: https://doi.org/10.1016/j.autcon.2016.02.009 (accessed on 29 June 2021).

Riveiro, B., González-Jorge, H., Varela, M., & Jauregui, D. V. (2013). Validation of terrestrial laser scanning and photogrammetry techniques for the measurement of vertical underclearance and beam geometry in structural inspection of bridges. Measurement: Journal of the International Measurement Confederation, 46(1), 784–794. Available online: https://doi.org/10.1016/j.measurement.2012.09.018 (accessed on 28 June 2021).

Rocha, Mateus, Fernández, & Ferreira. (2020). A Scan-to-BIM Methodology Applied to Heritage Buildings. Heritage, 3(1), 47–67. Available online: https://doi.org/10.3390/heritage3010004 (accessed on 30 June 2021)

Sattler, L., Lamouri, S., Pellerin, R., & Maigne, T. (2019). Interoperability aims in Building Information Modeling exchanges: a literature review. IFAC-PapersOnLine, 52(13), 271–276. Available online: https://doi.org/10.1016/j.ifacol.2019.11.180 (accessed on 01 July 2021).

Scozzese, F., Ragni, L., Tubaldi, E., & Gara, F. (2019). Modal properties variation and collapse assessment of masonry arch bridges under scour action. Engineering Structures, 199(March), 109665. Available online: https://doi.org/10.1016/j.engstruct.2019.109665 (accessed on 01 July 2021).

SpatialHumanities (n.d). Institute for Spatial Information and Surveying Technology. Academy of Sciences and Literature | Mainz. Terrestrial Laser Scanning. Available online: http://www.spatialhumanities.de/en/ibr/technology/terrestrial-laserscanning.html (accessed on 30 May 2021).

Tan, Y., Li, S., & Wang, Q. (2020). Automated Geometric Quality Inspection of Prefabricated Housing Units Using BIM and LiDAR. Remote Sensing, 12(15). Available online: https://doi.org/10.3390/RS12152492 (accessed on 01 July 2021)

Tang, Huber, Akinci, Lipman, & Lytle. (2010). Automatic reconstruction of as-built building information models from laser-scanned point clouds: A review of related techniques. Automation in Construction, 19(7), 829–843. Available online: https://doi.org/10.1016/j.autcon.2010.06.007 (accessed on 02 July 2021).

Tang, P., Anil, E. B., Akinci, B., & Huber, D. (2011). Efficient and Effective Quality Assessment of As-Is Building Information Models and 3D Laser-Scanned Data. Congress on Computing in Civil Engineering, Proceedings, 41182(June), 486–493. Available online: https://doi.org/10.1061/41182(416)60 (accessed on 01 July 2021).

Thomson, C. (2018) Common 3D point cloud file formats & solving interoperability issues. Vercator. Available online: https://info.vercator.com/blog/what-are-the-most-common-3d-point-cloud-file-formats-and-how-to-solve-interoperability-issues (accessed on 20 May 2021).

Tian, J. (2011). Basics of Photogrammetry. Geodetic Services, Inc. 62. Available online:

https://www.geodetic.com/basics-of-photogrammetry/ (accessed on 02 July 2021).

Tombari, F., & Remondino, F. (2013). Feature-based automatic 3D registration for cultural heritage applications. Proceedings of the DigitalHeritage 2013 - Federating the 19th Int'l VSMM, 10th Eurographics GCH, and 2nd UNESCO Memory of the World Conferences, Plus Special Sessions FromCAA, Arqueologica 2.0 et Al., 1(October), 55–62. Available online: https://doi.org/10.1109/DigitalHeritage.2013.6743713 (accessed on 02 July 2021).

Wang, C., & Cho, Y. K. (2015). Application of As-built Data in Building Retrofit Decision Making Process. Procedia Engineering, 118, 902–908. Available online: https://doi.org/10.1016/j.proeng.2015.08.529 (accessed on 02 July 2021)

Wang, Tan, & Mei. (2019). Computational Methods of Acquisition and Processing of 3D Point Cloud Data for Construction Applications. Archives of Computational Methods in Engineering, 27(2), 479–499. Available online: https://doi.org/10.1007/s11831-019-09320-4 (accessed on 02 July 2021).

Wang, Y., & Feng, H. Y. (2014). Modeling outlier formation in scanning reflective surfaces using a laser stripe scanner. Measurement: Journal of the International Measurement Confederation, 57, 108–121. Available online: https://doi.org/10.1016/j.measurement.2014.08.010 (accessed on 02 July 2021).

Yang, Koehl, Grussenmeyer, & Macher. (2016). Complementarity of historic building information modelling and geographic information systems. International Archives of the Photogrammetry, Remote Sensing and Spatial Information Sciences - ISPRS Archives, 41, 437–443. Available online: https://doi.org/10.5194/isprsarchives-XLI-B5-437-2016 (accessed on 02 July 2021).

YellowScan (2020). Three ways to determine distance using LiDAR. Available online: https://www.yellowscan-lidar.com/knowledge/three-ways-to-determine-a-distance-with-lidar/ (accessed on 15 June 2021).

Yunos, S. (2020). Refining The Scan to BIM Workflow for Further Automation and Visualisation. Autodesk University (p. 35). Autodesk. Available online: https://www.autodesk.com/autodesk-university/de/class/Refining-Scan-BIM-Workflow-Further-Automation-and-Visualization-2020#presentation (acessed on 02 July 2021).

Zhang, W., Qi, J., Wan, P., Wang, H., Xie, D., Wang, X., & Yan, G.(2016). An Easy-to-Use Airborne LiDAR Data Filtering Method Based on Cloth Simulation. Remote Sensing; 8(6):501. Available online: http://ramm.bnu.edu.cn/researchers/wumingzhang/english/default_contributions.htm (accessed on 03 July 2021).

Annex

This section presents the results of the face deviation analysis of the case study. The deviation analysis was performed for the main components of the bridge using Autodesk Point Layout Add-in for Revit. The heatmaps with signed colors in the model describes how much deviation the various faces of the BIM model have with respect to the point cloud data.

The maximum point distance from face was settled as 50 mm and the desired average distance between adjacent cloud point was 0.1 mm, as illustrated in the Figure A.1, and the analysis was performed individually for each structural family. The results are presented for each element of the model, which are identified and illustrated in the Figure A.2.

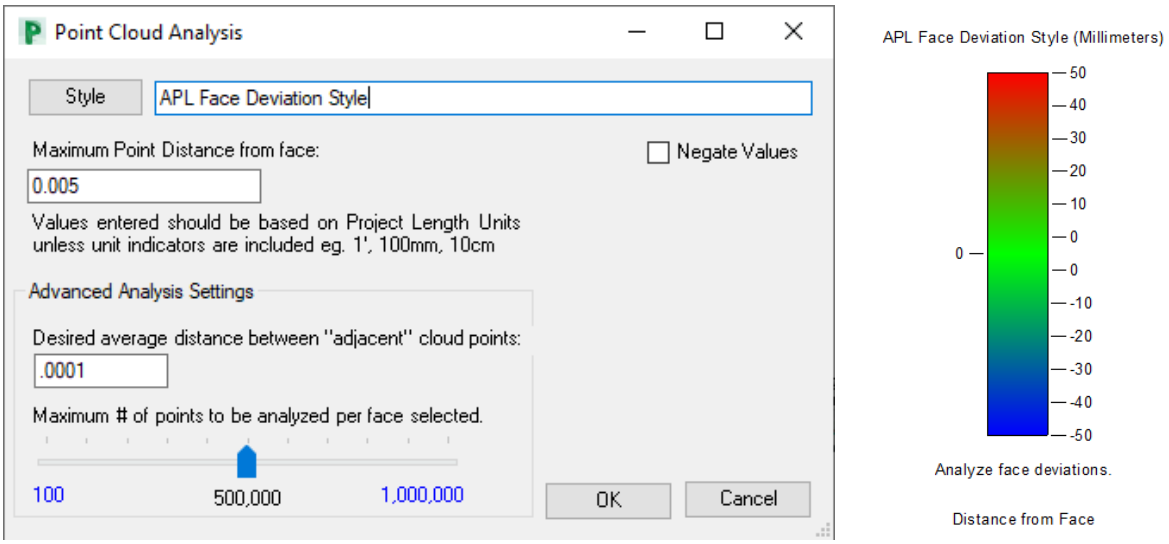

Figure A.1: Input for face deviation analysis.

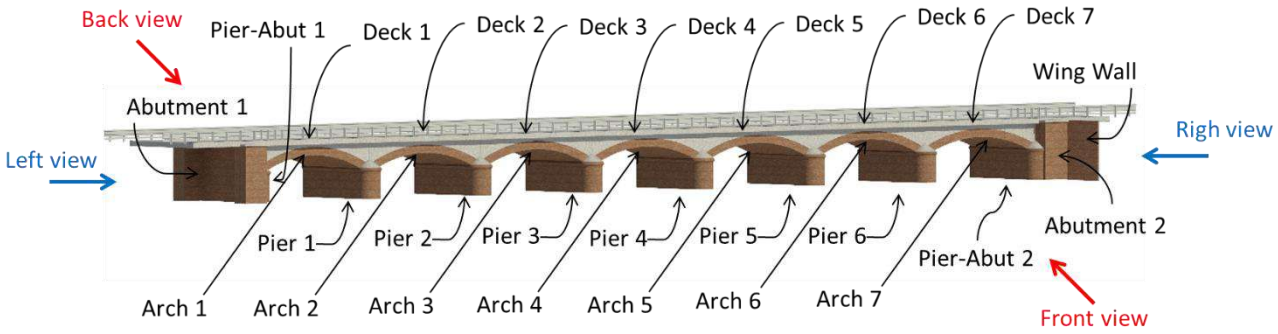

Figure A.2: Schematic representation of the bridge components.

A.1) Piers

PIER-ABUT 1

Front view

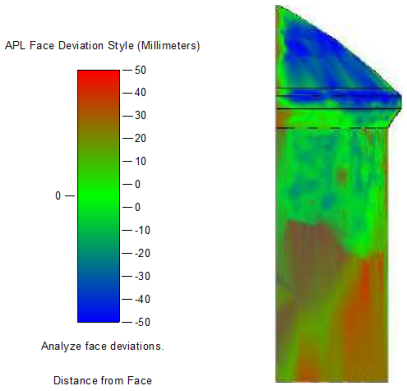

Back view

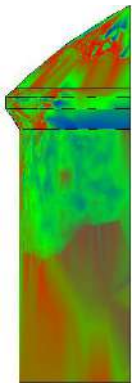

Right view

Top view

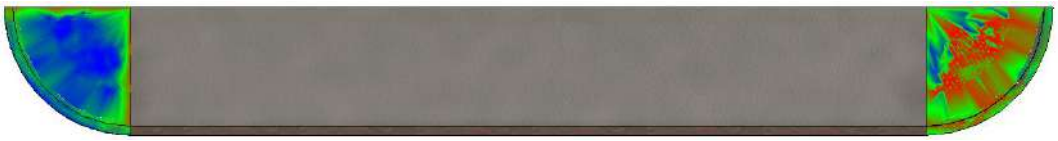

PIER-ABUT 2

Front view

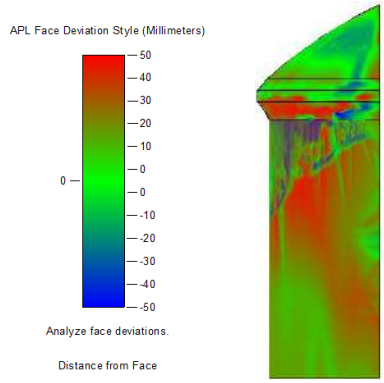

Back view

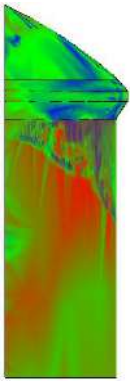

Left view

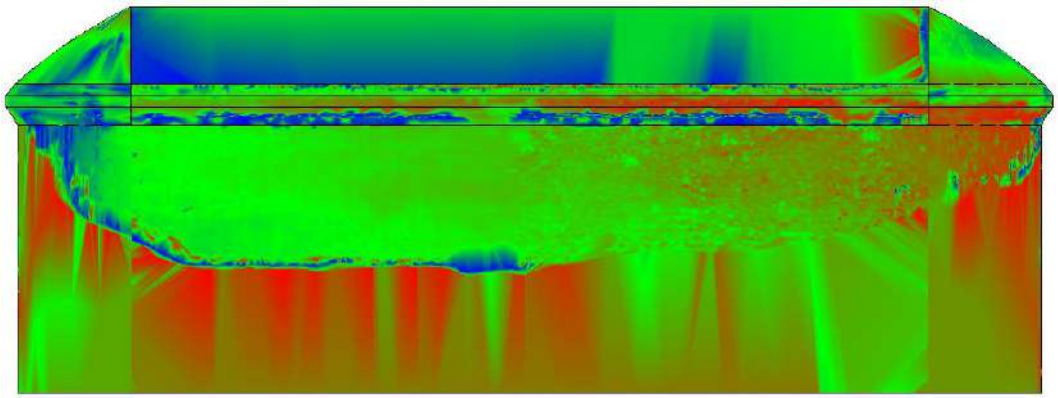

Top view

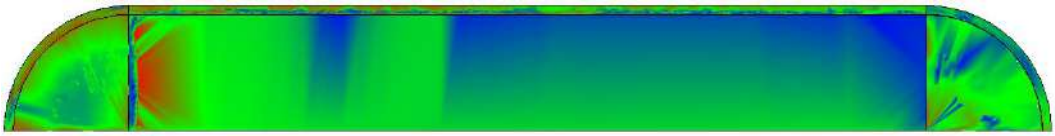

PIER 1

Front view

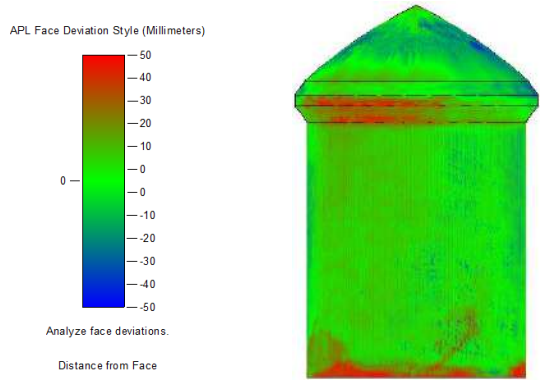

Back view

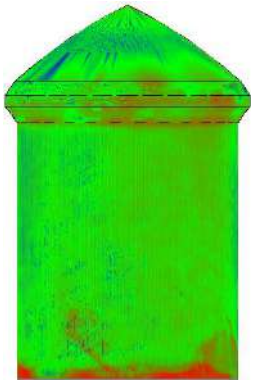

Right view

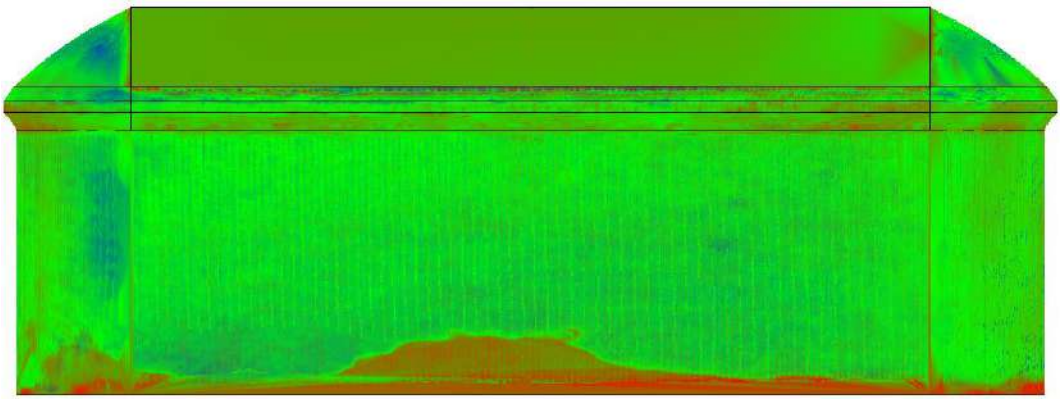

Left view

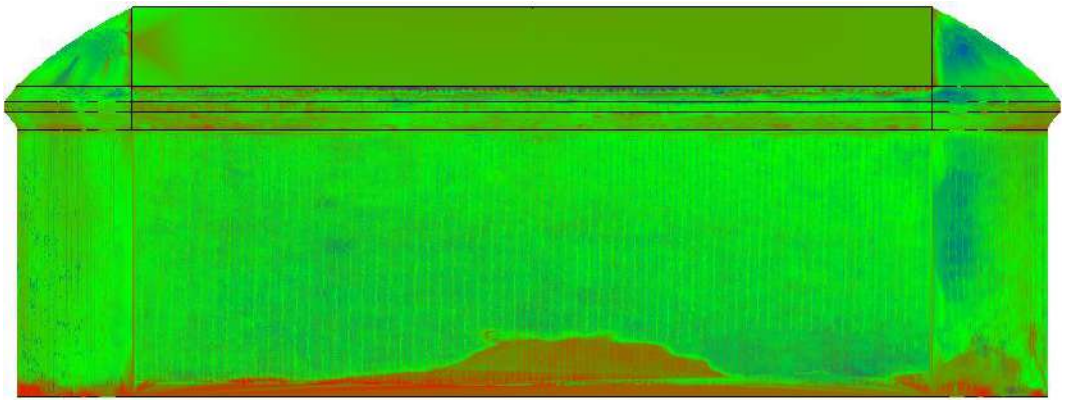

Top view

PIER 2

Front view

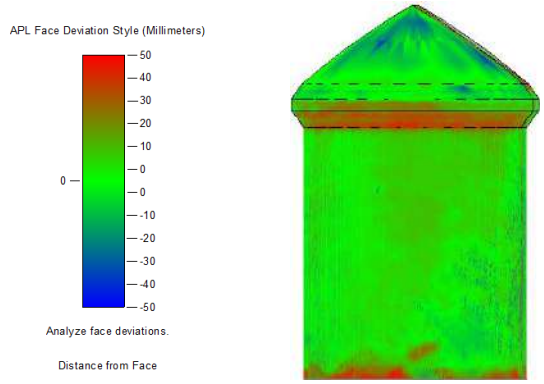

Back view

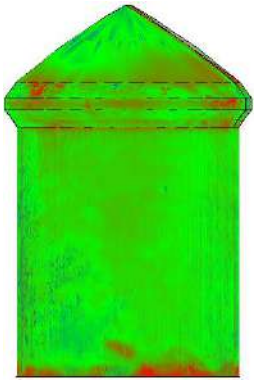

Right view

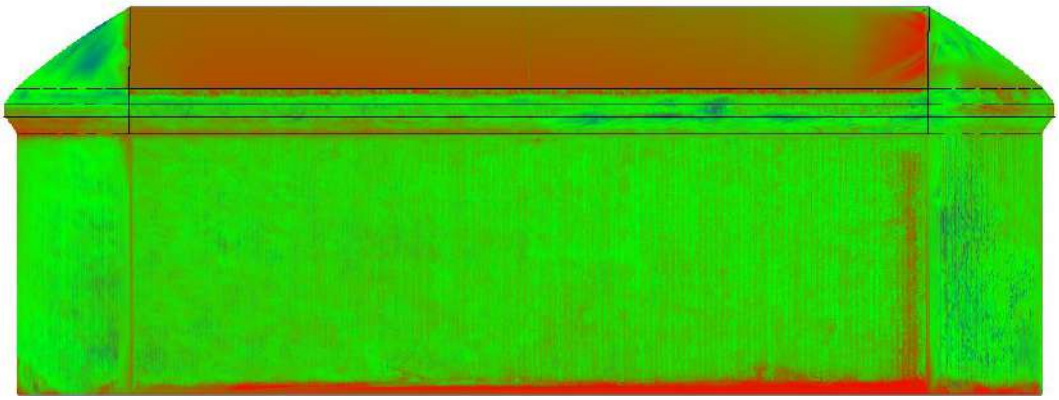

Left view

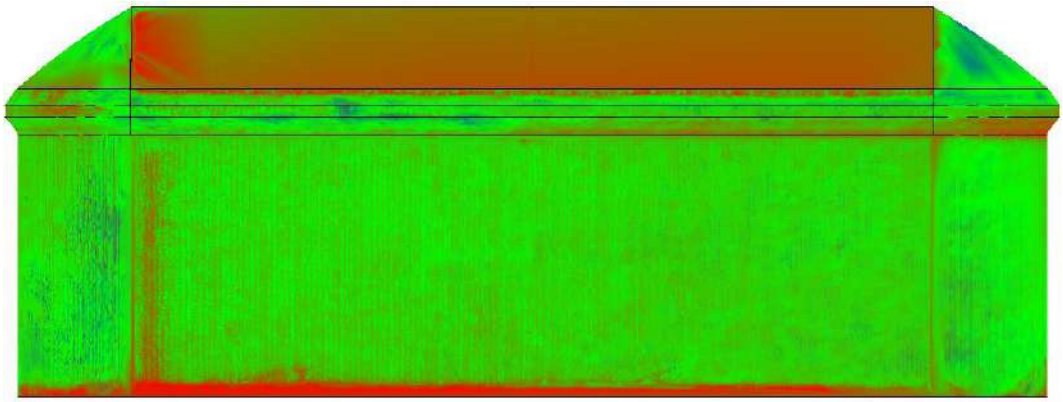

Top view

PIER 3

Front view

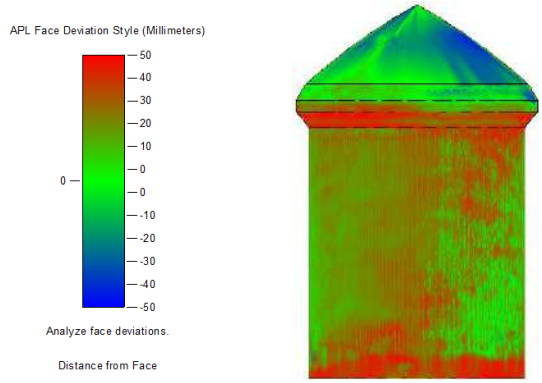

Back view

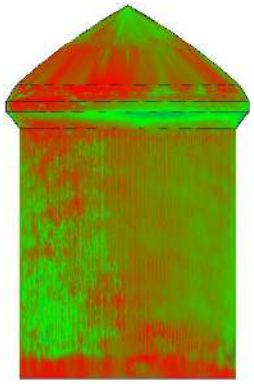

Right view

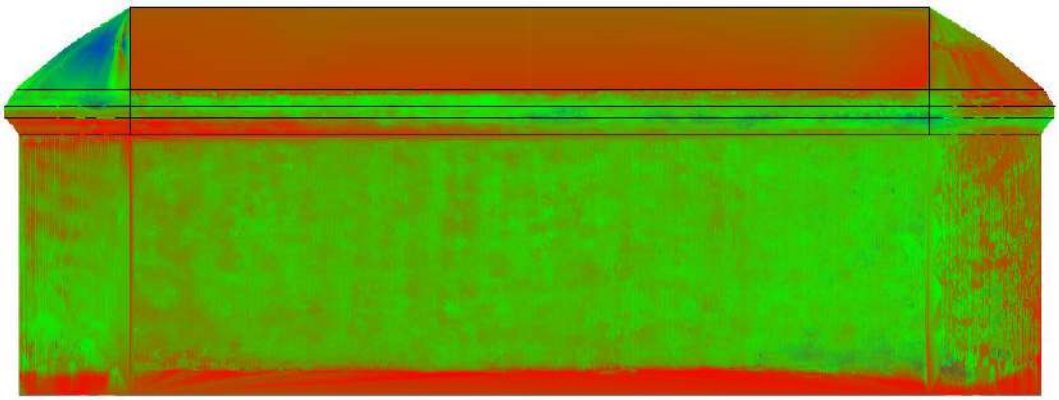

Left view

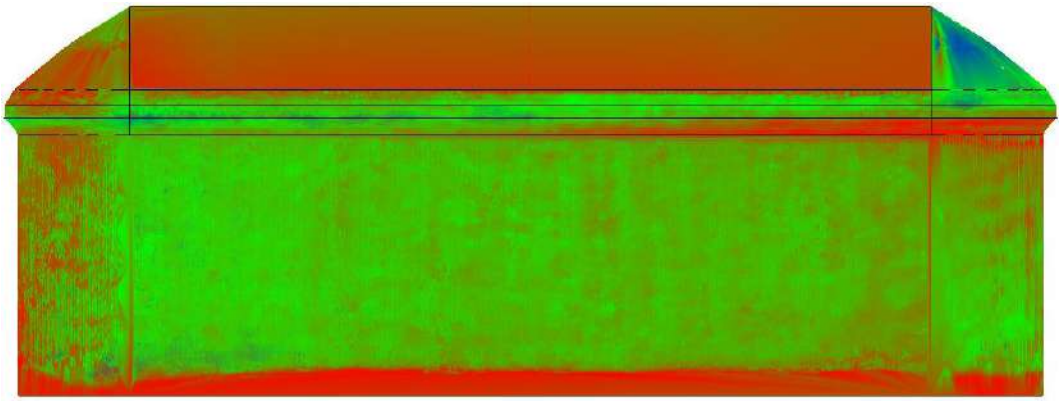

Top view

PIER 4

Front view

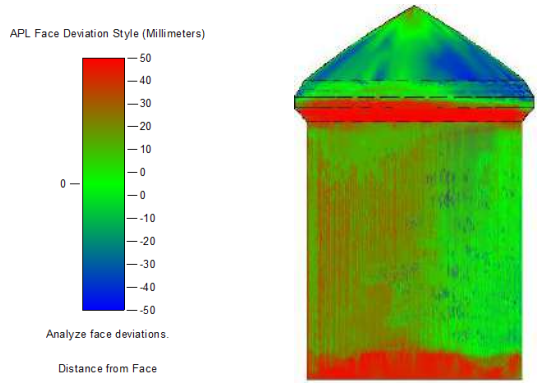

Back view

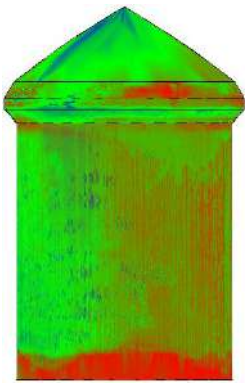

Right view

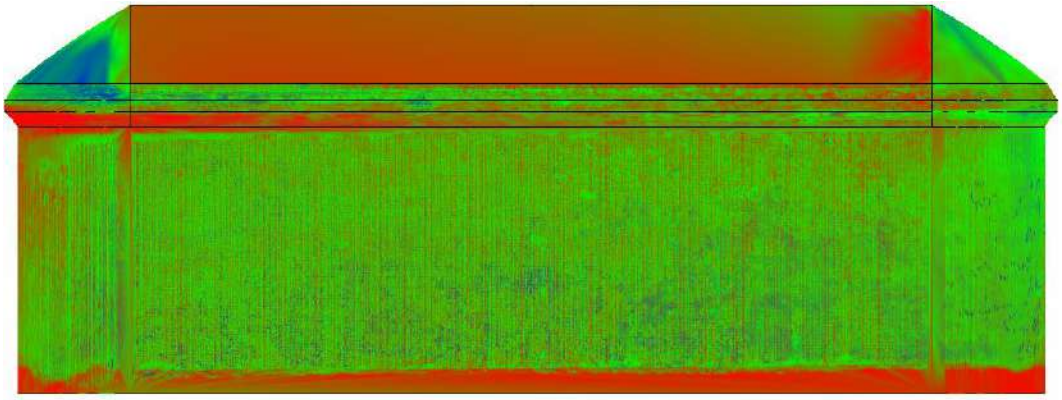

Left view

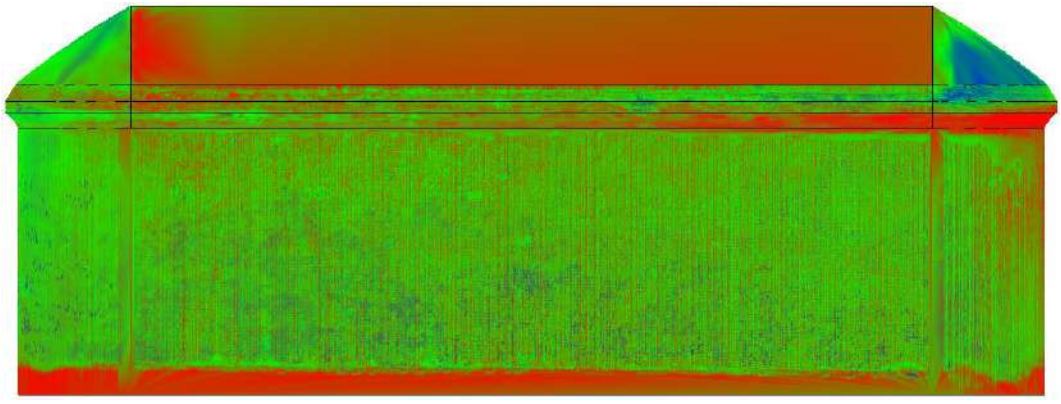

Top view

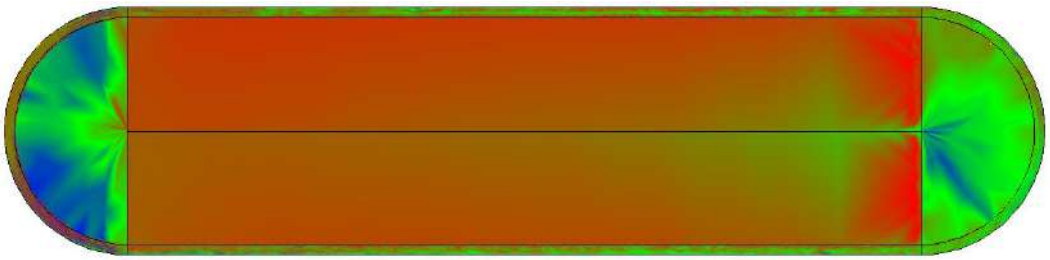

PIER 5

Front view

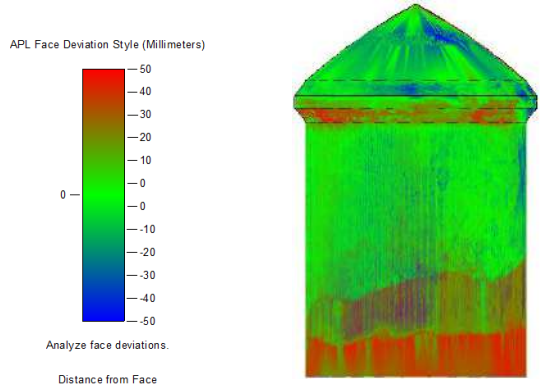

Back view

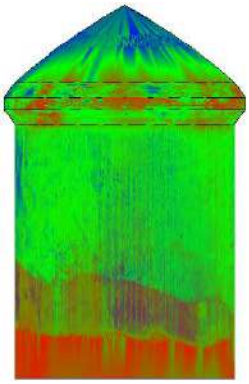

Right view

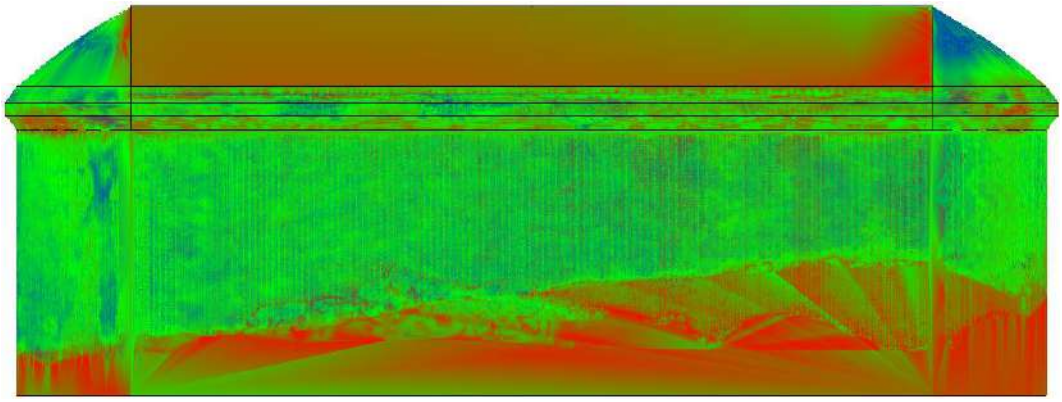

Left view

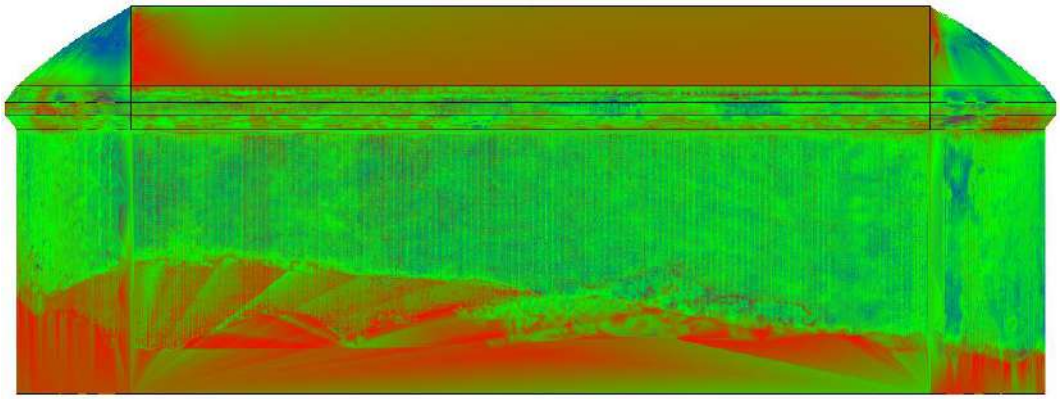

Top view

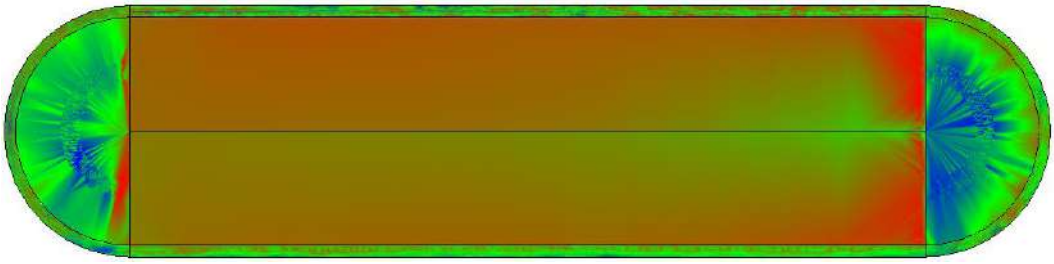

PIER 6

Front view

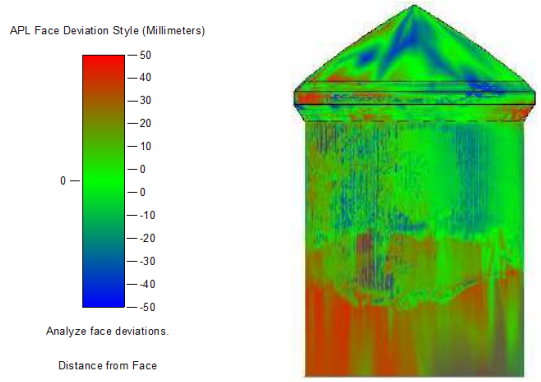

Back view

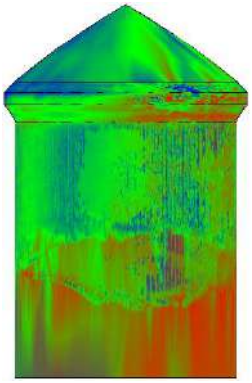

Right view

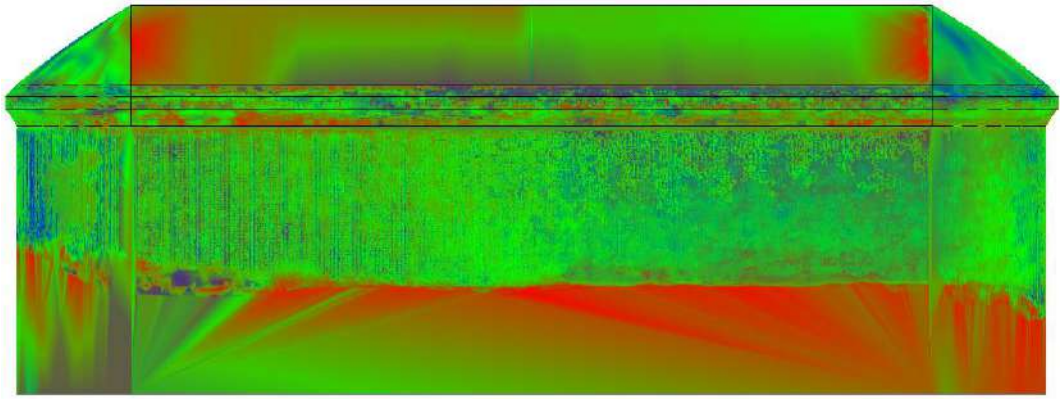

Left view

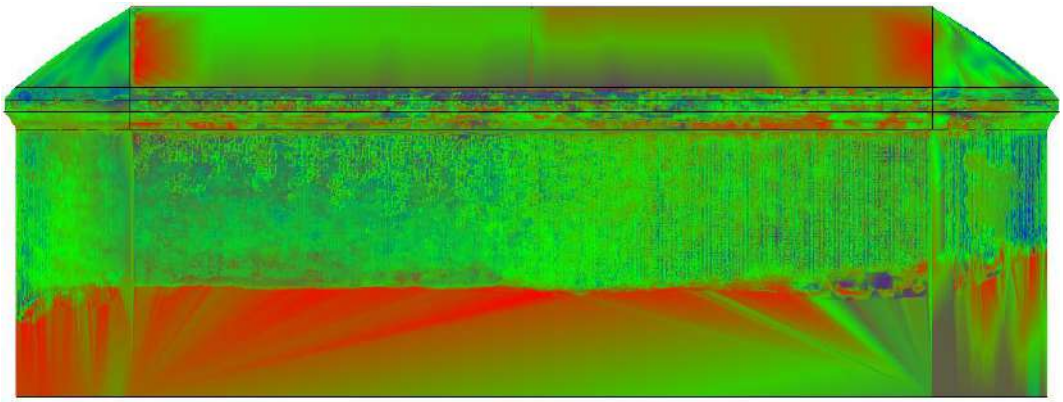

Top view

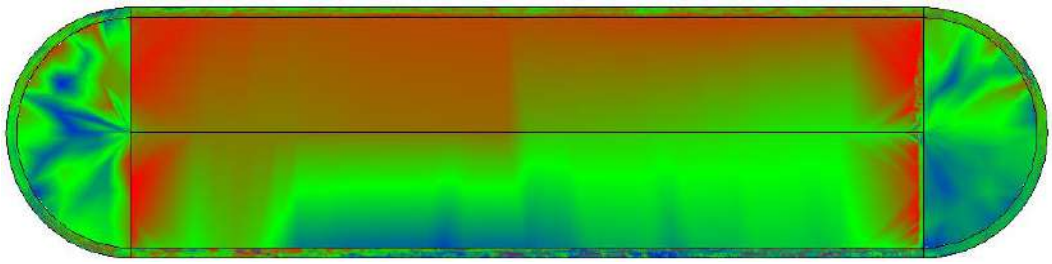

A.2) Abutments and Wing Wall

Isometric view

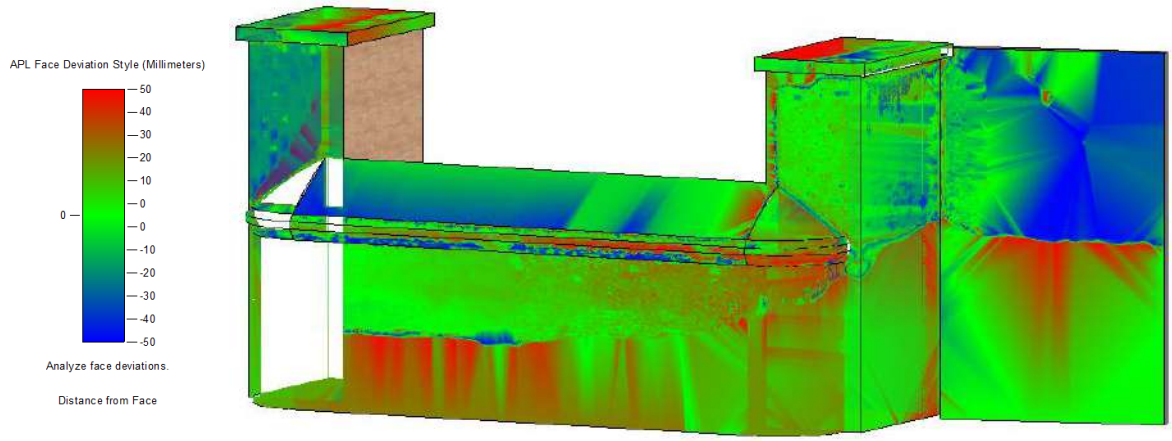

Front view

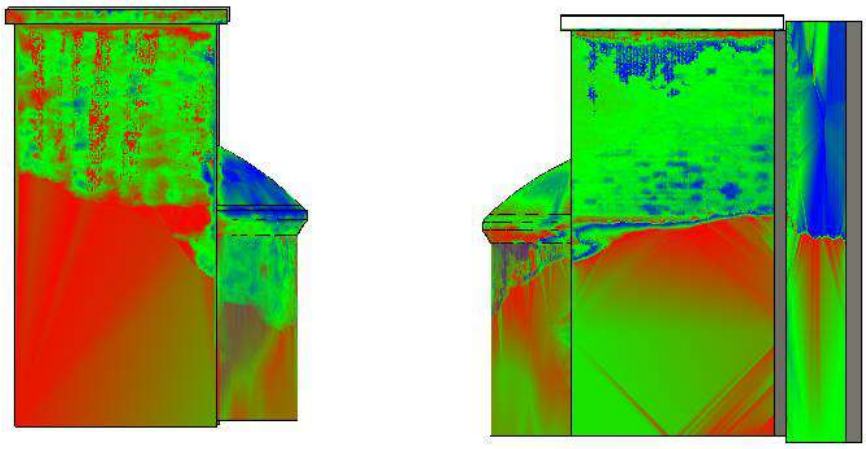

Abutment 1 – Abutment 2

Back view

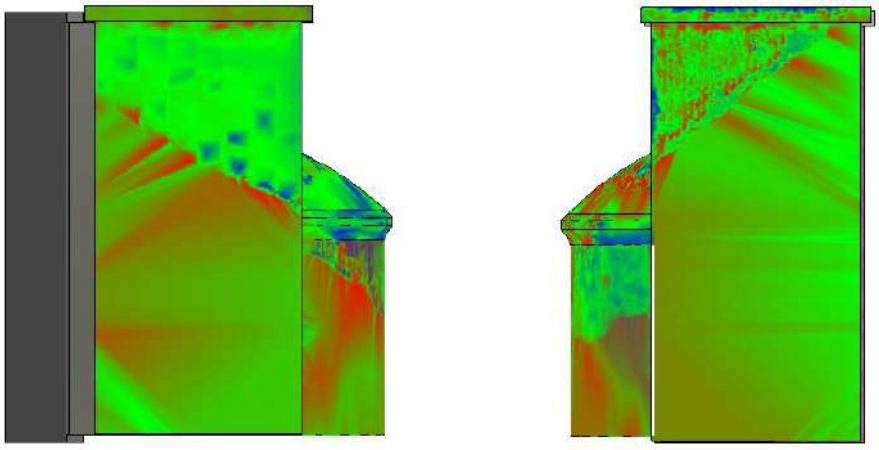

Abutment 2 – Abutment 1

ABUTMENT 1

Front view

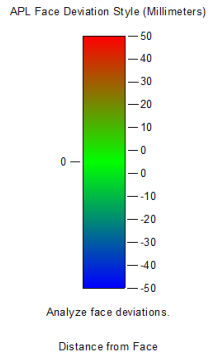

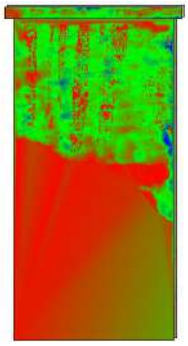

Back view

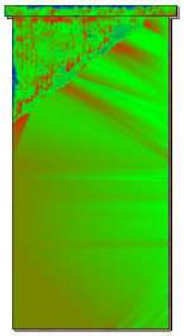

Right view

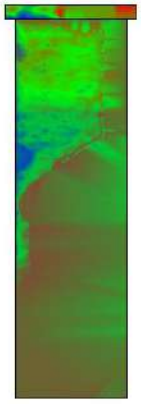

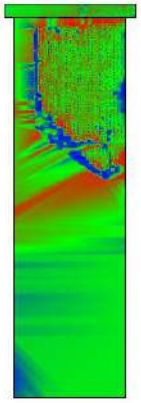

Left view

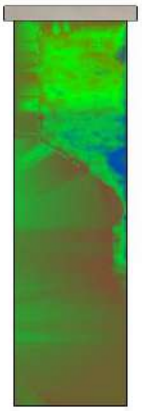

Top view

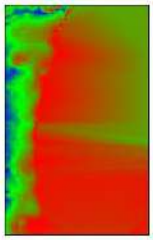

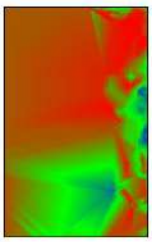

ABUTMENT 2

Front view

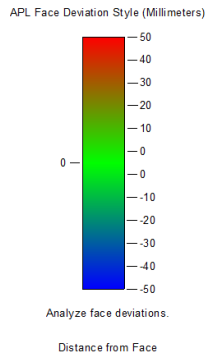

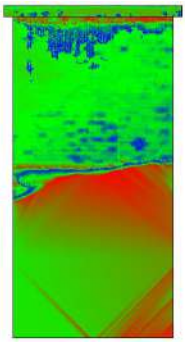

Back view

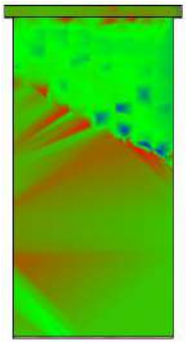

Right view

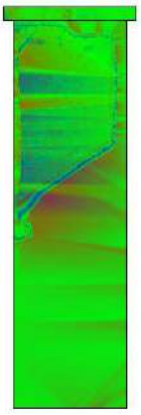

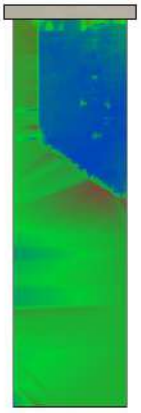

Left view

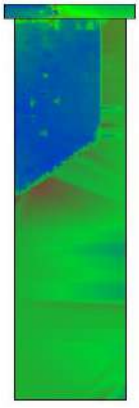

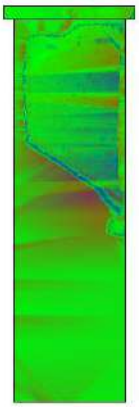

Top view

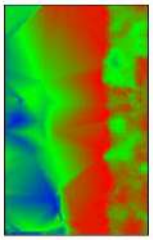

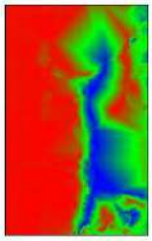

A.3) Spandrel Walls

Front view

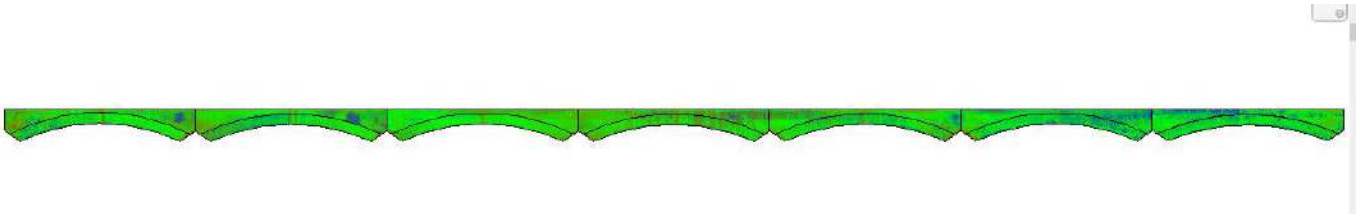

Back view

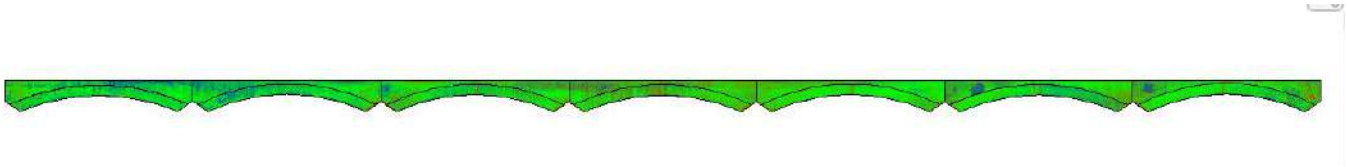

Top view

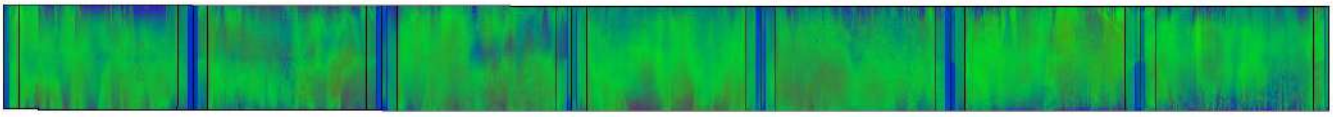

Bottom view

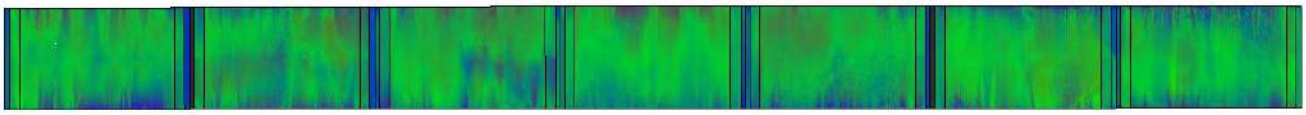

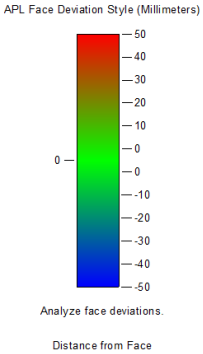

ARCH 1

Front view

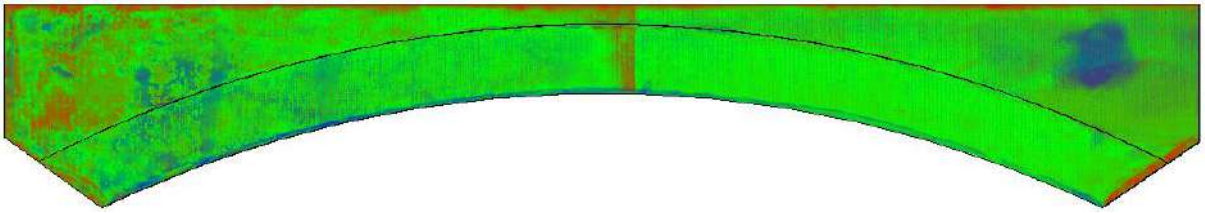

Back view

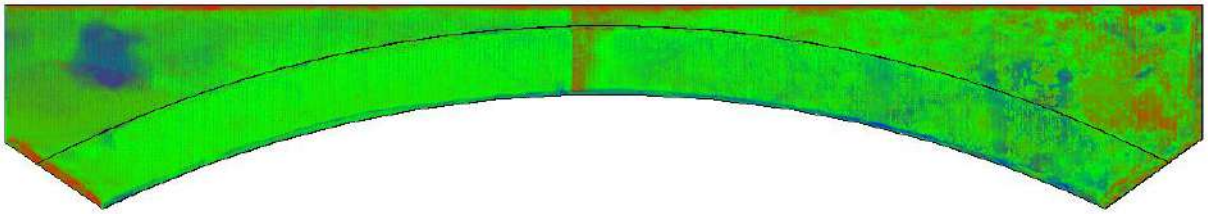

Bottom view

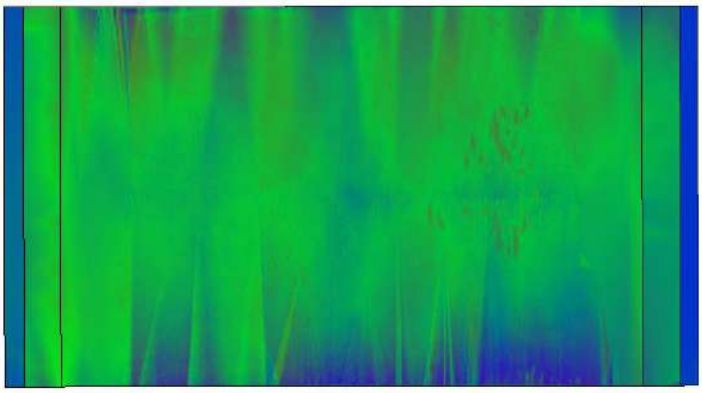

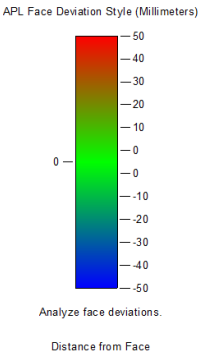

ARCH 2

Front view

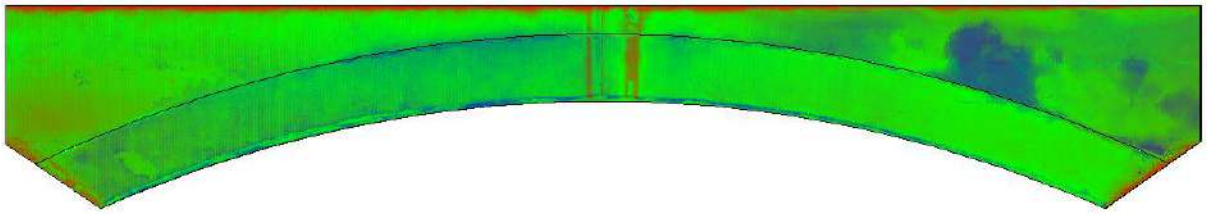

Back view

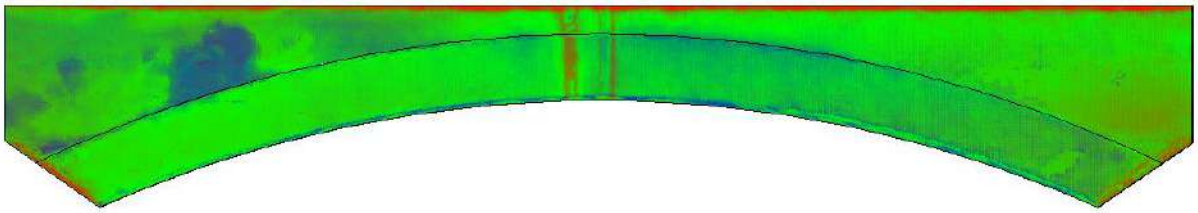

Bottom view

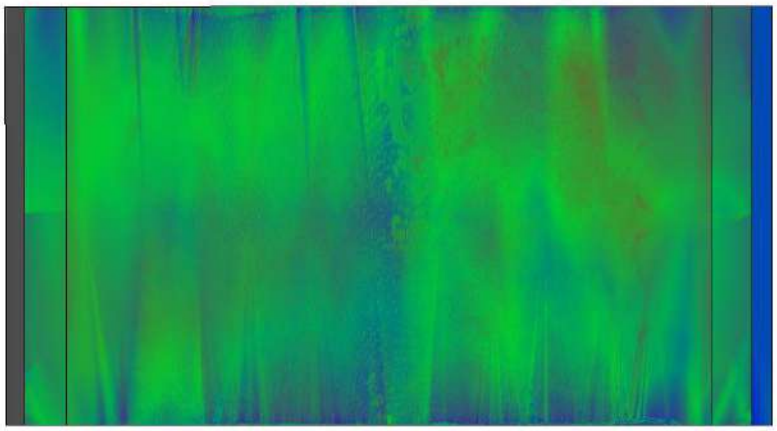

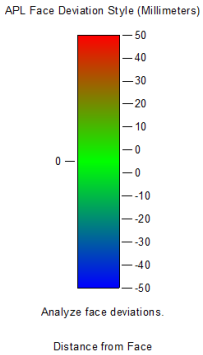

ARCH 3

Front view

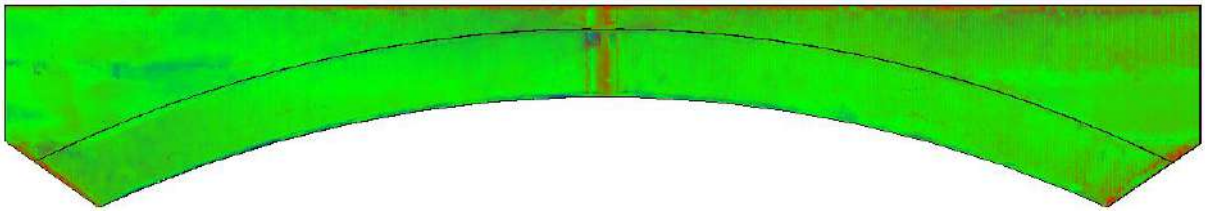

Back view

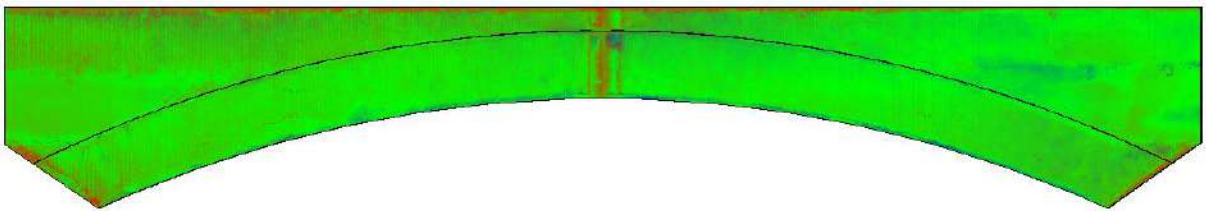

Bottom view

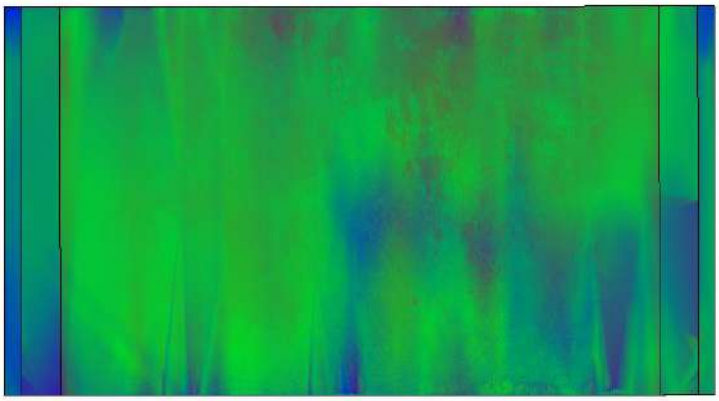

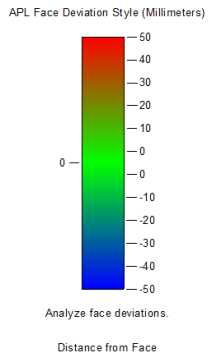

ARCH 4

Front view

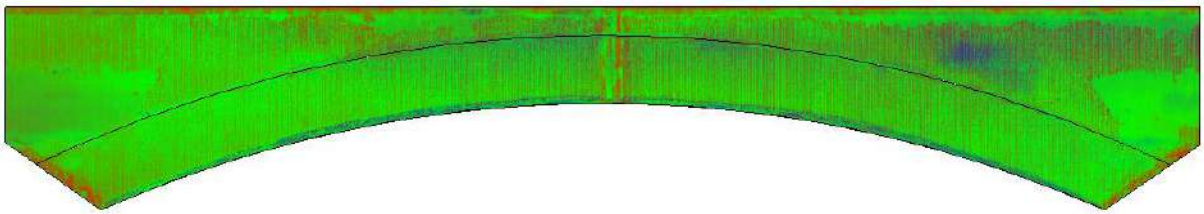

Back view

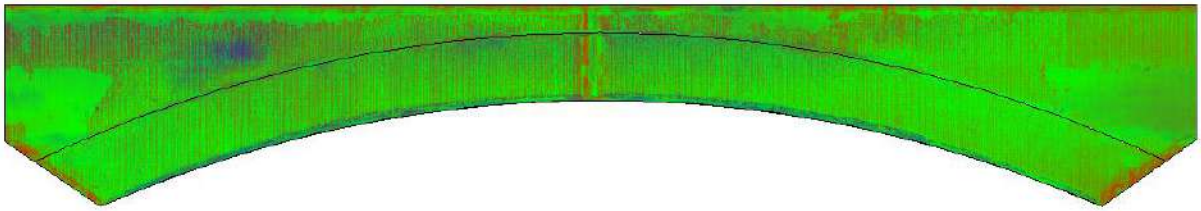

Bottom view

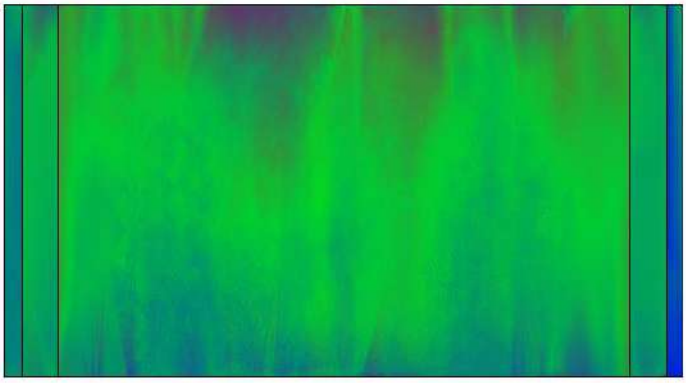

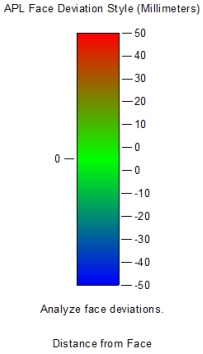

ARCH 5

Front view

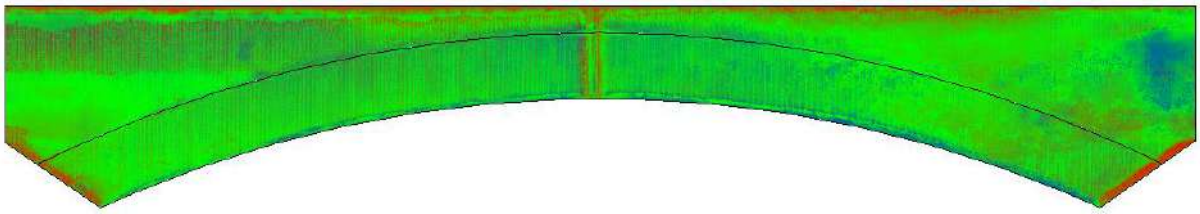

Back view

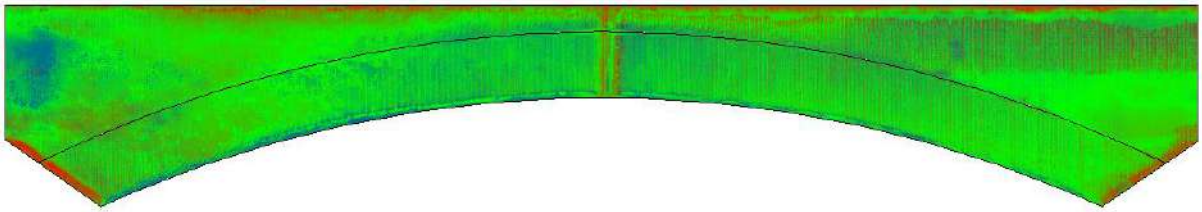

Bottom view

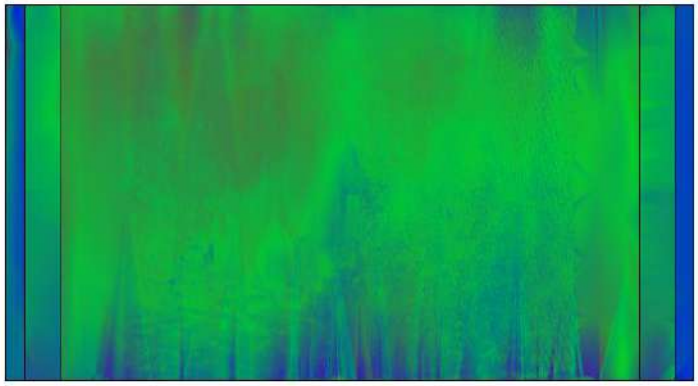

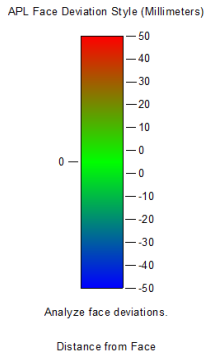

ARCH 6

Front view

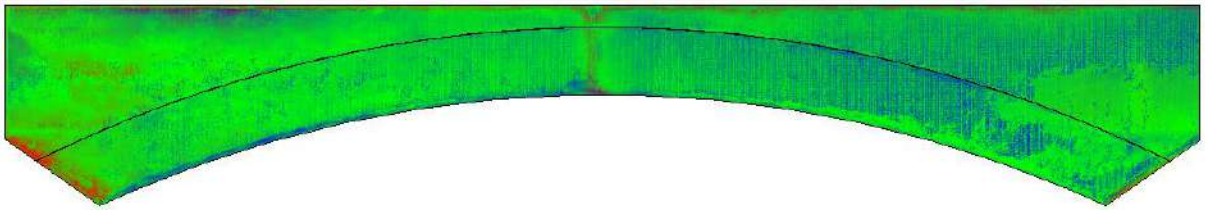

Back view

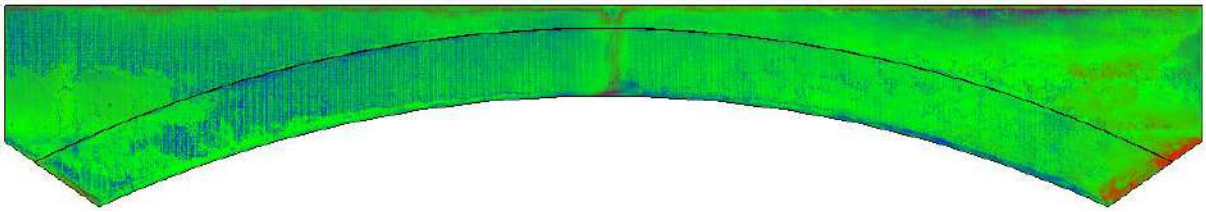

Bottom view

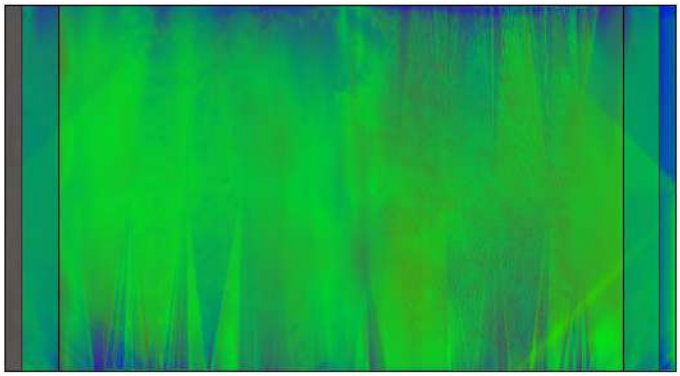

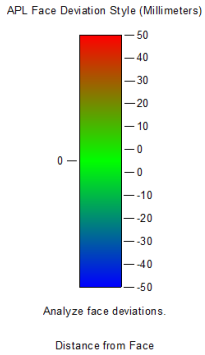

ARCH 7

Front view

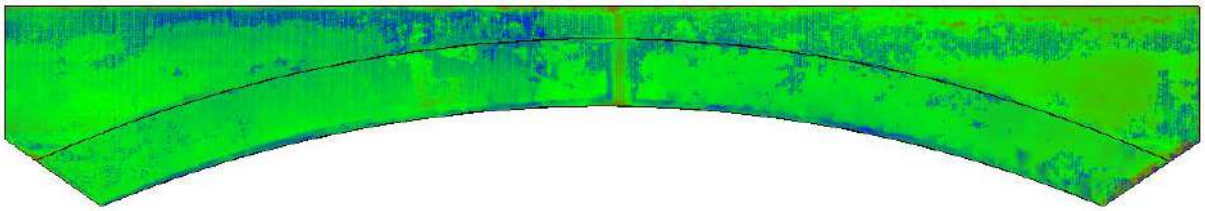

Back view

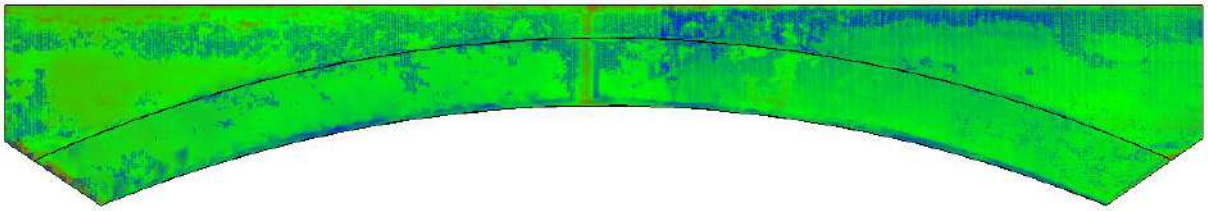

Bottom view

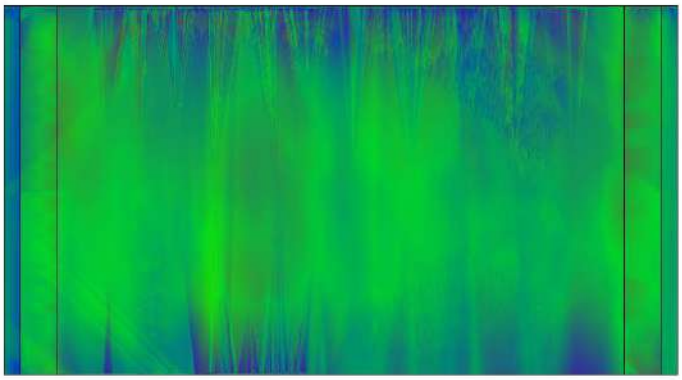

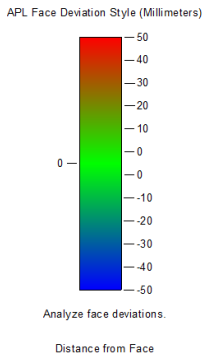

A.4) Decks

Top view

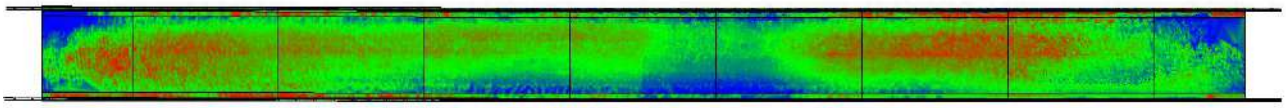

Entrance – Deck 1 – Deck 2 – Deck 3 – Deck 4 – Deck 5 – Deck 6 – Deck 7 – Exit

ENTRANCE

Front view

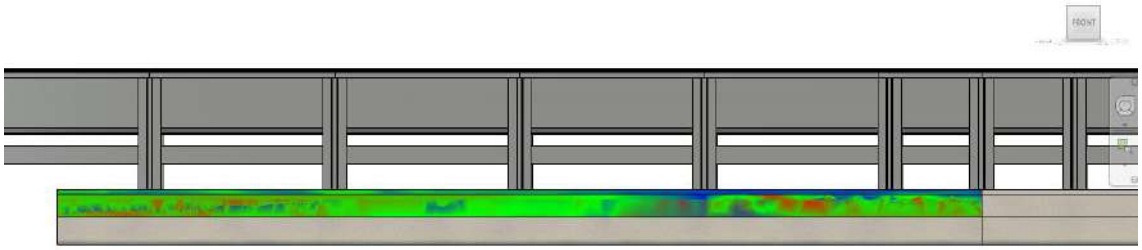

Back view

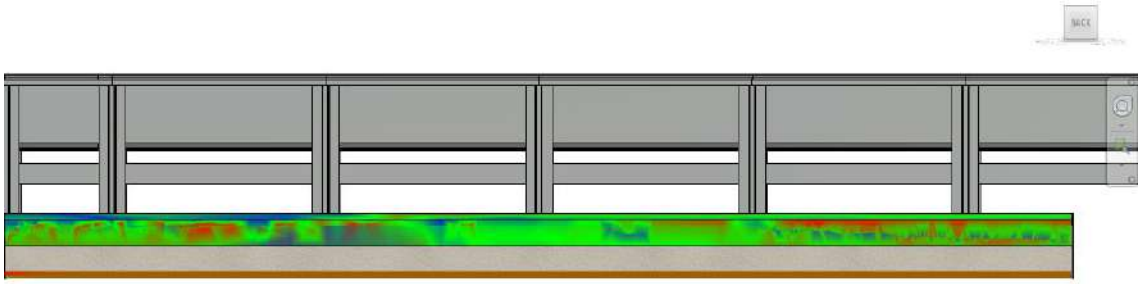

Top view

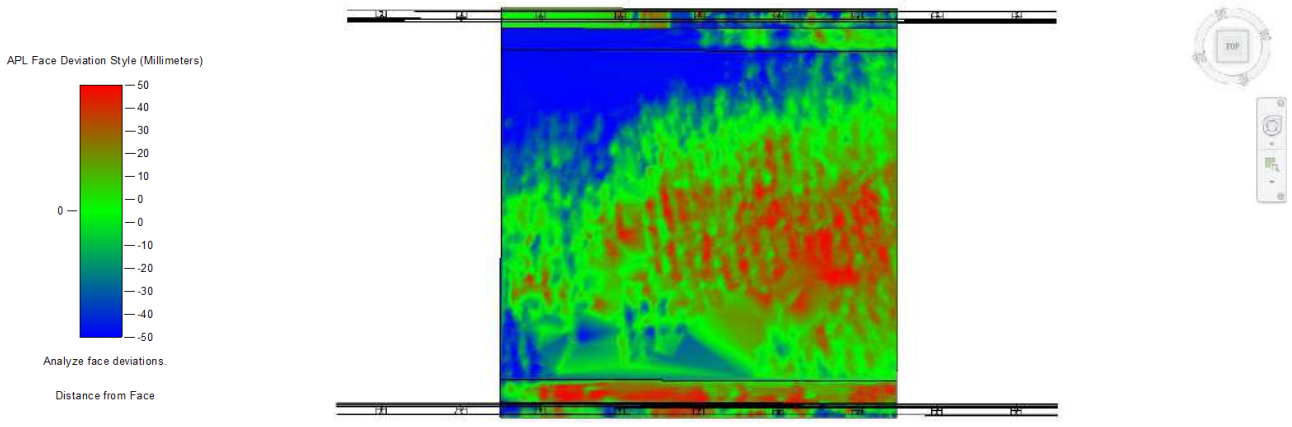

EXIT

Front view

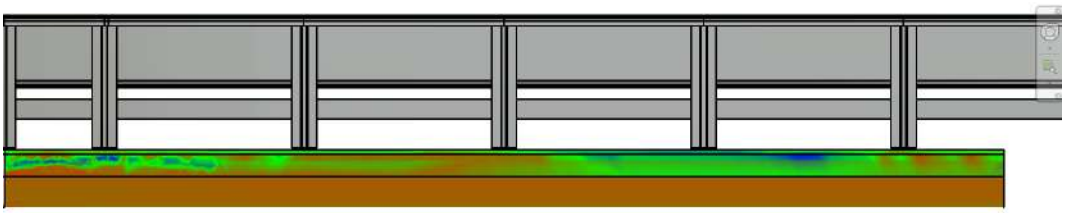

Back view

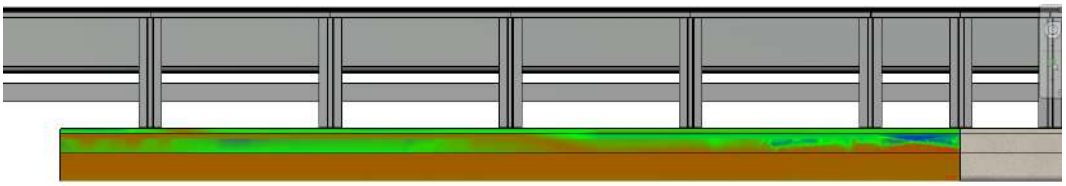

Top view

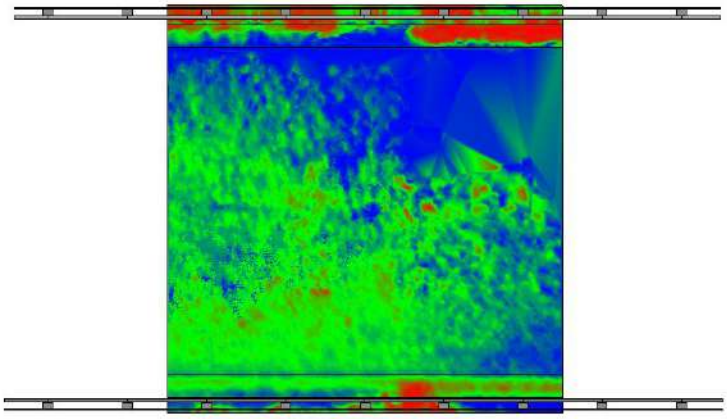

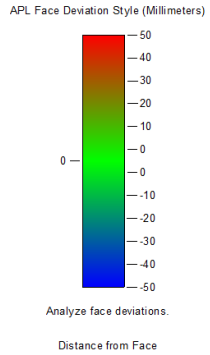

DECK 1

Front view

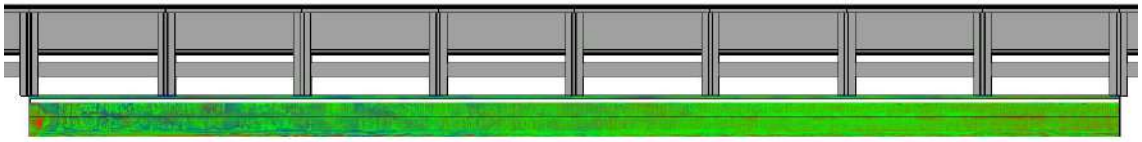

Back view

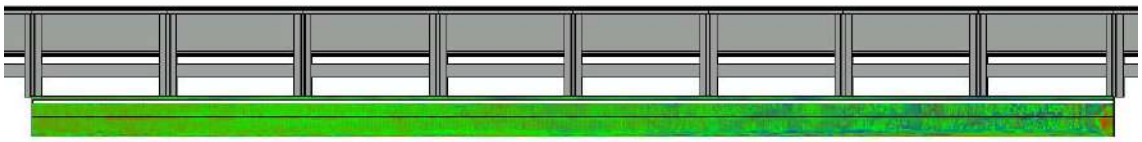

Top view

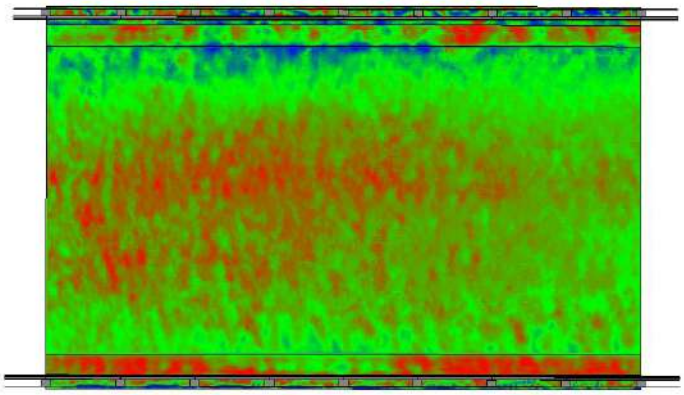

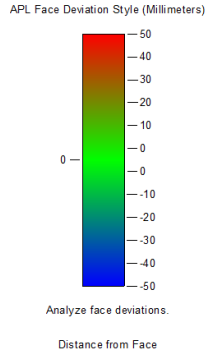

DECK 2

Front view

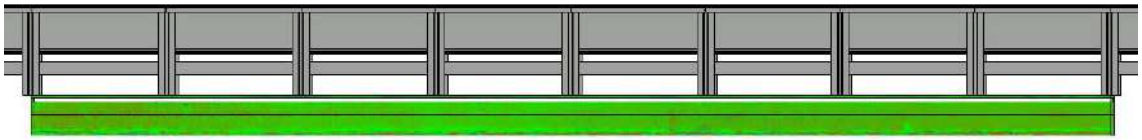

Back view

Top view

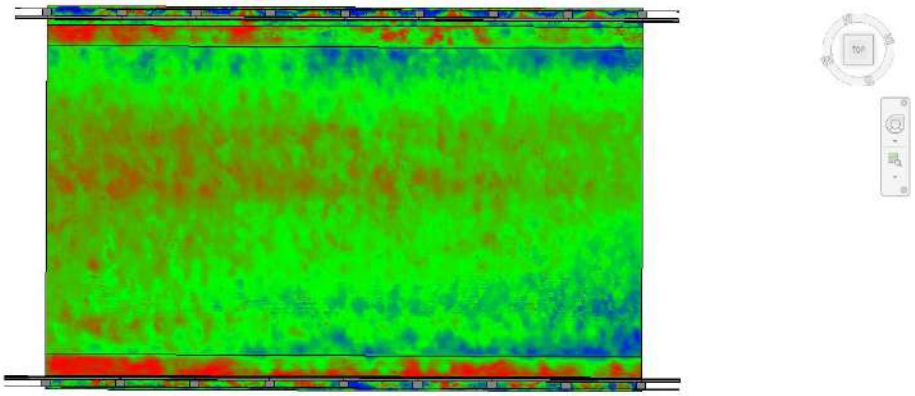

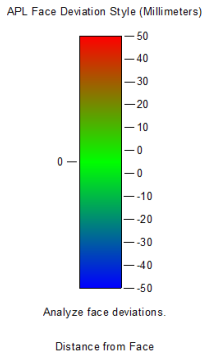

DECK 3

Front view

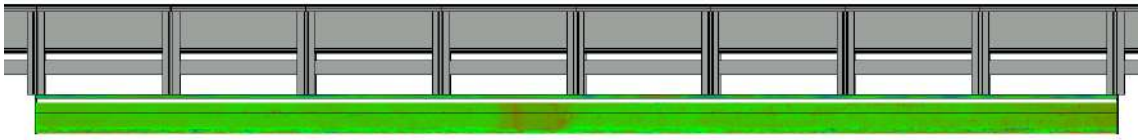

Back view

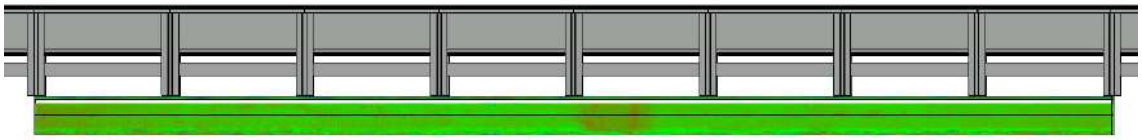

Top view

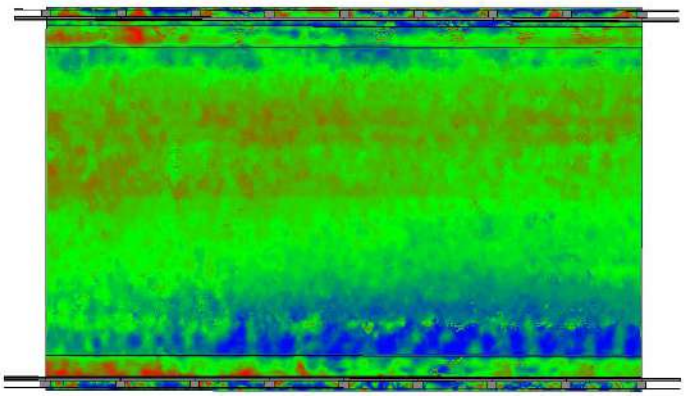

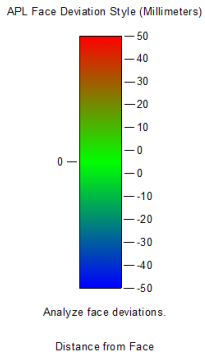

DECK 4

Front view

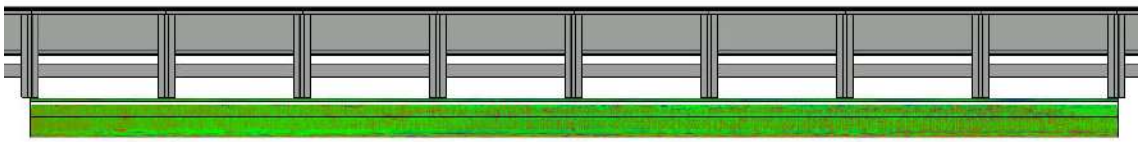

Back view

Top view

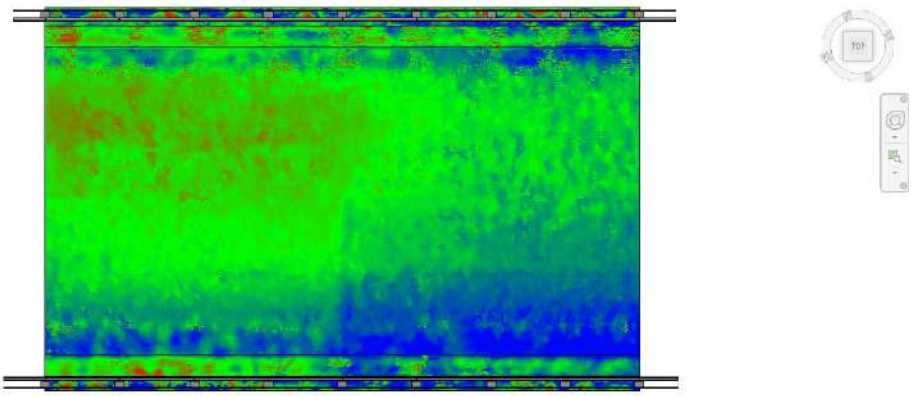

DECK 5

Front view

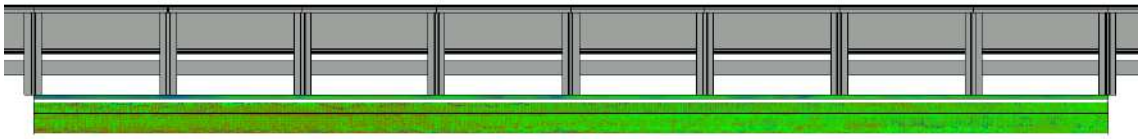

Back view

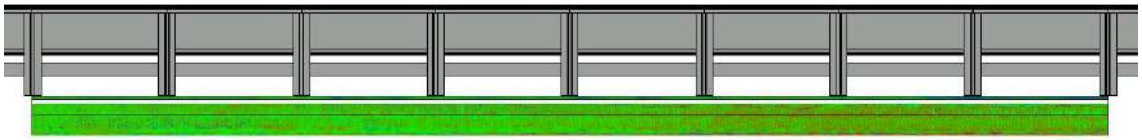

Top view

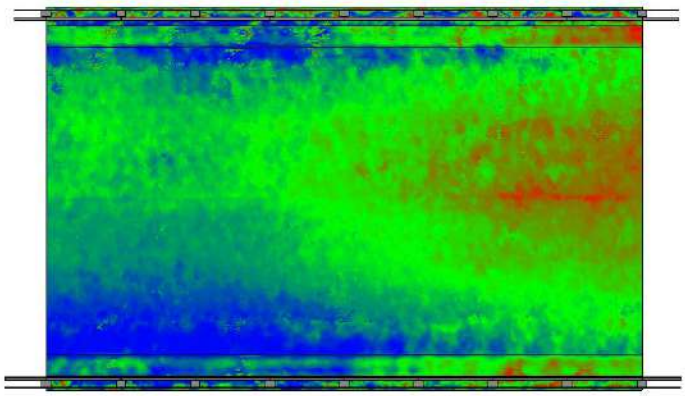

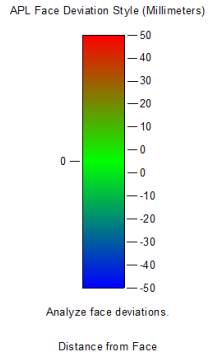

DECK 6

Front view

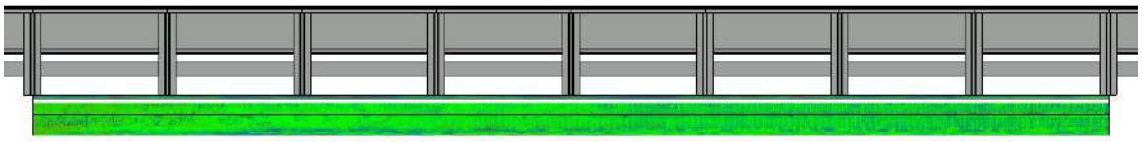

Back view

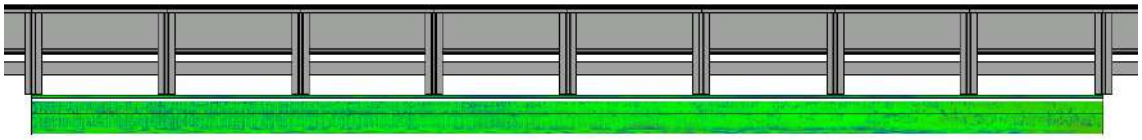

Top view

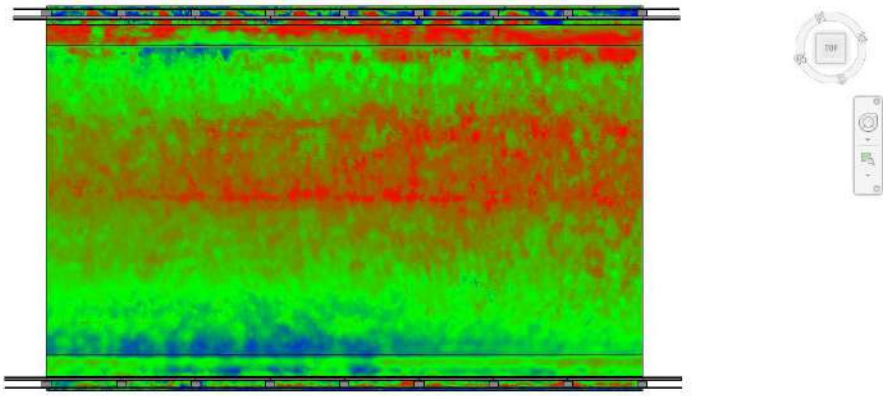

DECK 7

Front view

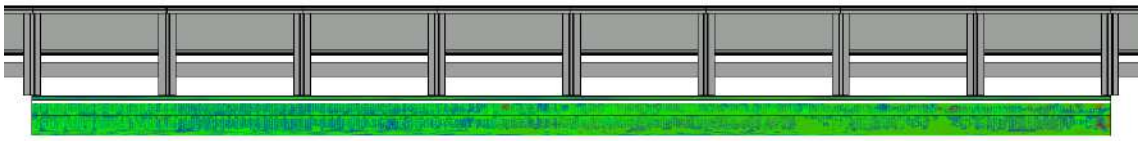

Back view

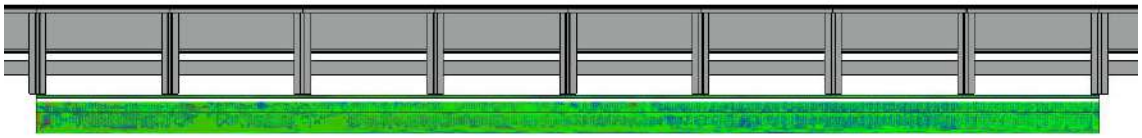

Top view

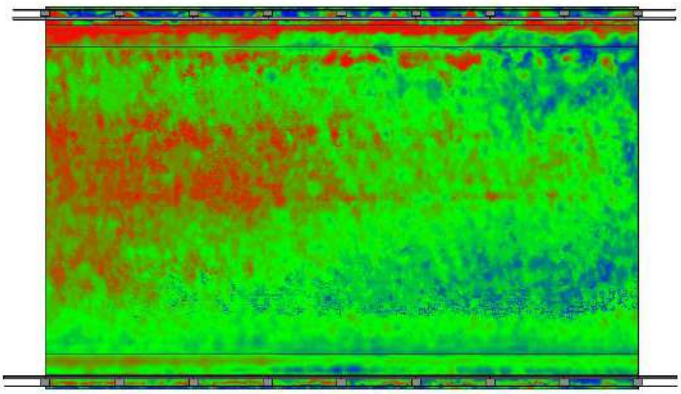

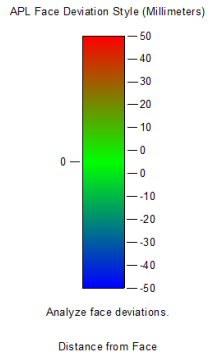

A.5) State of implementation of the public works of the Province of Piacenza

PROVINCIA DI PIACENZA
Servizio Viabilità
Dirigente Responsabile: Dott. Geol. Davide Marenghi
VERIFICA E MONITORAGGIO DELLO STATO DI CONSERVAZIONE DELLE OPERE DI COMPETENZA
REPORT DI SINTESI

Descrizione	*Importo stimato*
Strada Provinciale n. 654R di val Nure alla progressiva km. 45+150 in località Cantoniera. Lavori di adeguamento funzionale e miglioramento della sicurezza del ponte	€ 600.000,00
S.P. n. 6 bis di Castellarquato. Ponte sul torrente Chero in località Ciriano. Lavori di consolidamento delle fondazioni	€ 450.000,00
S.P. n. 4 Bardi. Ponte Lanzone alla progressiva km. 22+830. Lavori di consolidamento del manufatto e installazione di barriere di sicurezza.	€ 800.000,00
S.P. n. 10R Padana inferiore. Ponte sul torrente Chiavenna alla progressiva km. 202+520 in località Caorso. Lavori di consolidamento e installazione di barriere di sicurezza.	€ 400.000,00
S.P. n. 412R di Val Tidone. Ponte sul Rio Lentino alla progressiva km. 66+180. Lavori di consolidamento delle fondazioni dell'impalcato e di installazione delle barriere di sicurezza stradale.	€ 350.000,00
S.P. n. 654R di Val Nure. Ponte sul Canale del Vescovo alla progressiva km. 61+100 in località Retorto. Lavori di consolidamento del manufatto e installazione barriere di sicurezza.	€ 480.000,00
S.P. n. 586R di Val d'Aveto. Ponte sul Rio Remorano alla progressiva km.22+200. Installazione barriere di sicurezza.	€ 320.000,00
S.P. n. 588R dei Due Ponti. Ponte sul torrente Ongina alla progressiva km. 14+216. Lavori di consolidamento delle fondazioni	€ 210.000,00
S.P. n. 50 del Mercatello. Ponte sul torrente Cordarezza alla progressiva km. 24+150. Lavori di rifacimento del manufatto ai fini della riduzione del rischio idraulico residuo del centro abitato di Marsaglia	€ 650.000,00
S.P. n. 10 di Gropparello. Ponte sul torrente Vezzeno alla progressiva km. 6+950 in loc. Sariano. Lavori di consolidamento e installazione delle barriere di sicurezza.	€ 250.000,00
S.P. n. 654R di Val Nure. Ponte sul Rio Croso alla progressiva km. 65+758. Lavori di consolidamento del manufatto e installazione barriere di sicurezza.	€ 490.000,00
S.P. n. 26 di Busseto. Ponte sul torrente Arda nel centro abitato di Cortemaggiore alla progressiva km 0+645. Lavori di consolidamento delle fondazioni	€ 295.000,00
S.P. n. 587R di Cortemaggiore. Ponte sul Torrente Chiavenna alla progressiva km. 9+142 in centro abitato a Chiavenna Landi. Lavori di consolidamento del manufatto e installazione delle barriere di sicurezza	€ 300.000,00
S.P. n. 412R di Val Tidone. Viadotto sul Rio Ricò alla progressiva km. 61+800. Lavori di consolidamento del manufatto.	€ 1.400.000,00
S.P. n. 21 Val d'Arda Ponte sul torrente Arda in località Case Bonini alla progressiva km 9+755. Lavori di ripristino strutturale delle parti ammalorate in calcestruzzo armato	€ 400.000,00
S.P. n. 60 di Croce. Ponte sul torrente Tidone alla progressiva km. 0+200 in località Pianello. Lavori di consolidamento del manufatto e installazione barriere di sicurezza.	€ 850.000,00
S.P. n. 654R Ponte sul Rio Gambaro alla progressiva km. 57+868. Lavori di consolidamento del manufatto e installazione barriere di sicurezza.	€ 490.000,00
S.P. n. 56 di Borla. Ponte in località Comini alla progressiva km 13+250. Lavori di ripristino delle parti in muratura ammalorate.	€ 170.000,00
S.P. n. 16 di Coli. Ponte sul Rio Curdello alla progressiva km. 0+500. Lavori di consolidamento e installazione delle barriere di sicurezza.	€ 230.000,00
S.P. n. 60 di Croce. Ponte sul Torrente Chiarone alla progressiva km. 3+900. Lavori di consolidamento del manufatto e installazione barriere di sicurezza.	€ 240.000,00
S.P. n. 40 Statto. Manufatto di attraversamento del Fiume Trebbia alla progressiva km. 10+000, in località Bellaria. Lavori di consolidamento del manufatto e installazione barriere di sicurezza.	€ 950.000,00
S.P. n. 4 di Bardi. Ponte sul torrente Arda in loc Castell'Arquato alla progressiva km 9+000. Lavori di consolidamento del manufatto e installazione delle barriere di sicurezza.	€ 840.000,00
S.P. n. 10 di Gropparello. Ponte sul torrente Vezzeno alla progressiva km. 9+700 in località La valle. Lavori di consolidamento del manufatto e installazione barriere di sicurezza.	€ 190.000,00
S.P. n. 25 di San Nazzaro. Ponte sul Fiume Po alla progressiva km. 0+760. Lavori di consollidamento e rifunzionalizzazione.	€ 3.500.000,00
S.P. n. 34 di Pecorara. Ponte sul torrente Tidoncello in località Morasco alla progressiva km. 2+300. Lavori di ripristino strutturale delle parti in calcestruzzo armato ammalorate	€ 650.000,00
S.P. n. 15 di Prato Barbieri. Ponte sul Rio San Carlo alla Progressiva km. 0+900 in località Bettola. Lavori di consolidamento del manufatto e installazione barriere di sicurezza.	€ 290.000,00
S.P. n. 16 di Coli. Ponte sul fiume Trebbia alla progressiva km. 0+200 Lavori di ripristino della soglia idraulica e di installazione delle barriere di sicurezza.	€ 1.200.000,00
S.P. n. 10bis di Castellana. Ponte sul torrente Vezzeno alla progressiva km. 1+400 in località Gropparello. Lavori di consolidamento del manufatto e installazione barriere di sicurezza.	€ 410.000,00
S.P. n. 654R di Val Nure Ponte su torrente Nure alla progressiva km. 18+400, in località Pontedellolio. Lavori di consolidamento del manufatto e installazione barriere di sicurezza.	€ 3.800.000,00
S.P. n. 50 del Mercatello. Ponte sul Rio Grondana alla progressiva km. 0+500. Lavori di installazione delle barriere di sicurezza.	€ 180.000,00
S.P. n. 18 di Zerba. Ponte alla progressiva km. 0+650. Lavori di installazione delle barriere di sicurezza	€ 100.000,00
S.P. n. 18 di Zerba. Ponte alla progressiva km. 0+700. Lavori di installazione delle barriere di sicurezza	€ 150.000,00
S.P. n. 8 di Bedonia. Manufatto di attraversamento del rio dei Ratti al km. 8+000. Lavori di ripristino delle fondazioni e consolidamento manufatto	€ 250.000,00

Pagina 1